acta physica slovaca vol. 62 No. 5, 411 – 518 **October 2012**

MAGNETIZATION PROCESSES IN GLASS-COATED MICROWIRES WITH POSITIVE MAGNETOSTRICTION

Rastislav Varga[1]
Institute of Physics, Faculty of Science, UPJŠ Košice, Park Angelinum 9
SK-04 154 Košice, Slovakia

Received 31 March 2013, accepted 20 May 2013, in final form 4 June 2013

Glass-coated microwires are very interesting materials for theoretical study as well as for practical applications. Having positive magnetostriction, their domain structure consists of single axially magnetized domain and magnetization process runs through Large Barkhausen jump of a single domain wall along entire microwire. This gives us possibility to study a single domian wall propagation on large scales (few cm). As a result of their complex anisotropy distributon, the glass coated microwires exhibit very fast domain wall propagation, sometimes faster then sound speed. The domain wall dynamics can be very effectively modified by different anisotropies introduced in the wire by magnetic field, mechanical stress, thermal treatment, etc... In such a way, domain wall dynamics with the high domain wall velocity that is independent on magnetic field can be achieved. Stability of domain wall dynamics can be enhanced by using nanocrystalline compositions of microwire that combines low anisotropy of amorphous alloys with high structural stability of crystalline materials. On the other hand, sensitivity of domain wall dynamics on external parameters can be employed in the sensoric applications. The switching field at which the single domain wal starts to propagate is strongly sensitive to the temperature, mechanical stress, frequency of applied magnetic field etc... Knowing the physical origin of such sensitivies allows us to construct miniaturized multifunctional sensor that can even be embedded into the material structure.

DOI: 10.2478/v10155-012-0002-5

PACS: 75.60.Ej, 75.60.Jk

KEYWORDS: Magnetic microwires, Domain wall dynamics, Switching field, Magnetic anisotropy, Magnetic bistability, Nanocrystalline materials

Contents

[1]E-mail address: rvarga@upjs.sk

1 Introduction

Domain wall dynamics in thin magnetic wires is used in modern spintronic devices to store, transfer and manipulate information [1, 2, 3, 4]. The domain wall is forced to propagate either by magnetic field, or electrical current. Anyway, the speed of such devices is determined by the domain wall velocity. Hence, there is a demand for materials with fast domain walls with a very well controlable domain wall dynamics.

Magnetic glass-coated microwires are excellent materials to study the single domain wall propagation on large scales (few centimeters). As a result, a lot of new interesting results appeared during such studies. Due to the complex anisotropy distribution in the microwires, they show very fast domain wall propagation with the domain wall velocities up to 18 000 km/s [5]. Such velocities are much higher then sound speed. Hence, sometimes effects like "supersonic boom" appears as a result of magnetoelastic interaction of domain wall with phonons [6]. There are at least three reasons for such fast domain walls: 1. low Gilbert damping, 2. existence of shielding radial domain structure bellow the surface of the wire, that prevents the domain wall from pinning on surface defects and 3. existence of two perpendicular anisotropies that compensate each other. Applying a transversal magnetic field, the domain wall velocity increases up to 9 km/s and becomes independent on magnetic field [7]. Another effect that increase the domain wall velocity is a negative value of the critical propagation field [8], which results in a fast domain wall even in the case of low domain wall mobility [9]. Moreover, new contribution to the domain wall damping has been observed that arises from the structural relaxation of amorphous structure [8, 10].

The domain wall dynamics in glass-coated microwires is strongly dependent to external parameters like magnetic field, temperature, mechanical stress, etc... This leads us to idea to employ them in construction of miniature sensors that can even be introduced into the material stucture. It will be shown how understanding of basic physics can help in construction of multifunctional sensor of magnetic field, temperature and stress that consists of a single microwire and switching between the functions is provided by a simple change of the frequency of applied magnetic field.

The article is organized as follows: Chapters 2 describes production and magnetic properties of glass-coated microwires. Chapter 3 introduces a simple viscous model for single domain wall propagation. Chapter 4 presents the results on the domain wall dynamics in glass-coated microwires with respect to fast domain wall propagation, influence of thermal treatment on the domain wall velocity as well as it provides new compositions to obtain fast and stable domain wall dynamics in a wide temperature range. In Chapter 5 switching field of the single domain wall is introduced in terms of the domain wall potential. Chapter 6 shows dependence of the switching field on external parameters, showing also how it can be employed for construction of miniaturized sensors for temperature, magnetic field, mechanical load etc...

2 Glass-coated microwires

Glass-coated microwires are composite materials that consist of metallic nucleus and glass-coating (see Fig. 2.1). The diameter of metallic nucleus is from 100 nm up to 50 μm, whereas the glass-coating thickness is from 2 up to 20 μm [11]. Their bigest advantage is the simple and cheap method of preparation, efficiency (up to few kilometers of microwire can be produced from 1 g of master alloy), glass-coating that provides electrical insulation, small dimensions and circular symmetry [12, 13]. They are prepared by drawing and rapid quenching of molten master alloy [14]. It was firstly introduced by Taylor in 1924 in USA, according to whom this method is named [15]. Later, this method was improved by Ulitovski in USSR in 1950 in order to be able to produce large amount of such microwires [16]. in 70-ies of 20. century, the amorphous magnetic glass-coated microwires were produced and studied in GDR [17]. New boom appers at the end of 20. century when amorphous glass-coated microwires became to be produced and studied in different countries and main interest has been focused to magnetic microwires with specific magnetic properties.

As a result of their amorphous structure, amorphous glass-coated microwires are characterized by a low anisotropy (since the most important -crystalline anisotropy is missed). Hence, their magnetic properties are given mainly by magnetoelastic and shape anisotropy. The main -magnetoelastic anisotropy arises from the interaction of local magnetic moments with applied mechanical stress induced during microwire's production by drawing, quenching as well as due to different thermal expansion coefficients of metallic nucleus and glass-coating. As it was shown in [18, 19, 20], axial tensile stress dominates in the center of metallic nucleus, whereas compressive axial and tensile radial stresses prevails just below the surface. Such a distribution of mechanical stresses is crucial for magnetic properties of amorphous glass-coated microwires. Depending on the sign of magnetostriction, the glass-coated microwires are usually divided into the three groups.

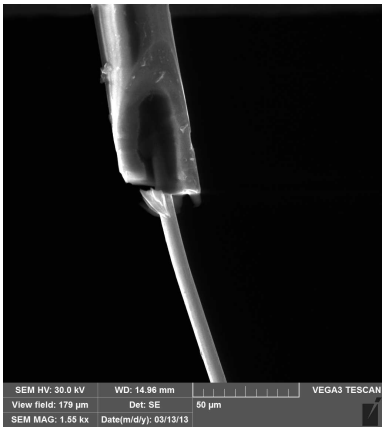

Fig. 2.1. SEM picture of glass-coated microwire

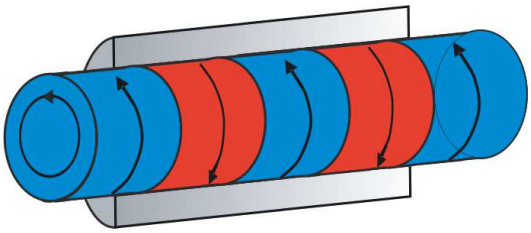

Fig. 2.2. Schematic domain structure of glass-coated microwires with negative magnetostriction

2.1 Microwires with negative magnetostriction

There are mainly CoSiB-based microwires that are characterized by relatively high and negative magnetostriction. As a result of stress distribution (described above) the easy axis in theses microwires will be circular. Hence, they are characterized by a domain structure that consists of circular domains (see Fig. 2.2) [21]. Magnetization process in axial direction runs through reversible rotation of magnetic moments inside domains. Hysteresis loop of such microwires is unhysteretic and manetization is proportional to the applied magnetic field. They are ideal for construction of miniaturized sensors, transformers, etc...

2.2 Microwires with low magnetostriction

There are usually CoFeSiB (3-5 at.% of Fe) -based microwires that are characterized by very low, but negative magnetostriction. This results in small circular magnetoelastic anisotropy. The domain structure of such microwirers is characterized by circular domains below the surface of metallic nucleus and axial domain structure in the center of the wire (see Fig. 2.3) [22]. Hysteresis loop of microwires with low magnetostriction is characterized by very low coercivity and high initial permeability. Apart from possibility to study the circular domain wall propagation theoretiacally [23], high sensitivity of initial susceptibility to external parameters (like temperature, magnetic field, mechanical stress, etc...) can be employed in construction of miniaturized

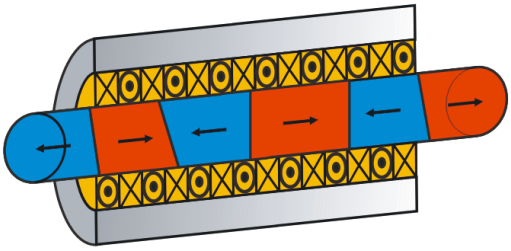

Fig. 2.3. Schematic domain structure of glass-coated microwires with low and negative magnetostriction

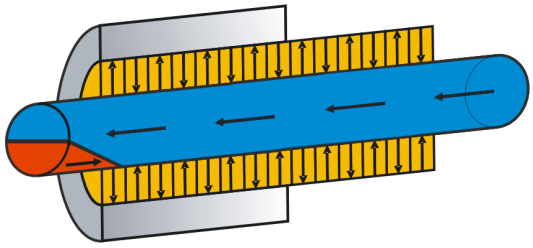

Fig. 2.4. Schematic domain structure of glass-coated microwires with positive magnetostriction

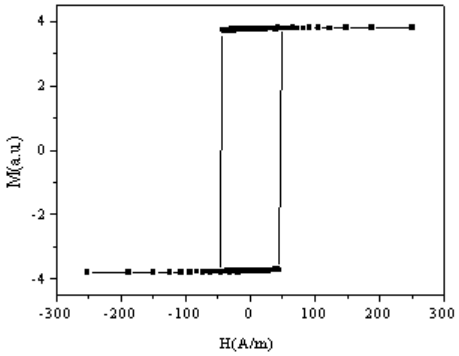

Fig. 2.5. Hysteresis loop of glass-coated microwires with positive magnetostriction

very sensible sensors. Particularly, the microwires with low and negative magnetostriction are already employed in sensors of magnetic field based on the GMI effect [24] that is one of the most promissing application of glass-coated microwires.

2.3 Microwires with positive magnetostriction

Last group that has been intensively studied in last years is the group of glass-coated microwires with positive magnetostriction. Due to the magnetoelastic interaction of magnetic moments with stress distribution introduced during the microwire's production, their domain structure consists of large single domain in the center of metallic nucleus that is covered by a radial domain structure (see Fig. 2.4) [25, 26]. Moreover, small closure domains appear at the end of the wire in order to decrease the stray fields [27].

As a result of the peculiar domain structure, the magnetization process runs through the depinning and subsequent propagation of closure domain along entire microwire in a single large Barkhausen jump. Such a domain structure and magnetization process is ideal to study the single domain wall propagation on large distances (few centimeters). On the other hand, hysteresis loop of such microwire is perfectly rectangular (see Fig. 2.5) and magnetization can have only

two values $\pm M_s$ (where M_s is the saturation magnetization). The switching between the two magnetization values appreas when external field exceeds the so-called switching field H_{sw}. The switching field is strongly dependent on external parameters like temperature, mechanical stress, external magnetic field, etc... Moreover, it is easy to detect, therefore the glass-coated microwires can be employed in construction of miniaturized sensors.

3 Model for domain wall dynamics

The domain wall propagation in real material can be described similarly as the movement of linear harmonic oscillator under external force $F(t)$ in a viscous medium [28]. Its time (t) dependent oscillation is described [28]:

$$m_{dw}\frac{d^2x}{dt^2} + \beta\frac{dx}{dt} + \alpha\, x = F(t), \tag{3.1}$$

where m_{dw} is the effective mass of the domain wall, β is the damping coefficient that characterizes the viscous medium, α is the stiffness coefficient, x is the displacement of the domain wall from its equilibrium position. In the case of domain wall, the force F is represented by the force, acting on the domain wall by the applied magnetic field H and it is expressed as:

$$F = b\mu_0 M_s H, \tag{3.2}$$

where b is the constant that depends on the domain wall configuration and is equal to 2 for 180° domain wall or to $\sqrt{2}$ for 90° domain wall, μ_0 is the permeability of vacuum and M_s is the saturation magnetization. Assuming the domain wall propagation at constant velocity ($d^2x/dt^2 \rightarrow 0$), linear dependence of the domain wall velocity v on the applied magnetic field H can be simply obtained [29]:

$$v = S(H - H_0). \tag{3.3}$$

Here S is the so-called domain wall mobility and H_0 is the critical field, below which the domain wall propagation cannot be observed, neither theoretically. Comparing the Eq. (3.1) and Eq. (3.3), it can be shown that domain wall mobility is inversely proportional to the domain wall damping parameter β:

$$S = \frac{b\mu_0 M_s}{\beta}. \tag{3.4}$$

The critical propagation field H_0 is a more mystic parameter. Sometimes, it is taken to be a meaningless constant [29]. However, according to Eq. (3.1) and (3.3), it is expressed:

$$H_0 = \frac{\alpha x}{b\mu_0 M_s}, \tag{3.5}$$

which is very similar to expression for the coercive field [28]. Therefore, some authors take it simply as coercivity [30]. Another authors called it dynamic coercivity [31], since it differs from the static coercivity measured from hysteresis loops. In the following sections, we will show some interesting aspect that are connected to the critical propagation field and that strongly affects the domain wall velocity. However, the most important parameter that controls the domain wall velocity is the domain wall damping. At the beginning, the only domain wall damping was assumed to arise from the eddy current [31]. In the case of magnetic wire, the domain wall damping due to eddy current β_e is expressed as [33]:

$$\beta_e = \frac{4\mu_0^2 M_s^2 r_0}{\rho}(ln\frac{r_0}{r_b} + \frac{8}{\pi^2}), \tag{3.6}$$

where ρ is the resistivity, T is a temperature and r_0 and r_b are the radii of the wire and that of the inner domain core, respectively. However, the strong damping for highly insulated materials, such as ferrites, cannot be explained by the eddy current damping. Therefore, another damping mechanism, based on Landau-Lifshitz equation has been introduced [34], which is still basis for many theoretical approaches to solve the domain wall propagation [35, 36]. The idea starts from famous Landau - Lifshitz model [37] of the domain wall that assumes the homogeneous distribution of magnetization within the domain wall. In such case, the spin dynamics can be described by the famous Landau-Lifshitz equation [30]:

$$\frac{d\vec{M}}{dt} = -\gamma(\vec{M} \times \vec{H}) + \frac{\alpha_G}{M_s}(\vec{M} \times \frac{d\vec{M}}{dt}), \tag{3.7}$$

where α_G is the so-called called Gilbert damping parameter. The switching motion of magnetization is more viscous as the Gilbert damping parameter becomes large. However, the switching time becomes very large, too, as the Gilbert damping parameter becomes small, since the magnetization performs too many precession rotations [32]. Hence, the fastest switching is attained for an intermediate value of Gilbert damping parameter α_G, called critical damping. It is possible to obtain the relation between the domain wall damping β and Gilbert dampig parameter α_G [30, 32]. Such damping, called relaxation β_r, is inversely proportional to the domain wall width δ_w:

$$\beta_r = \frac{\alpha_G}{|\gamma|\,\delta_w} \approx \frac{\mu_0 M_s}{\pi}\sqrt{\frac{K}{A}} \approx \frac{\mu_0 M_s}{\pi}\sqrt{\frac{3\lambda_s\sigma}{2A}}, \tag{3.8}$$

where γ is gyromagnetic ratio, K is the magnetic anisotropy energy density (in the case of amorphous microwires magnetoelastic), A the exchange stiffness constant, λ_s is the saturation magnetostriction and σ is mechanical stress. Anyway, neither eddy currents, nor magnetic relaxation could explain a strong variation of domain wall damping with the temperature for some magnetic materials [8,38]. Therefore, another damping was suggested in [38] that arises from the structural relaxation of the mobile defects on atomic scale. Such contribution, called structural relaxation damping β_s, was firstly approved in amorphous microwires [8]:

$$\beta_s \approx \tau \left\langle (\epsilon_{eff})^2 \right\rangle (c_0/kT) G(T,t), \tag{3.9}$$

where τ is the relaxation time of the defects, ϵ_{eff} is the interaction energy of the domain wall with the defects, c_0 is the concentration of mobile defects, k is Boltzman constant and $G(T,t)$ is so-called relaxation function defined as [39]:

$$G(T,t) = (1 - exp(-t/\tau)), \tag{3.10}$$

Here t is time and τ obbeys Arrhenious law:

$$\tau = \tau_0 exp(Q/kT), \tag{3.11}$$

where τ_0 is the pre-exponential factor and Q is the activation energy of mobile defects.

The structural relaxation damping was approved also by a thermal treatment [40], and it is specially important at low temperature, when the atomic mobility decreases, leading to the

increase of a local anisotropy and therefore to the increase of the structural relaxation damping [8, 41].

Amorphous microwires are in metastable state and they can relax even at low temperatures. Hence the structural relaxation influences the domain wall damping significantly [8, 42] through the mobile defects that exist as a consequence of the atoms appearing in the vicinity of the so-called free-volumes (e.g. the volume fractions with the volume density lower than the average one [43]). In contrary to previous contributions (eddy current and magnetic relaxation) to the domain wall damping, the structural relaxation component can be modified by properly setting the experimental conditions or by thermal treatment [40]. During the experiment, three time parameters are important:

1. τ relaxation time of mobile defects
2. t_1- time necessary for domain wall to propagate across the defect (given by the domain wall width and its velocity)
3. t_2- time between two domain wall propagations (given by the frequency f of the applied magnetic field H, $t_2 \sim 1/f$).

The relative value of τ with respect to t_1 and t_2 determines five thermal ranges for the domain wall propagation [40]:

1. Metastable range: $\tau > t_2 > t_1$. Defects have no time to relax (they are frozen-like) and they appear in the non-thermodynamical equilibrium. The amplitude of the structural relaxation damping is given by the history of the material. If the material was stabilized, by annealing below the Curie temperature, β_s is high. But if the system was destabilized, by demagnetization or by heating above the Curie temperature, β_s is small. Such range corresponds to low temperatures (see Arrhenius law - Eq. (3.11)).
2. Structural relaxation range: $\tau \approx t_2 > t_1$. Defects are able to relax between two domain wall propagations. This makes β_s increase hindering the domain wall propagation. By properly setting the driving frequency, that range can be moderated and the structural relaxation damping β_s can be increased or decreased [10].
3. Adiabatic range: $t_2 > \tau > t_1$. The defects system is in thermal equilibrium and β_s reaches a maximum, at a given temperature (see Eq. (3.10)), but the defect cannot follow the propagating domain wall.
4. Diffusion damped range: $t_2 > t_1 \approx \tau$. In this regime, the time at which the domain wall crosses a single defect is comparable to its relaxation time. The defect relaxes during the domain wall propagation making decrease the domain wall speed. Increasing the applied field amplitude, the domain wall velocity rises until $t_1 < \tau$, when the domain wall is able to depin from the defect and goes into the adiabatic regime [45].
5. Isothermal range: $t_2 > t_1 > \tau$. Although the whole system relaxes between two domain wall propagations, the relaxation time of defects is short and they are able to follow rapidly the domain wall during its propagation. β_s is small and the domain wall velocity increases. Such regime corresponds to high temperatures.

Now, the situation should be easy if one wants to achieve the fast domain wall. According to Eq. (3.3) and (3.4), one should simply keep domain wall damping, β, low (in order to obtain high domain wall mobility S) and critical field H_0 also low (even negative, if possible). However, the situation is much more complicated in practice. Generally, the viscous domain wall motion occurs only up to a certain limit. For a very high magnetic field, the magnetization precession inside the domain wall becomes non-uniform and the conditions of validity of the above-described model (constant velocity of the domain wall, homogeneous distribution of the magnetization inside the domain wall) are not fulfilled anymore. This situation occurs at the so-called Walker limiting velocity v_w [46], which is mostly taken as the maximum domain wall velocity for its propagation in viscous regime. Walker limiting velocity can be estimated as [30]:

$$v_W = \frac{|\gamma|\,\mu_0 M_s \delta_w}{2}. \tag{3.12}$$

However, the field range in which the domain wall velocity is proportional to the applied magnetic field depends on the presence of the transverse anisotropy. The Walker limiting velocity appears at the so-called Walker field, H_W, which is proportional to the transverse anisotropy field H_K [47]:

$$H_W \approx \alpha_G H_K/2. \tag{3.13}$$

Above this Walker field, the domain wall propagation is not uniform, the domain wall velocity decreases and its mobility is negative [31]. Although nice, the Walker model cannot describe fast domain walls observed experimentally in some Garnet films when a perpendicular field, $H_\perp$, was applied [48]. These velocities exceed the Walker limiting velocity more than ten times. The maximum velocity, v_m, can be related to the Walker limiting velocity, v_W, by the following expression [30]:

$$\frac{v_m}{v_W} = \frac{2H_\perp(Q+1)}{M_s Q}, \tag{3.14}$$

being Q dimensionless parameter representing the anisotropy of material ($Q = 2K_u/\mu_0 M_s^2$). K_u is the uniaxial anisotropy constant.

Finally, very fast domain walls have been observed in ortoferrites [49, 50, 51]. Such domain wall velocity exceeds the sound velocity with a maximum $\approx$ 20 000 m/s. Quasi relativistic behaviour was found with the maximum velocity equal to the spin waves velocity [50, 51]. The theory for such quasirelativistic behaviour was worked out by Zvezdin [52] or Baryakhtar [53].

This is an overview of the physical models mostly used currently for description of the domain wall dynamics. However, new materials and new measuring conditions bring new, surprising results that do not fit to the above given model. Surely, there are much more parameters that defines the domain wall velocity, therefore new experiments on new materials are necessary in order to understand the thing. In the following section, the most interesting results obtained during the study of domain wall dynamics in glass-coated microwires are shown.

4 Domain wall dynamics in glass-coated microwires

4.1 Experimental methods

Sixtus and Tonks were in between the first scientists trying to study the domain wall dynamics in 30-ies of last century [54, 55]. They have built up a simple method to measure domain wall velocity in magnetic wires, which is used up to now. Apparatus consists of primary coil to produce a homogeneous magnetic field necessary for domain wall propagation (see Fig. 4.1). Inside the primary coil, two pick-up coils are inserted coaxially. Magnetic microwire is placed in the center of the coil's system. At the end of the wire, nucleation coil is placed in order to nucleate reverse domain. Doman wall between the main and reversed domain propagates along entire microwire and its movement induces *emf* signal when it propagates inside the pick-up coils. The domain wall velocity is simply estimated as a ratio between the distance between the pick-up coils and time between the two *emf* maxima induced in pick-up coils. In the case of glass-coated microwires, such a method is even more simple. Due to a presence of reverse domain at the end of the wire (see Fig. 2.4), no nucleation coil is necessary. It is employed only in the case of measurements in low magnetic field.

In our case, the length of the primary coil is 10 cm and the distance between the pick-up coil is 6 cm. The width of pick-up coil is 3 mm. We have slightly improved the Sixtus Tonks method to fit better the conditions in microwires. Firstly, the position of microwire in primary coil is not symmetrical. Instead, one end of the wire is placed outside of soleniod (in lower magnetic fields), while the other end is placed inside [5]. This improvement assure the domain wall propagation always from one end of the wire. Such improvemement was finally applied also in theoretical works on domain wall propagation [56]. Secondly, the pick-up coils are connected anti-series. This allows us to control the direction of the domain wall propagation, since one pick-up coils induces *emf* maximum, whereas the other pick-up coil induces *emf* minimum. Moreover, anti-series connections compensate the influence of external magnetic field change. Thirdly, symmetrical pick-up coils were replaced with antisymmetrical ones, in which asymmetrical *emf* signal

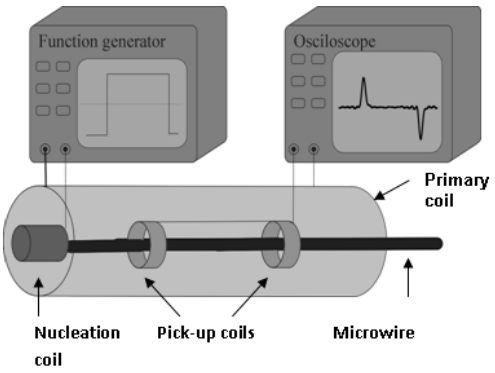

Fig. 4.1. Schematic picture of Sixtus-Tonks apparatus for maesuring the domain wall velocity in magnetic wires

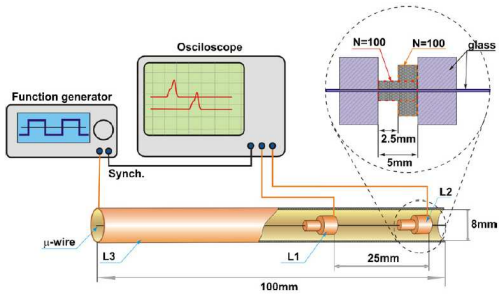

Fig. 4.2. Schematic picture of improved Sixtus-Tonks apparatus with antisymmetrical pick-up coils [57]

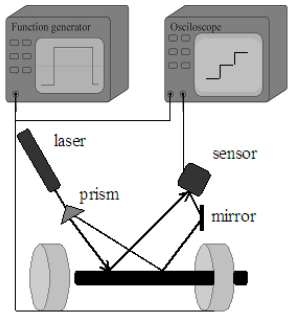

Fig. 4.3. Schematic picture of improved Sixtus-Tonks apparatus by its combination with Kerr effect [58]

is induced depending on the domain wall propagation direction (see Fig. 4.2) [57]. This gives us possibility to recognize multidomain wall propagation, nucleation of the reversed domain in the center of the wire, etc...

The dimensions of the system allows it to be placed in crysostats and to performe the domain wall dynamics study in a wide range of temperature.

Another improvement of the method consists of replacing the pick-up coils by Kerr effect reflection point (see Fig. 4.3) [58]. This combination allows us to measure very high domain wall velocities. Moreover, it allows to study the domain wall shape, too [59].

4.2 Domain wal dynamics in viscous regime

Our first results [8] on the domain wall dynamics in glass-coated microwires showed that it fits perfectly to the linear dependence of the domain wall velocity on applied magnetic field in a wide temperature range according to Eq. (3.3) (see Fig. 4.4). However, it shows some peculiar characteristics. First of all, the domain wall dynamics shows negative critical propagation field H_0. Such a fact has already been observed in glass-coated microwires, but it was ignored [60,61, 62,63]. Theoretically it should mean that the domain wall propagation velocity is positive in the case of no applied external field. However, the things is more complex as will be shown below.

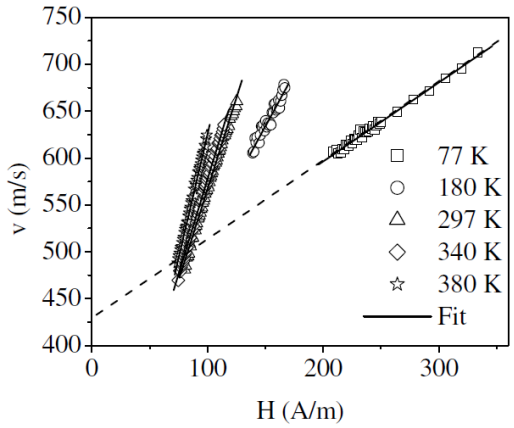

Fig. 4.4. Domain wall velocity dependence on applied magnetic field in FeSiB microwire [8]

On the other hand, the temperature dependence of the domain wall damping β shows strong increase at low temperatures. This increase cannot be described by eddy-currents (Eq. (3.6)), neither by magnetic relaxation of magnetic moments (Eq. (3.8)). However, it can be explained by the structural relaxation damping introduced by Kitttel in 1956 [38]. Glass-coated microwires are metastable in nature because of their amorphous character, therefore they should exhibit strong structural relaxation leading to the stabilization of the magnetization in the domain walls as well as in the domains [64, 65]. Consequently, it is reasonable to introduce a new damping mechanism arising from the structural relaxation. Let us imagine the nearly planar 180° domain wall propagating along the wire with an angle of about 90°. The wall interacts with the defects present in the amorphous structure. These defects are mobile and able to follow the change of the local magnetization direction in order to decrease the total free energy [66]. But they also play a role as pinning centers for the wall when they lose their mobility. The interaction energy of the wall with these defects has been expressed in the form [67]:

$$E_S = \frac{2}{15}\left[-2\delta_w\right]\frac{\left\langle\left(\epsilon_{eff}^2\right)\right\rangle c_0}{kT}G(t,T). \tag{4.1}$$

As the wall propagates with velocity v, local moments rotate 180°, and it takes a time, $t = \delta_w/v$, until the wall traverses the position of a mobile atomic defect. If t is much longer than the relaxation time τ of the defect, it will be able to follow the magnetization change and no damping is visible. This happens at high temperature since τ obeys the Arrhenius law (Eq. (3.11)). However, at low temperatures τ increases and for values of $\tau >$t, the atomic defects are no longer able to relax within t. This process enhances the wall pinning and contributes to the additional damping. Consequently, this damping through the structural relaxation takes place when $\delta_w = v\tau$. Introducing this into Eq. (4.1), considering the energetic balance between the interaction energy E_S and the energy provided by the external field $\mu_0 M_s H$, as well as the correlation between the domain wall mobility and damping coefficient, yields an expression for the structural relaxation

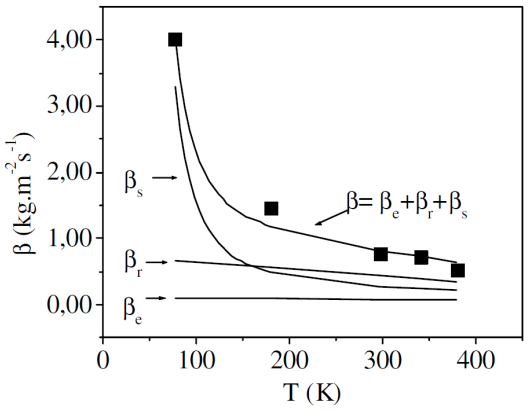

Fig. 4.5. Temperature dependence of the domain wall damping β: experimental (square points) and calculated (lines) [8]

wall damping (Eq. (3.9)).

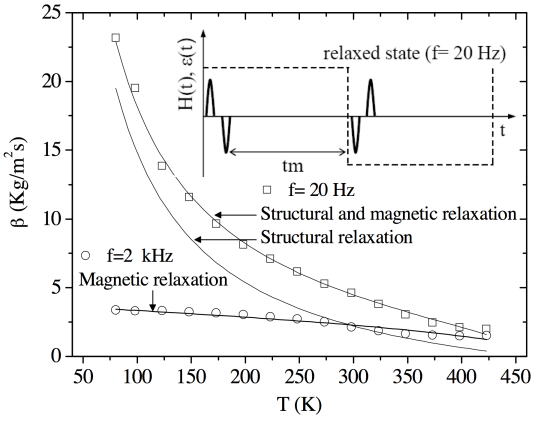

Fig. 4.6. Temperature dependence of the domain wall damping β for the relaxed (20 Hz) and unrelaxed (2 kHz) states. Full lines represent a fit according to corresponding contributions. Inset shows a schematic illustration for the relaxed state. Uniform drive field (dashed line) is shown as $H(t)$, induced voltage in sensing coils (full line) is depicted as $\epsilon(t)$. [10]

The fitting to the experimental damping in Fig. 4.5 denotes that the stabilization through structural relaxation plays a major role at low temperatures. From experimental results, the activation energy for structural relaxation per defect of around 20 meV is deduced, comparable to the thermal energy, kT, at temperatures when the structural relaxation becomes relevant.

The structural relaxation contribution to damping can be recognized from measurements by

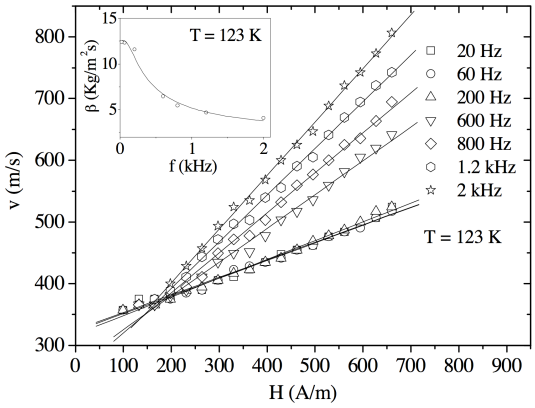

Fig. 4.7. Domain wall velocity as a function of applied field for T=123 K. Frequency as a parameter. Full lines represent a linear fit. Inset shows the corresponding frequency dependence of the domain wall damping β. Full line represent an exponential fit. [10]

properly setting the measuring conditions [10]. As given in the Section 3, the structural relaxation damping is sensible to the frequency of measurement f. Such a fact has been confirmed by measuring the temperature dependence of domain wall dynamics at different frequencies (Fig. 4.6). These frequencies, 20 Hz and 2 kHz, correspond to the sample been relaxed or unrelaxed, respectively. At high frequency , change of polarity of of exciting magnetic field occurs immediately after the domain wall propagation along the wire. At low frequencies, there is sufficient time for structural relaxation between the domain wall propagation and the change of polarity of exciting field. In the unrelaxed state, the damping is due to magnetic relaxation of magnetic moments. The domain wall damping β decreases slowly with temperature as a result of small variation of resistance and stresses applied on metallic nucleus by glass-coating. In contrary, measurement in relaxed state (at 20 Hz) shows strong increase of domain wall damping at low temperatures that was ascribed to structural relaxation damping. Inset of Fig. 4.7 shows the exponential dependence of structural relaxation damping on the frequency of applied exciting field according to Eq. (3.9). The overall damping varies by one order in the frequency interval 20-2000 Hz, beeing high at low frequency and low at high frequency of exciting magnetic field see inset of Fig. 4.7. This gives us possibility to tailor the domain wall damping according to desired conditions by simply varying the frequency of external magnetic field.

An alternative mechanism to increase the domain-wall velocity is to decrease the critical propagation field H_0. In some materials, H_0 can even be negative, as is the case of orthoferrites [49, 69], where a negative critical field was ascribed to the change of the domain wall structure. A negative critical propagation field has been observed many times in amorphous glass-coated microwires [60, 61, 62, 63]. However, no change of the domain structure has been observed during the domain wall propagation at low fields. Hence, there must be another explanation for the negative critical propagation field.

One possible explanation arises from the critical propagation field definition (Eq. (3.5)). Basically, Eq. (3.3) describes the domain-wall propagation in a domain-wall potential E (that can

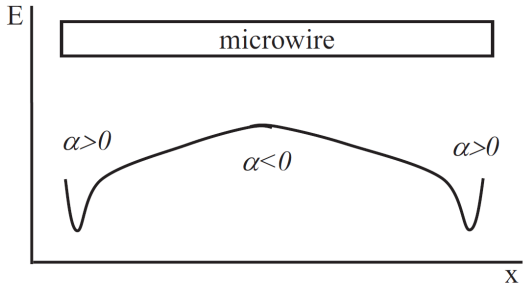

Fig. 4.8. Schematic dependence of the domain-wall potential E ($E \approx \alpha x^2$) in amorphous glass-coated microwire. [68]

be approximated by the parabolic shape $E \approx \alpha x^2$). However, the domain wall, in the case of microwires, propagates between the two potential minima that are separated by a potential barrier (Fig. 4.8) [68]. At the end of the microwires, the restoring force parameter α is positive. However, α is negative in the center of microwires where the domain-wall dynamics is studied. Negative restoring force parameter gives a negative critical propagation field (Eq. (3.5)). If this is true, the only necessary condition to observe the negative critical propagation field is to have domain-wall propagation between two local minima that are separated by the energetic barrier. The higher is the barrier, the higher is the amplitude of negative critical propagation field and the higher is also the domain-wall propagation (even in the case of low domain-wall mobility).

Such a fact is confirmed by the temperature and frequency dependence of the critical propagation field H_0. We have shown, that the critical propagation field H_0 is proportional to the switching field H_{sw}. This points to the fact, that both fields are driven by the same mechanism. Similarly to H_{sw} [64, 65], the H_0 has two contributions: i) magnetoelastic that arises from the interaction of local magnetic moments with local stress and ii) structural relaxation that arises from structural relaxation of mibile defects presented in the amorphous structure. Similarly, H_0 in the center of microwires can be expected to arise from the same contributions. Magnetoelastic contribution is given:

$$H_0^\sigma = \frac{2K}{\mu_0 M_s}. \tag{4.2}$$

The structural relaxation contribution is given by [64]:

$$H_0^s \approx \frac{\left\langle (\epsilon_{eff}^2) \right\rangle c_0}{kT} G(t,T). \tag{4.3}$$

Finally, the total critical propagation field H_0 is given by the sum of these two contributions:

$$H_0 = H_0^\sigma + H_0^s. \tag{4.4}$$

It was shown above [10] that the temperature dependence of the domain-wall damping within this temperature range can be successfully described by the two main contributions (magnetoelastic and structural relaxation). Similarly, the critical propagation field H_0 can be described by

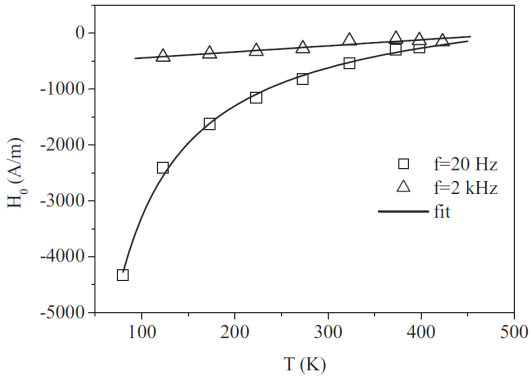

Fig. 4.9. Dependence of critical propagation field H_0 on temperature. Frequency of applied field as a parameter. Full lines correspond to the fit according to Eq. (3.10) [68].

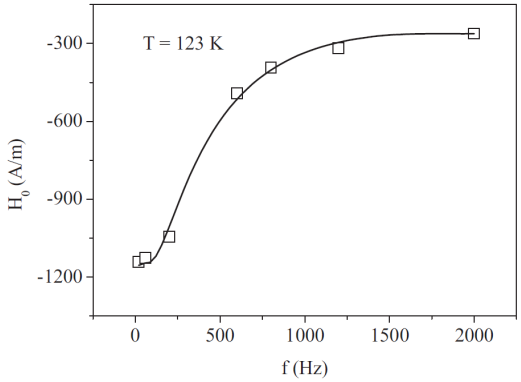

Fig. 4.10. Dependence of critical propagation field H_0 on frequency of excitation field. Full lines correspond to the fit according to Eq. (4.3) [68].

the sum of its two contributions given by Eq. (4.4) (Fig. 4.9). Two dependences are given: the first one measured in unrelaxed state, at 2 kHz (where $G(T,t) \rightarrow 0$), is given mainly by the magnetoelastic contribution (Eq. (4.2)). The amplitude of H_0 increases with the decreasing temperature as the stresses applied on the metallic nucleus by the glass coating increases. The second dependence of H_0 was measured in relaxed state (at 20 Hz) and is much more sensitive to the temperature. This is the result of the structural relaxation contribution (Eq. (4.3)) that is inversely proportional to the temperature. Stabilization of the domain structure in this case can increase the critical propagation field by one order of magnitude (being still negative). The amplitude of the critical propagation field, H_0, decreases with the frequency as a result of the stabilization of the domain structure (Fig. 4.10). At low frequency, the domain structure has enough time to relax

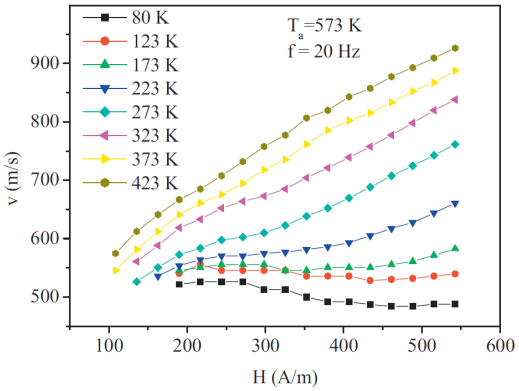

Fig. 4.11. Dependence of the domain-wall velocity v on applied magnetic field H for amorphous FeSiBP microwire annealed at 573 K/1 h. Temperature of measurement as a parameter [68].

after the domain-wall propagation. At high frequencies, there is no time for the domain structure to relax. Hence, the H_0 dependence on the frequency of applied field follows the exponential dependence given by the relaxation function $G(T,t)$ (Eq. (4.3)). Similarly to the structural relaxation damping, such an effect gives us the possibility to control effectively the domain-wall dynamics by simply changing the frequency of measurement.

Structural relaxation can even be employed to get negative domain wall damping S (Fig. 4.11) [68,70]. It appears at low temperatures where structural relaxation damping β_s is dominant. Negative domain-wall mobility has already been predicted by Schryer and Walker [71] and measured in different magnetic wires [72, 73]. It can appear at large applied fields, above the so-called Walker limit, when the domain-wall propagation is no longer in the viscous regime. Instead of that, something like a turbulent propagation of the domain wall appears. The field value, at which the Walker limit takes place, is called the Walker field and depends on the anisotropy (axial or transversal) present in the sample. However, it appears at a much higher field than in our case. Hence, the negative mobility must have another origin.

We have found that the negative-mobility effect can be enhanced or hindered by changing the frequency of the measurement (Fig. 4.12). This leads us to one possible explanation that can be offered in terms of complex domain structure of amorphous glass-coated microwires and its stabilization by heat treatment. It consists of single core domain with axially oriented magnetization that is surrounded by the radial domain structure (Fig. 2.4). The actual diameter of the inner core domain is given by the stress distribution and applied magnetic field. When the amorphous microwire is annealed at elevated temperature (but well below the Curie temperature) 573 K in our case, its domain structure is stabilized by pair ordering [29, 74]. When the axial field is applied, the diameter of the axial domain changes. If the field is in the direction of the axial magnetization, the diameter increases in comparison to that of the axial domain without external field. If the field has the opposite direction to the axial magnetization, the diameter of the axial domain decreases.

At high frequencies, when there is no time for structural relaxation between the two sub-

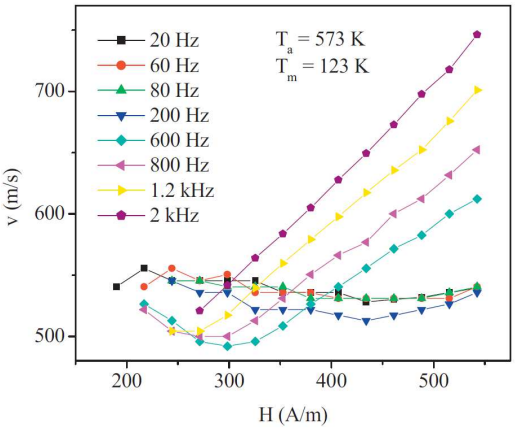

Fig. 4.12. Dependence of the domain-wall velocity v on applied magnetic field H for amorphous FeSiBP microwire annealed at 573 K/1 h. Frequency of measurement as a parameter [68].

sequent domain wall propagations, the domain structure occupies its stabilized state and the domain-wall dynamics is described by the linear dependence of the domain-wall velocity on the applied magnetic field. However, when the axial field of low frequency is applied, the situation changes. After each domain-wall propagation, the domain structure has enough time to relax and to increase the diameter of axial domain. Hence, the new domain wall propagates through the axial domain with larger diameter. Therefore, the domain-wall propagation is slower. The higher the amplitude of the applied field, the higher is the diameter of the relaxed axial domain. Such an effect is observed up to a certain field (where the minimum of the velocity appears). Above this field, the diameter of the core domain is saturated and increasing the field results in the increase of the domain-wall velocity according to Eq. (3.3). Although there is no direct (by optical methods) evidence for the domain-structure relaxation, such a model can describe the temperature (since the relaxation amplitude is inversely proportional to the temperature) as well as frequency (since the relaxation amplitude is proportional to the relaxation function $G(T,t)$) dependence of the domain wall dynamics having negative domain-wall mobility. Moreover, the negative domain-wall mobility appears in the microwire annealed well below the Curie temperature (in our case 573 K). However, it disappears in the microwire annealed at 673K that is the temperature very close to the Curie temperature and the effect of domain structure stabilization by magnetic annealing is hindered by high thermal activation of magnetic moments. Similar behavior has been found in Ref. [73], however, without any detail explanation. Although such effect increases energetic looses in magnetic materials, it gives us possibility to obtained the relatively high domain wall velocity (cca. 550 m/s) that does not depends on applied magnetic field (see Figs. 4.11 and 4.12 at 123 K, 20-80 Hz) which is higly desirable in some applications and also in multiple domain wall propagation synchronization.

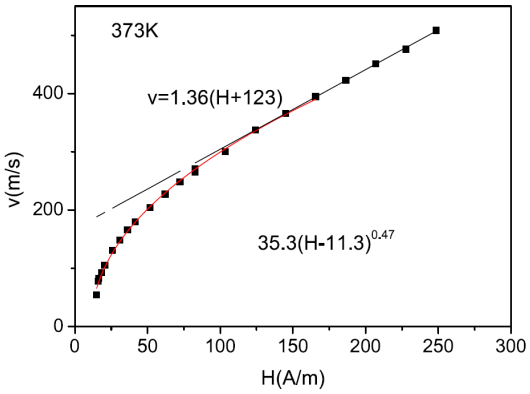

Fig. 4.13. Domain wall velocity v as a function of magnetic field amplitude H for FeSiB [42].

4.3 Low-field domain wall dynamics

As given above, the domain wall dynamics in glass-coated microwires shows interesting results at low fields. Negative critical propagation field should be very interesting phenomena if it would be possible to measure it. Hence, our next interest has been focused on the domain wall dynamics in low magnetic fields [42, 75, 76]. We have shown that the domain wall velocity is far from linear dependence on applied magnetic field (Fig. 4.13). Alternatively, the low-field domain wall dynamics can be described by a power law:

$$v = S'.(H - H'_0)^{\eta}, \tag{4.5}$$

where S' is the effective domain wall mobility parameter, H'_0 is the dynamic coercive field and η is the power exponent. Such a power law results from the interaction of the propagating wall with the defects of the material, different sources of which in the actual amorphous microwire have been described before [8, 65, 77]. As it was shown in [64] and [65], the domain wall potential W consists of two terms: the long-range magnetoelastic one and the short-range terms arising from the pinning of the domain wall on the defects in the amorphous medium. The pinning centres are randomly distributed along the amorphous microwire and the pinning field. Therefore, the domain wall potential fluctuates as the domain wall moves through the material, and the restoring force α acting on the domain wall due to the gradient of the internal potential is given by $\alpha = dE/dx$. When the domain wall passes the region with a local maximum of the restoring force α, a local jump occurs until the wall reaches a new site with the restoring force α greater than the force $2\mu_0 M_s H$ acting on the domain wall.

Therefore, the domain wall motion in the low-field limit is adiabatic. Under the action of a small force $2\mu_0 M_s H$, the domain wall moves slowly close to some local minimum in its potential that arises from the elastic interactions within the domain wall and from the impurities pinning. At some point, the local minimum disappears and the domain wall moves forward rapidly to another local minimum. Such motion is characterized by intermittent jumps of domain wall from defect to defect. Hence, the local domain wall dynamics description is governed by the

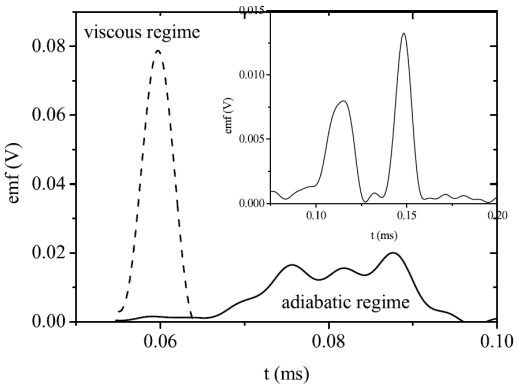

Fig. 4.14. The *emf* recorded waveform measured in the viscous and adiabatic regime (at very low domain wall velocity) at 273 K. The inset shows how the peak is separated into two peaks when the pinning is so strong that the domain wall stops inside the pick-up coil (below H_0') [42].

generalized Eq. (3.3):

$$v = S(H - (H_{dm} + H_p)), \tag{4.6}$$

where H_{dm} includes all long-range contributions (such as the geometry dependent demagnetizing field and the magnetoelastic contribution) and is separated from a random component, H_p, that includes all short-range counterfield contributions. The pinning field, H_p, is assumed to exhibit statistical properties governed by details of the local pinning potentials that inhibit domain wall motion. In the first approximation, the distribution of the pinning field takes Gaussian shape with the width of R. Then the magnetization change during the domain wall jump is given by the power law [78]:

$$\Delta M = \left(\frac{R - R_c}{R_c}\right)^{\eta}, \tag{4.7}$$

where R_c is a critical distribution width, below which the small intermittent domain wall jumps do not appear. As a result, the domain wall moves with average velocity ($v = \Delta M/\Delta t$) given by Eq. (4.5) [79, 80, 81]. The different shape of the induced peaks at the pick-up coils (obtained by a single shot acquisition) also confirms the presence of the two regimes (Fig. 4.14). The perfect symmetric shape measured in the viscous regime confirms the planar shape of the domain wall, which propagates at constant velocity. The emf waveform measured in the adiabatic regime (at very low domain wall velocity 50 m/s) suggests the fluctuation of the domain wall velocity during its motion across the randomly distributed defects. When the applied field is very close to the critical field H_0', the domain wall can even stop in the centre of the pick-up coil (see inset of Fig. 4.14). Then one can observe two peaks that correspond to two Barkhaussen jumps, similarly to the experiments in [82]. The domain wall can depin from the defect due to the thermal activation [83, 84]. In this case it does not propagate along the entire wire since it finally remains pinned somewhere in the middle of the wire.

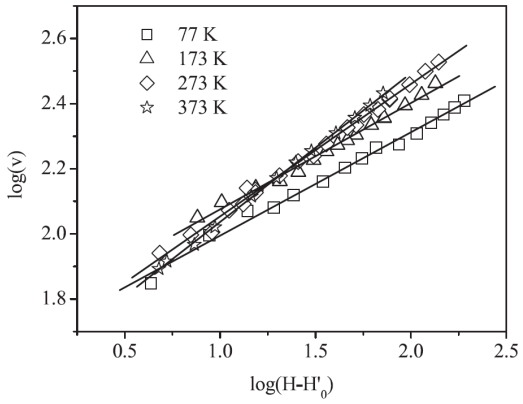

Fig. 4.15. Domain wall velocity as a function of magnetic field amplitude for a range of indicated measuring temperatures. Full lines represent the linear fit [42].

The observed nonlinear dynamics at low fields in Fig. 4.13 is not surprising. It was first calculated by Nakatani et al. for thick sub-micron strip line [85], and assumed theoretically from the measurement of Yang and Erskine [86]. We have confirmed the scaling behaviour of the single domain wall during its propagation over large distances [42], which has been taken as a manifestation of the nonlinear dynamics and criticality in complex systems [87].

The power law is universal and valid on a wide range of scales where crackling noise is detected [88,89,90,91,92,93]. The power law at low fields is confirmed also in a wide temperature range, as proved in the log-log plot in Fig. 4.15. However, the power exponent is temperature dependent (see Fig. 4.16) and increases from $\eta = 0.32$ at 77 K up to $\eta = 0.48$ at 373 K. This evolution can be treated in terms of the change of the domain wall shape. We can assume two contributions to the domain wall potential in amorphous microwires [8, 65]: firstly, the long-range magnetoelastic one that changes with temperature due to the different thermal expansion coefficient of metallic nucleus and glass coating. A short-range contribution comes from the interaction of the domain wall with the defects on the atomic level. Due to the interaction energy with local spontaneous magnetization these mobile defects try to align into the most favourable orientation. Amorphous alloys have a low packing density because of the steric misfit between atoms of different atomic radii. Therefore, even at low temperature small rearrangements of atoms are possible by jumps of atoms into the neighbouring free volumes. It was shown earlier [8,65], that structural relaxation becomes an important mechanism especially at low temperatures. When the temperature decreases, the mobile defects lose their mobility that increase the local anisotropy and the pinning of the domain wall on such defects is stronger. Hence, one possible explanation of the temperature dependence of power exponent η arises from the domain wall shape change due to pinning. At high temperatures, the long-range magnetoelastic contribution prevails, the domain wall pinning on the local defects is small (see Fig. 4.16 contributions to the switching field) and the domain wall prefers to keep a planar (rigid) shape in order to decrease the stray fields. According to the random field theory [79, 80, 81], the coefficient $\eta = 1/2$. At low temperature, the pinning forces from the randomly distributed defects are much stronger than elastic

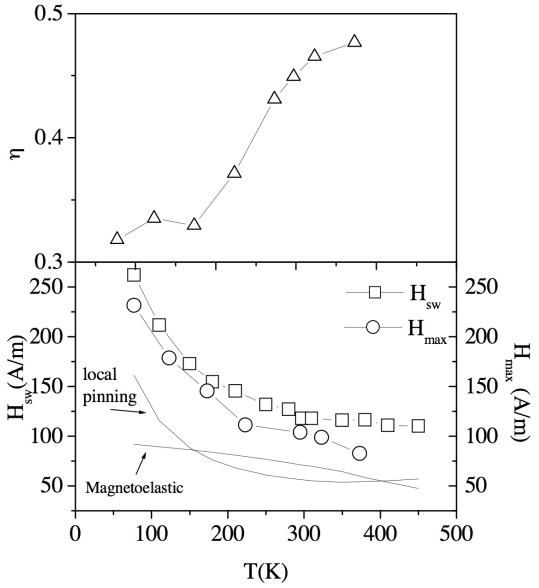

Fig. 4.16. Temperature dependence of the scaling exponent η (up). Temperature dependence of the switching field H_{sw} and its contributions taken from [64] and theoretically estimated H_{max} according to Eq. (4.11) (down). [42].

forces and the interface breaks up [80]. The domain wall motion at any point depends on its pinning on the local defects and the domain wall takes a flexible shape. This results in the decrease of the power exponent η down to 0.32 at 77 K. This value corresponds well with the random field model [80, 81]. These results are also consistent with the temperature dependence of the switching field and its contributions (see also Fig. 4.16) [64]. Moreover, such a temperature dependence of η does not occur in microwires, where the pinning contribution to the hysteresis mechanism is negligible [75]. Unfortunately, there is no direct experimental evidence for the domain wall shape change. The propagating domain wall in microwires is shielded by the radial domain structure so the direct observation of the domain wall is impossible.

Another important parameter is the effective domain wall mobility parameter S' given in Eq. (4.5). Its role is not clear and there is also speculation that the nonlinear domain wall dynamics can be treated in terms of the field dependence of the mobility parameter S', keeping the power exponent η = 1 [79]. Anyway, according to Eq. (4.5) and (4.7), the domain wall velocity can be expressed as:

$$v = \left(\frac{H - H_0'}{H_0'} \right)^{\eta} . \tag{4.8}$$

Then, the mobility parameter S' is equal to

$$S' = \frac{S^*}{(H_0')^{\eta}} . \tag{4.9}$$

The new parameter S^* is proportional to the domain wall mobility in the viscous regime S given by Eq. (3.3), where the proportionality constant, H_{max}, has the dimensions of magnetic field:

$$S^* = S.H_{max}. \tag{4.10}$$

As observed in Fig. 4.16, H_{max} takes similar values to the switching field obtained in [64]. In addition, it has the same temperature dependence, which points to the fact that both fields are governed by the same mechanism. Finally, the relation between the mobility parameter S' given by Eq. (4.5) and domain wall mobility in the viscous regime S has beenfound as:

$$S' = \frac{SH_{max}}{(H_0')^{\eta}}, \tag{4.11}$$

which supports the fact that the domain wall mobility can be taken as a constant and it is not field dependent. At least in the adiabatic and viscous regime. At higher fields, larger than the fluctuations of the wall potential, Eq. (4.5) transforms into Eq. (3.3). In this viscous regime, above H_{max}, when the wall propagates at constant velocity it is not locally pinned so it propagates in a single continuous step without interaction with local defects. Accordingly, Eq. (4.5) can be modified as:

$$v = v(H_{max}) + S(H - H_{max}). \tag{4.12}$$

An analytical description in the whole range is:

$$v = \begin{cases} 0 & \text{for} \quad H < H_0' \\ \dfrac{SH_{max}}{(H_0')^{\eta}}(H - H_0')^{\eta} & \text{for} \quad H_0' < H < H_{max} \\ v(H_{max}) + S(H - H_{max}) & \text{for} \quad H_{max} < H \end{cases} \tag{4.13}$$

Same behaviour has been confirmed by other groups that show the existence of power law for single domain wall propagation at low magnetic fields in the environment with defects. [94, 95, 96].

4.4 Fast domain wall dynamics

According to Eq. (3.3) there are only two parameters to control the domain wall velocity at a given field: domain wall mobility, S, and critical propagation field, H_0. Usualy, the increase of domain wall mobility is used to increase the domain wall velocity in magnetic material. In order to increase domain wall mobility, one must use material with high electrical resistivity and small dimensions (to decrease the eddy current damping β_e - see Eq. (3.6)), low anisotropy and Gilbert damping (to decrease the magnetic relaxation damping β_r - see Eq. (3.8)) and low structural relaxation (to decrease the structural relaxation damping β_e - see Eq. (3.9)).

Amorphous glass-coated materials are ideal material to expect the fast domain wall velocity as they have high resistivity [61], small dimensions, low Gilbert damping [97, 98, 99], low anisotropy (due to amorphous structure) and they show low structural relaxation at room temperature [8, 10].

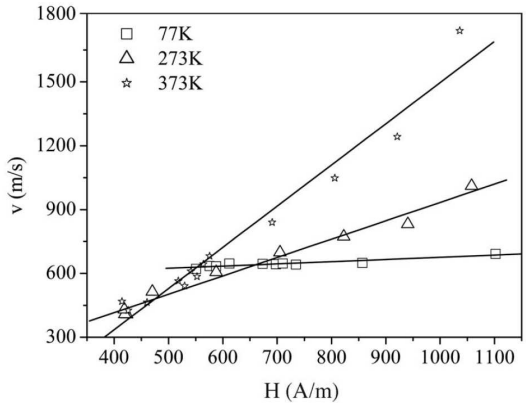

Fig. 4.17. Domain wall velocity as a function of magnetic field amplitude for various temperatures in amorphous FeCoSiB microwire. [9].

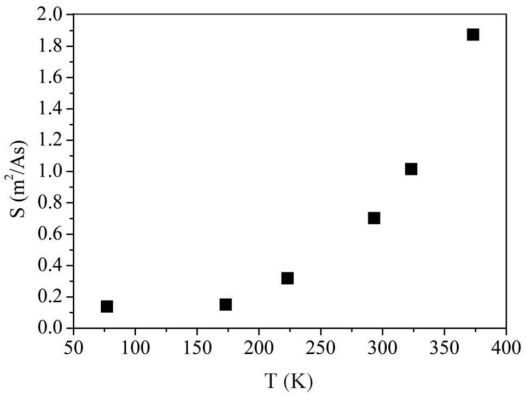

Fig. 4.18. Temperature dependence of the domain wall mobility in amorphous FeCoSiB microwire. [9].

Figure 4.17 shows the domain wall velocity v as a function of the applied magnetic field H. Domain wall velocity in microwires is very high, attaining values up to 1800 m/ s at a field of 1050 A/m and a temperature of 373 K. A key dynamic parameter for the domain wall motion is the domain wall mobility S. The average mobility in microwires (taken from the linear fit of the data in Fig. 4.17) varies with temperature from 0.14 m^2/As at 77 K up to 1.93 m^2/As at 373 K (Fig. 4.18), in contrast to the domain wall mobility for a trilayer submicron magnetic wire, which was constant [100]. The value of S at 373 K is a factor of 5 higher than that reported for Permalloy nanowires in [101]. On the other hand, the mobility at low temperature (77 K) is almost zero. Nevertheless, the velocity remains relatively high (over 600 m/s) over the whole range of applied field investigated.

Apart from low anisotropy and low Gilbert damping, two more mechanisms that are respon-

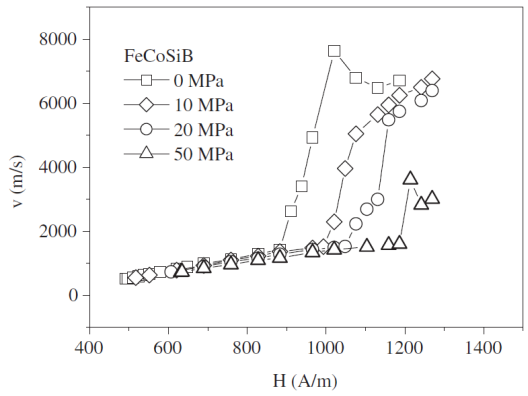

Fig. 4.19. Domain wall velocity v as a function of the magnetic field amplitude H for FeCoSiB microwire with the applied tensile stress as a parameter. [5].

sible for fast domain wall propagation in glass-coated microwires have been recognized [5, 9]. Firstly, it is the existence of a complex domain structure. We can assume that the propagating closure domain wall does not interact with any surface irregularities because it is shielded by the external radial domain structure. Therefore, the strong damping that would arise from the pinning of the propagating domain wall within the inner axially magnetized core on such surface irregularities can be neglected. Another possible mechanism, which could result in very rapid domain wall movement, might arise from the external domain structure having a radial magnetization vector (see Fig. 2.4). It has been shown that introduction of defects below the surface would result in an increase of the domain wall velocity [47]. The external domain structure could play the role of such defects, giving rise to an increase in the domain wall velocity. Moreover, radial structure introduced on the surface of axial domain produces magnetostatic interactions that hinders the appearence of the Walker limit and allows the domain wall to increase its velocity over Walker limit [102].

However, fast domain wall propagation has been observed even in microwires with relatively high magnetic anisotropy [5, 9]. Hence, another mechanism must be taken into account to be responsible for fast domain wall propagation. It is the existence of two, perpendicular anisotropies that are present in the metallic nucleus. As given above, the domain structure of bistable microwire is a result of energetic equilibrium of magnetoelastic anisotropies. Radial just below the surface and axial in the center of metallic nucleus. The presence of two perpendicular anisotropies results in averaging out of total effective anisotropy acting in the center of the wire. As a result, the domain wall moves very fast (Fig. 4.19).

Observed domain wall propagation exceeds the sound velocity ($\sim$4500 m/s) measured in similar magnetic microwires [103]. However, the domain wall dynamics is not linear like given by Eq. (3.3). Instead, two linear dependencies are found. One possible explanation for the slope change could be attributed to the change of the domain wall structure. It was shown by micromagnetic simulations that the vortex-type domain wall is faster than transversal one [104, 105].1 The transversal domain wall creates the surface stray field that interacts with the radial

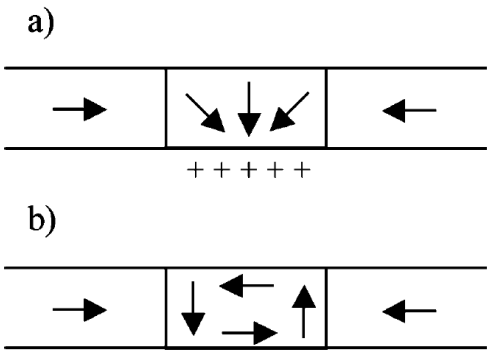

Fig. 4.20. Schematic structure of different 180° domain wall configuration in thin magnetic wires. (a) Transversal, (b) Vortex [110].

domain structure (Fig. 4.20). The vortex-type domain wall does not create surface stray fields. Therefore, it does not interact with the radial domain structure and the movement is faster. On the other hand, it has complicated structure with higher exchange energy. Therefore, the vortex domain wall is more preferable for the case of thick magnetic wires than the transversal one [104]. At low fields, a transversal-type domain wall structure should be expected due to the axial and radial anisotropies present in the microwire. Increasing the axial field leads to the increase of the diameter of the internal single domain. Moreover, the rise time of the applied square magnetic field is very short and the change of the field is abrupt. Therefore, instead of depinning of the closure domain wall, the nucleation of a reversed domain could occur. This fact is supported by the change of the critical propagation field H_0, which is much higher for the vortex structure. Vortex-type domain wall should now be expected, since the velocity of the domain increases steeply. As the micromagnetic simulations show [104], once the wall is nucleated into a certain structure, its structure remains the same during wall motion. However, we have no direct evidence for the domain wall structure change.

The maximum domain wall velocity is fixed by the restoring forces that oppose precession inside the domain wall (Walker model [46]). Thus, it could be increased by adding an anisotropy with transverse easy axis. Theoretically, the domain wall velocities can reach up to 1000 m/s [47, 106, 107]. However, domain wall velocities up to 2000 m/s are experimentally observed [101, 5, 9]. The main problem of the micromagnetic simulations in [104, 105, 106, 107] is that they do not take into account the anisotropy. It was shown that the domain wall velocity increases with the presence of the transversal anisotropies [35,46]. Glass-coated microwires exhibit strong radial anisotropy arising from the stresses induced by the glass-coating through the difference in the thermal expansion coefficients of the metallic nucleus and the glass-coating. In the case when both anisotropies (axial as well as transversal) are compensated, the restoring force that opposes precession inside the DW is minimum. This happens just at the boundary in between the axial and radial domain structures. Therefore, the critical Walker field H_w at which the maximum velocity appears is enhanced by the presence of radial anisotropy ($H_w = (\alpha_G H_k/\mu_0 M_s$, where

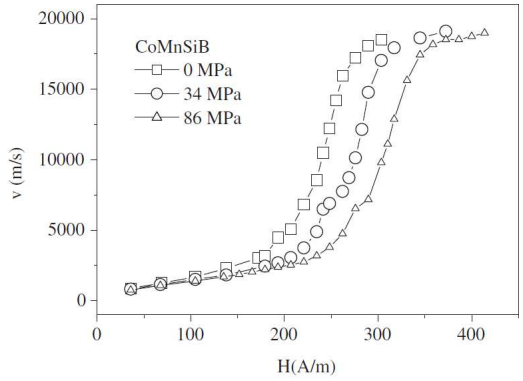

Fig. 4.21. Domain wall velocity v as a function of the magnetic field amplitude H for CoMnSiB microwire with the applied tensile stress as a parameter [5].

α_G is the Gilbert damping, H_k is the transversal anisotropy field).

The effect of the stress-induced anisotropy on the domain wall propagation is shown by applying a tensile stress on the microwire (Fig. 4.19). The threshold field associated with the nucleation of the vortex domain wall increases as a result of the nucleation field increase. At the same time, the velocity at which the type of the domain wall changes remains roughly the same for all applied stresses. The application of a tensile stress increases the domain wall damping and therefore the domain wall velocity decreases. Although such an effect is not very clear at low fields, maximum is not observed at high fields, where the maximum velocity is expected. We assume that to obtain high velocity of the domain wall, strong anisotropy is needed, but in opposition, strong transversal anisotropy results in an increase of the domain wall damping and the decrease of the domain wall velocities.

As a result of their amorphous nature, the glass-coated microwires have high resistivities. Therefore, the eddy current damping is very low in these materials [8]. The most important damping mechanism in glass-coated microwires at room temperature was found to arise from spin relaxation. It was shown in [8] that damping contribution coming from the spin relaxation,β_r is proportional to the square root of the anisotropy [8, 108]. In the case of amorphous glass coated microwire, the anisotropy is determined mainly by the magnetoelastic interaction of the local magnetic moments with the stresses, σ, introduced during the microwires preparation (see Eq. (3.8)). In contrast to the FeCoSiB microwire in Fig. 4.19, the microwire with nominal composition $Co_{68}Mn_7Si_{10}B_{15}$ is characterized by the lowest possible magnetoelastic anisotropy (due to its low magnetostriction λ_s [109]) among the microwires with single domain axial structure. In fact, it has ten times smaller magnetoelastic anisotropy in comparison to the FeCoSiB microwire and therefore extremely small domain wall damping. Anyway, the stresses applied on the metallic nucleus are of the same directions like in the FeCoSiB microwire and it presents the same domain structure. As a result of the small damping, the domain wall mobility is extremely high (16 m^2/As at low fields) and it reaches the maximum value of 272 m^2/As at the field of 255 A/m (Fig. 4.21). Although the Walker field is small ($\sim$ 300 A/m), the maximum velocity

reaches a value of 18 500 m/ s. Such fast domain wall velocity is dificult to model. We think that the maximum velocity is given not only by the transversal anisotropy but mainly by the high mobility as well as by the counterbalance between the uniaxial and transversal anisotropy [31].

Application of a tensile stress shifts the Walker fields to higher values, but the effect on the maximum velocity is not so strong as in the case of FeCoSiB microwire. It is believed that this behavior is as a consequence of small magnetoelastic anisotropy (depending on the small magnetostriction $\lambda_s \sim 10^7$).

The extremly low anisotropy is not the only parameter to obtain fast domain wall propagation. High domain wall velocities can be observed also in relatively high magnetostrictive microwire (like FeNiSiB [110]). Moreover, the new effect arises in the domain wall propagation when the domain wall approaches the sound speed limit. Since the amorphous bistable microwires are highly (with respect to soft magnetic materials) magnetostrictive, the domain wall produces an elastic wave when it propagates. Such a wave always accompanies the propagating domain wall in magnetostrictive materials. Elastic waves in magnetic microwires are very fast. ($\sim$ 4700 m/s [103, 111].) They disappear much faster then domain wall propagation. However, when the domain wall approaches the sound speed limit, the dissipation in the elastic subsystem of a microwire grows substantially and the domain wall transfers part of its magnetic energy to the elastic subsystem [112]. As a result, the domain wall velocity remains constant. The magnetic energy transferred to the elastic subsystem can be calculated from the constant part of the domain wall velocity dependence [113]:

$$E = 2\mu_0 M_s \Delta H, \tag{4.14}$$

where ΔH is the width of the constant part in dependence. The transferred magnetic energy increases the amplitude of the elastic waves until the elastic waves damping becomes equal to $2\mu_0 M_s \Delta H$. Finally, the domain wall exceeds the sound speed when the driving field became greater than the force of dynamic breaking of the domain wall by the elastic waves. Then, domain wall velocity jumps steeply to higher values. Such an effect is already well known in ferrites [112, 113, 114] that have much smaller magnetization compared to the amorphous Fe-based microwires.

Generally, the sound velocity s in solids is given by:

$$s = \sqrt{\frac{E_Y}{\omega}}, \tag{4.15}$$

where E_Y is the Young modulus and ω is mass density. In solids, there is a non-zero stiffness for volumetric and shear deformations. Hence, it is possible to generate sound waves with different velocities depending on the deformation mode.

In amorphous FeNiSiB microwire, the interaction of the domain wall with the elastic waves appears three times at the velocities of 3130, 4070, and 5430 m/s, respectively (Fig. 4.22). These velocities correspond well to the sound velocitiy obtained for Fe-based microwires (4700 m/s [103]) or the sound velocity for crystalline iron (5100 m/s). The existence of three sound velocities can be treated in terms of different sound waves that can be created in a finite solid body. For example, three phonon waves were measured in a stainless-steel rod [115]: 1) longitudinal, 2) transversal, and 3) extensional one (see Table 4.1). The values measured for microwires correspond almost perfectly to the longitudinal (5790 m/s) and transversal (3100 m/s) phonon

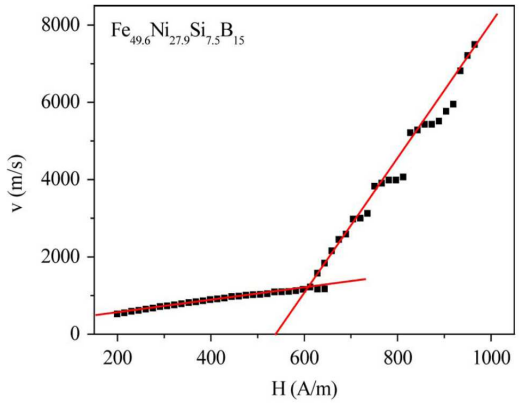

Fig. 4.22. Domain wall velocity v as a function of the magnetic field amplitude H for FeNiSiB microwire [110].

wave. However, sound speed (4070 m/s) either does not represent the extensional wave or one should take into account the stress applied by the glass coating as well as different dimensions of the microwires in order to explain discrepancies. Similar values were obtained for whole series of $Fe_{77.5-x}Ni_xSiB$ microwires.

The effect of the domain wall interaction with the phonons is undesired due to its power consumption. On the other hand, it can be used to synchronize the multi-domain wall movement in some devices, such as race-track memories [1] or domain wall logic [2].

Tab. 4.1. Sound velocities as measured for stainless steel and amorphous FeNiSiB microwire [110].

phonon wave	longitudinal v(m/s)	transversal v(m/s)	Extensional v(m/s)
Stainless steel [115]	5790	3100	5000
FeNiSiB microwire	5430	3130	4070

4.5 Effect of transversal field

As it has been shown previously, the application of a transverse field in addition to the longitudinal driving field can modify the speed of a domain wall [116, 117, 118, 119]. Kunz and Reiff in [119] have shown via micromagnetic simulations that a transverse field, H_t, oriented parallel (antiparallel) to the core magnetic moments within a transverse domain wall could increase (decrease) the domain wall velocity below the Walker limit, while no effect was found above that limit. In turn, micromagnetic simulations by Bryan et al. [120] have demonstrated that beyond the Walker limit, a strong transverse field H_t could increase the domain wall velocity. In addition, Bryan et al. reported a dependence of the Walker field, H_w, on the polarity of the transverse

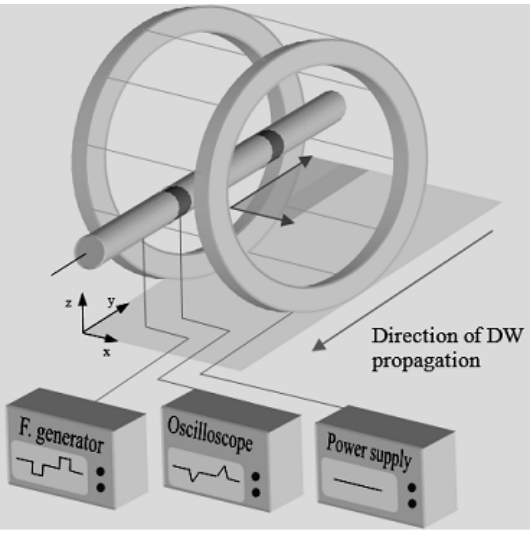

Fig. 4.23. Schematic picture of Sixtus-Tonks apparatus for maesuring the domain wall velocity in perpendicular field [121].

field, H_t. For alignment of transverse field parallel or antiparallel to the core magnetic moments within the transverse domain wall, they observed a small increase or decrease in H_w, respectively. The total suppression of the Walker breakdown process was deduced in micromagnetic simulations when an out-of-plane transverse field was applied.

In all cases, the changes in the domain wall velocity, v, under the influence of a transverse field have been explained taking into account the two following mechanisms [119, 120]: i) the presence of a transverse field modifies the angular distribution of magnetic moments within the wall, changing its width and consequently, the domain wall velocity. ii) The presence of a transverse magnetic field rotates the magnetic moments within the domains adjacent to the wall, which reduces the domain wall angle. According to the model of Sobolev et al. [117], the speed of domain wall is also a function of the domain wall angle, hence the change of domain wall speed in transverse field could be assisted by changing the domain wall angle. Nevertheless, Glathe et al. [120] have experimentally shown that the transverse field speeds the domain wall velocity up to 5 km/s, around four times the maximum velocity obtained in the same material without transverse field. Such a large increase in velocity cannot be explained considering the two mechanisms mentioned above.

Amorphous microwires are ideal material to study the single domain wall propagation at different external conditions. Hence, it is easy to improve the Sixtus -Tonks system for measuring the domain wall dynamics under the influence of transversal magnetic field (see Fig. 4.23).

The dependence of the domain wall velocity on the axial driven magnetic field having constant transverse field as a parameter is shown in Fig. 4.24 [7]. Here two regimes are clearly identified as they were described before. The low-field regime is characterized by reduced domain wall mobility and a negative critical field, while at higher field the mobility takes higher

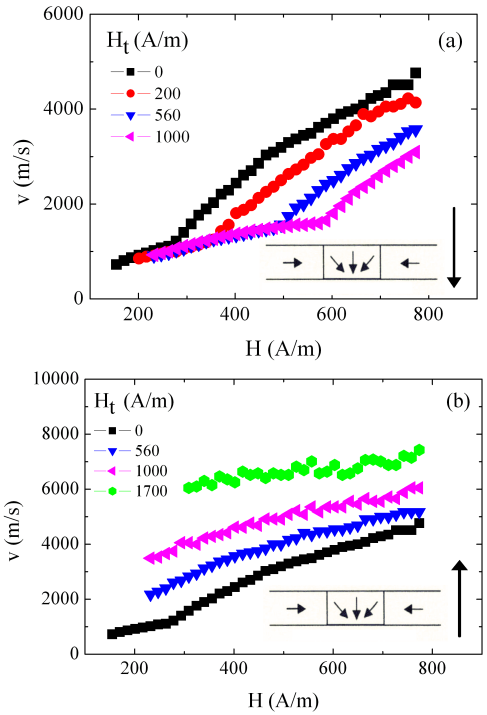

Fig. 4.24. Dependence of the domain wall velocity v on the driving magnetic field H when weak transverse fields H_t are applied along opposite directions. Schematics of the transverse domain wall (in the lowfield regime) and transverse field (denoted by downwards (a) and upwards (b) arrows) are included [7].

values and the critical field is positive. The two linear regimes of the domain wall motion corresponds to two different domain wall structures. The maximum velocity of steady state motion of a transverse domain wall is defined as a Walker velocity, v_w. Below the Walker velocity, the domain wall dynamic follows a linear regime and propagates as a rigid plane along the microwire, while beyond this limit, vortex type domain wall is nucleated.

The application of a transverse field, H_t, gives rise to two different situations, depending on its sign and magnitude. For a given value of the driving field, the wall velocity decreases or increases depending on the direction of H_t, as can be observed in Figs. 4.24(a) and (b), respectively. When the transverse field is applied in a given direction (Fig. 4.24(a), the Walker field, H_w, increases from 300 A/m to the almost its double value of 560 A/m under 1000 A/m transverse field. The shift in the Walker limit shown in Fig. 4.24(a) indicates that the presence of transverse fields reinforces the stability of the transverse domain configuration and enables an increase in the domain wall velocity to much higher values. This conclusion is relevant for spintronic devices based on transverse domain wall motion, for increasing its speed rate by placing

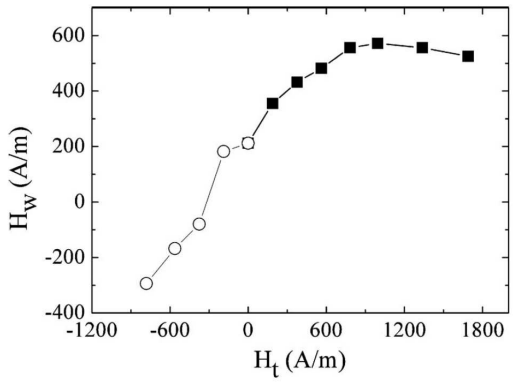

Fig. 4.25. Walker field, H_w, as a function of applied transverse field H_t. Full rectangles correspond to H_w determined from Fig. 4.24(a), while open circles correspond to H_w determined by extrapolation of data from Fig. 4.24(b) (the Walker field was not directly observed in that case) [7].

them under a transverse field. However, the domain wall mobility S changes very weakly (if any) in this regime of relatively weak transverse fields. Hence, this effect cannot be described properly in terms of changes of the domain wall width, δ_s, which is directly proportional to the mobility. In turn, a transverse field of equal strength but opposite sign leads to destabilization of transverse domain wall and vortex domain wall configuration alone is observed. Here, the transverse field induces a decrease in the Walker field, H_w, as shown in Fig. 4.24(b). This interesting result could be explained in terms of micromagnetic simulations [120] that indicate how even a weak applied transverse field is able to substantially modify the Walker field, H_w, depending on the relative orientation of transverse field to the core magnetization within the transverse domain wall. When transverse field is parallel oriented to the core magnetization within the transverse domain wall (Fig. 4.24(a)), the change from transverse to vortex domain wall occurs at higher fields. In this case, the transverse field favors transverse domain wall. Alternatively, when the transverse field is oriented antiparallel to the core magnetization within the transverse domain wall, it leads to destabilization of transverse domain wall.

The evolution of the Walker field, H_w, with the amplitude of the applied transverse field is shown in Fig. 4.25. A nearly linear behavior is observed (at least within the field range from -1000 to 1000 A/m) as it was suggested theoretically [35].

The asymmetrical effect of transversal field on the domain wall dynamics can be easily understood in planar nanowires [35], however it is difficult to understand it in case of microwires with circular cross-section. One explanation is offered when we returns to the method of preparation. Microwires are prepared by drawing and rapid quenching of molten master alloy. Quenching is provided by a water jet from one side. Hence, they are not quenched symmetrically from whole surface to the center. Instead a stress distribution is induced that arises from single point into the whole Section of microwire. One example of such stress distribution is provided in Fig. 4.26. The crystalline microwire of NiMnInCo prepared by Taylor Ulitovski method shows inhomogeneous distribution of crystallites that has grown up according to the stress distribution in the

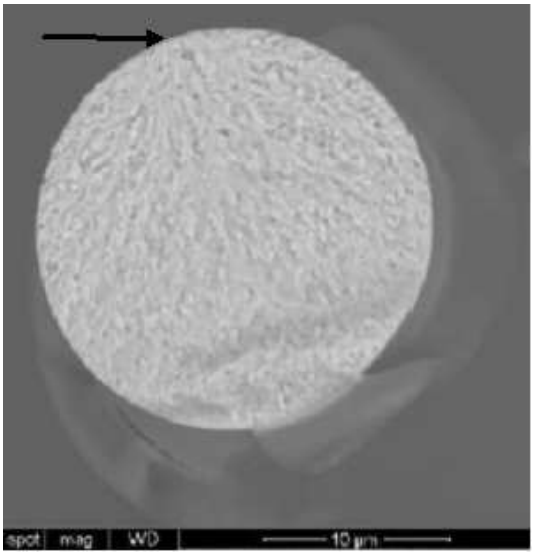

Fig. 4.26. SEM picture of cross-section of crystalline glass-coated microwire shows asymmetrical distribution of the stresses introduced by rapid quenching.

metallic nucleus. The crystalls starts to grow from a single point (shown by arrow) where water jet touch the surface of microwire. Than they continue to grow in all direction untill they reach the surface of metallic nucleus. Such asymmetry surely brings asymmetry in the domain wall structure and finally the transversal domain wall is also asymetrical with respect to the wire's axis. Such a behaviour can be used to controll and store magnetic domain walls in spintronic devices, where propagation of multiple domain walls in the same direction is not driven by current, but by combination of transversal and axial magnetic fields [122, 123].

The dependence of the domain wall velocity on axial magnetic field when a high transverse fields is applied, is shown in Figs. 4.27(a) and (b). Here, the transverse field produces an increase in the domain wall velocity irrespective of the transverse field orientation, and the vortex domain wall structure configuration is stabilized, contrary to the transverse wall regime. In addition, increasing the transverse field reduces steeply the domain wall mobility, and increases the amplitude of the critical propagation field, H_0, which remains at negative values. At the highest transverse fields of around H_t =2700 A/m, the wall mobility almost vanishes while the wall velocity approaches its limit of 9 km/s. One possible explanation can be found in terms of the domain wall width compression. It was shown [30] that when the domain wall approaches the critical velocity v_c given by:

$$v_c = \sqrt{2Q}v_w, \tag{4.16}$$

it starts to reduce its width significantly, proportionally to the actual velocity. The compressed

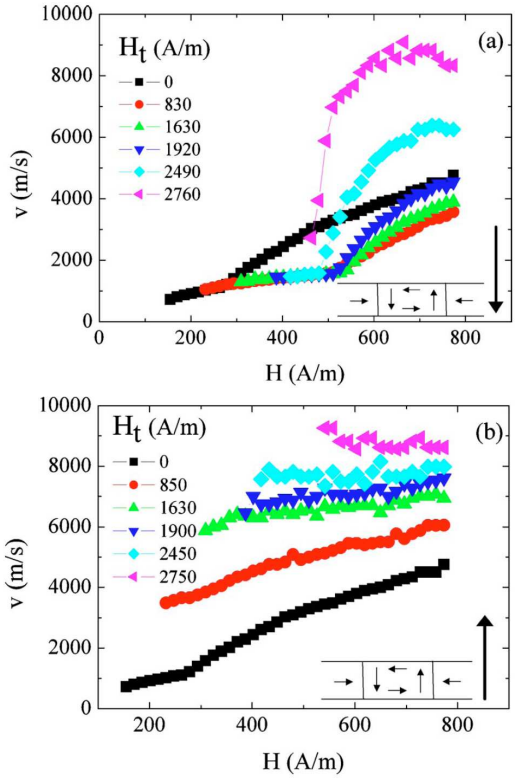

Fig. 4.27. Dependence of the domain wall velocity on driving magnetic field when strong transverse field is applied in first (a) and second (b) direction with respect to the axis of microwire. Strong transverse field leads to saturation of domain wall velocity up to value of about 9 km/s and zero domain wall mobility independently on orientation of strong transverse field with respect to the microwire [7].

domain wall width δ_s' is given:

$$\delta_s' = \frac{\delta_s}{(1+\frac{v^2}{2Qv_w^2})^2}, \tag{4.17}$$

where $Q = K/(2\mu_0 M_s^2)$ is the quality factor, which characterizes the strength of uniaxial anisotropy (in our case Q <1) and δ_s is the domain wall width at the zero velocity. As the domain wall mobility S is proportional to the domain wall width, Eq. (3.3) can be rewritten as:

$$v = S(H-H_0) = \frac{S}{(1+\frac{v^2}{2Qv_w^2})^2}(H-H_0). \tag{4.18}$$

This result is very interesting, since it indicates that under given conditions of transverse applied field the domain wall velocity does not depend on the driving axial magnetic field. It can

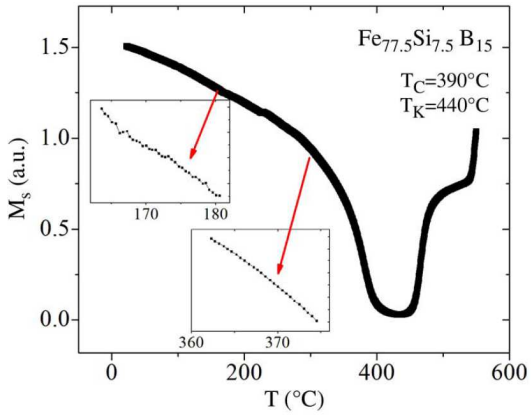

Fig. 4.28. Saturation magnetization as a function of temperature for FeSiB microwire. Insets show discontinuity of measured data at two temperatures, which is connected to the relaxation of internal residual stresses [125].

be used in applications where domain walls with well-defined velocity are needed (race track memory and domain wall logic). However, it needs more experiments to clarify the reason for extremly high domain wall velocity at low domain wall mobility.

4.6 Thermal treatment

As a result of their preparation, strong stresses are introduced into the amorphous glass-coated microwires by rapid quenching and drawing. These stresses increase the overall anisotropy of metallic nucleus and strongly affect the domain wall dynamics. Hence, it is desirable to control the stress distribution somehow. One possibility is to remove the stresses by thermal treatment. However, the first attempt was not very succesfull [40]. On the other hand we have shown [124] that it is possible to affect the domain wall dynamics by thermal treatment but the temperature must be selected carefully.

In order to estimate a proper annealing temperature, the temperature dependence of saturation magnetization has been measured (Fig. 4.28) [125]. At low temperature (below 200°C), the magnetization curve is characterized by intermittent course due to a relief of the stress introduced by microwire's production (see inset of Fig. 4.28). Such process is already completed at 300°C where magnetization shows continuous course because mechanical stresses are already relaxed during thermal treatment. The Curie temperature is 390°C and crystallization of FeSi crystalline phase appears at 440°C. To confirm the stress relaxation we have checked the domain wall dynamics for both annealing temperatures 200 and 300 °C.

Using the annealing at 200°C for 1 hour bring very small effect on the domain wall dynamics (Fig. 4.29). It does not change neither the critical field nor domain wall velocity. This is in a good agreement with previous attempts [40], where annealing of FeSiB wires at 200°C caused only 10% increase of domain wall velocity. Annealing at this temperature leads to the reversible

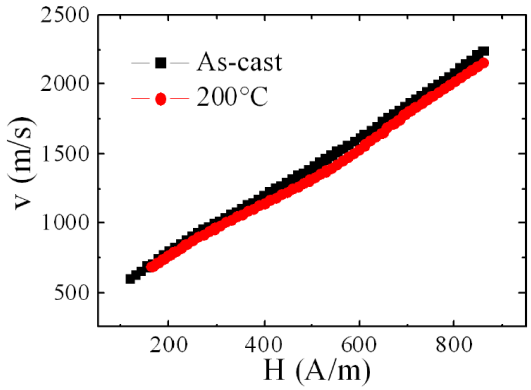

Fig. 4.29. The dependence of the domain wall velocity on driving field before and after thermal treatment at 200°C for FeSiB microwire [124].

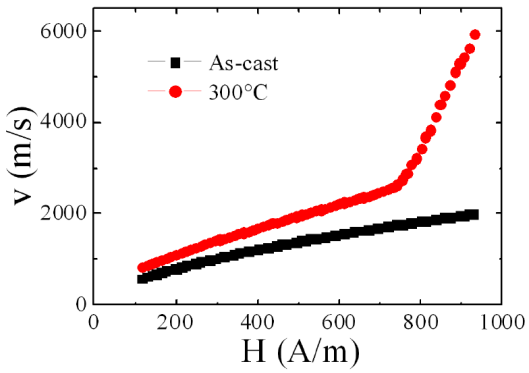

Fig. 4.30. The dependence of the domain wall velocity on driving field before and after thermal treatment at 300°C for FeSiB microwire [124].

structure changes only. Such result has been obtained in several measurements of amorphous FeSiB alloys, where annealing at 200°C did not change its magnetic properties in comparison to the as-cast state [126].

In contrary to the annealing at 200°C, annealing at the higher temperature 300°C leads to the two significant effects (Fig. 4.30): i) remarkable increase of domain wall mobility of primary regime and ii) introduction of a new, secondary regime (with positive critical field). The increase of domain wall mobility is caused by decrease of magnetic relaxation damping (caused by relaxation of internal stresses) and by decrease of structure relaxation damping (caused by annealing out of free volumes). It has been shown previously that regime with positive critical field is caused by change of the internal domain wall structure from the transversal to the vortex

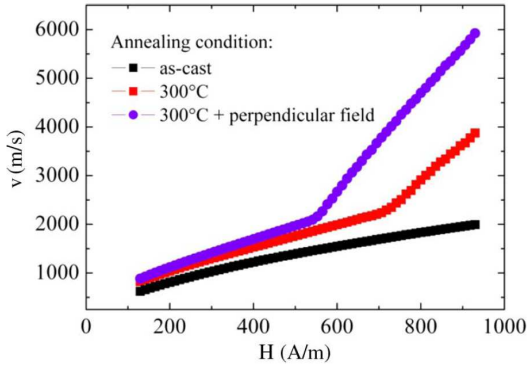

Fig. 4.31. The dependence of the domain wall velocity on driving field before and after thermal treatment at 300°C with and without perpendicular magnetic field of 1 T for FeSiB microwire [125].

one. On contrary to the transversal domain wall, the structure of the vortex domain wall contains higher amount of magnetic moments oriented out of easy axis. Hence, the magnetoelastic part of the total domain wall energy is more important in the vortex domain wall in comparison to the transversal one [105]. Since the thermal treatment at 300°C decreases the residual internal stresses, the magnetoelastic part of the energy of the domain wall then also decreases, which allows to form the vortex domain wall, even in the wire, where the vortex domain wall has not been present before thermal treatment.

However, low anisotropy is not necessary condition for fast domain wall velocities. As it was shown above, application of perpendicular magnetic field can increase the domain wall velocity significantly. Perpendicular magnetic field can even be induced by magnetic annealing. Such annealing is particularly succesful in the case of amorphous materials where strong pair ordering appears when the are annealed under proper conditions [127].

In order to underline the importance of two perpendicular anisotropies in microwires on mediating the fast domain wall dynamics, the domain wall velocity was also measured in the wires annealed in strong perpendicular field of 1 T [125]. Samples were annealed separately with and without presence of perpendicular magnetic field. Then, the domain wall dynamics in both wires were compared to the domain wall dynamics in as-cast state. As it is shown in Fig. 4.31, annealing in perpendicular field leads to the slight increase of domain wall mobility similarly to the annealing without perpendicular field. The domain wall mobility has increased from 2.5 m^2/As to 2.7 m^2/As for transversal domain wall, whereas for vortex domain wall the increase from 10 m^2/As to 10.2 m^2/As was observed. However, more remarkable effect of annealing in perpendicular field is shift of the transition field at which the internal domain wall structure changes from transversal to vortex one. Induced perpendicular anisotropy enhances multi-axis structure of the domain wall and magnetoelastic part of the vortex domain wall energy decreases. As a result, vortex domain wall could appear at lower field. This is in good agreement with the previous measurements of domain wall dynamics, where transition field was shifted by perpendicular field, too [7]. As it is seen in Fig. 4.31, effect of induced perpendicular anisotropy speeded up do-

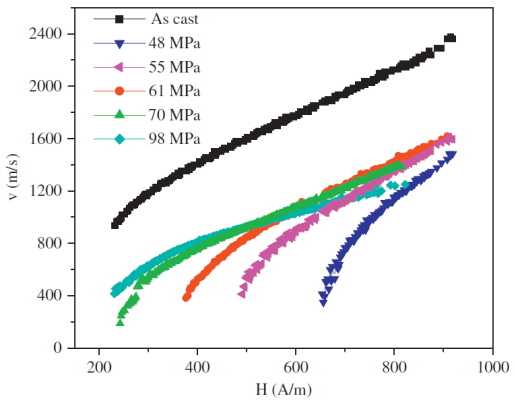

Fig. 4.32. Dependence of the domain wall velocity on the applied magnetic field for as-cast FeSiB microwire as well as for wire annealed at 300°C for 1 hour under the axial stress of 77 MPa [128].

main wall velocity by factor of 2 (from 3.5 km/s to 6 km/s) in comparison to microwire annealed without perpendicular field. It points out, that perpendicular anisotropy inside the microwires plays very important role in mediating fast domain wall dynamics. Especially, this is important for microwires, where two perpendicular anisotropies are always present.

As shown above, higher annealing temperature increases possibility to release the stress introduced by production as well as to induce anisotropy. However, even though annealing at 400°C releases the stress applied on metallic nucleus of microwire, another stress is introduced when cooling down to room temperature because of different thermal expansion coefficient of glass-coating and metallic part. Moreover, annealing above the Curie temperature (390°C in this case; see Fig. 4.28) hinders the possibility to induce anisotropy by magnetic annealing.

Finally, the annealing temperature 300°C appears to be the optimum to release the stress significantly as well as to induce proper magnetic anisotropy.

Due to their amorphous nature, the magnetic properties of glass-coated microwires are governed mainly by the magnetoelastic anisotropy. Naturally, the stress annealing should affect strongly the domain wall dynamics, too. Figure 4.32 shows the effect of annealing the glass-coated FeSiB microwire for 1 h at the temperature 300°C under the mechanical stress of 77 MPa applied axially [128]. After such annealing, the microwires loose its bistability. In order to obtain the bistable structure, axial texsile stresses of 48 MPa must be applied. However, the domain wall velocity decreases comparing to the as-cast state and the critical field increases. On the other hand, the domain wall mobility increases almost twice to 3.16 m^2/As (comparing to that of as-cast state 1.76 m^2/As). Further application of axial stress increases the domain wall velocity although the domain wall mobility decreases. It is because of the decrease of the critical propagation field H_0 (as given by Eq. (3.3)).

Another possibility to tailor the domain wall dynamics is to introduce circular anisotropy. This can be provided by current annealing. Figure 4.33 shows the domain wall dynamics of FeCoMoB microwires in as-cast state, after annealing for 1 h at 450°C and after current annealing

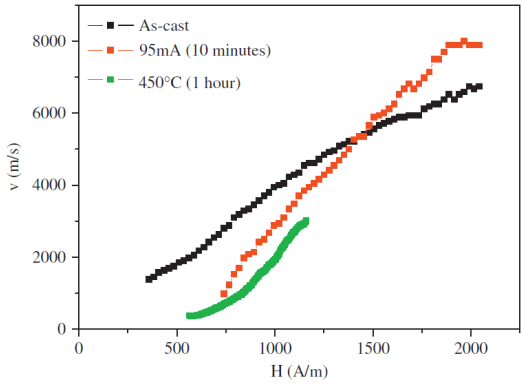

Fig. 4.33. Dependence of the domain wall velocity on the applied magnetic field for as-cast FeCoMoB microwire as well as for wire annealed for 1 h at 450°C and annealed for 10 min at 95 mA in order to get nanocrystalline state [128].

for 10 min by a current of 95 mA. As-cast FeCoMoB microwire shows very fast domain wall that can reach velocities above 6000 m/s. Annealing of the microwire at 450°C leads to the appearance of nanocrystalline state [129]. In such case, the microwire consists of crystalline grains of diameter $\sim$ 12 nm [130] oriented randomly. Such structure is characterized by a very stable domain wall dynamics in a quite wide range of temperature [73]. On the other hand, high stability is paid by lower domain wall velocity. However, when the nanocrystalline state is obtained by a currrent annealing, (that produces simultaneously the circular magnetic field during annealing), the domain wall velocity increases up to 8000 m/s. This is because the circular anisotropy introduced by current annealing favours the appearance of the vortex domain wall structure that was shown to be able to reach very high domain wall velocities.

4.7 Nanocrystalline microwires

4.7.1 Structure of nanocrystalline materials

High domain wall velocities in magnetic materials are usually paid by low time or temperature stability of domain wall dynamics. It is because in order to obtain high mobility, low anisotropy is required. Hence, even small variations of anisotropy results in high variations of domain wall mobility [131, 132]. As it was shown above, also amorphous glass coated microwires shows very low anisotropy and hence high domain wall velocity. However, their temperature and time stability is very poor [8, 9, 10]. On the other hand, some crystalline materials shows excellent stability of domain wll mobility, but the magnitude of mobility is by orders lower [100].

The solution is offered in terms of nanocrystalline soft magnetic materials. They are composite materials that consist of nano-crystalline grains (of diameter $\sim$ 10nm) randomly embedded in amorphous matrix. Random orientation of crystalline grains, together with their small dimansions - lower than exchange length, results in exchange coupling between the crystalline grains and in averaging out of effective crystalline anisotropy [133, 134]. They were discovered in

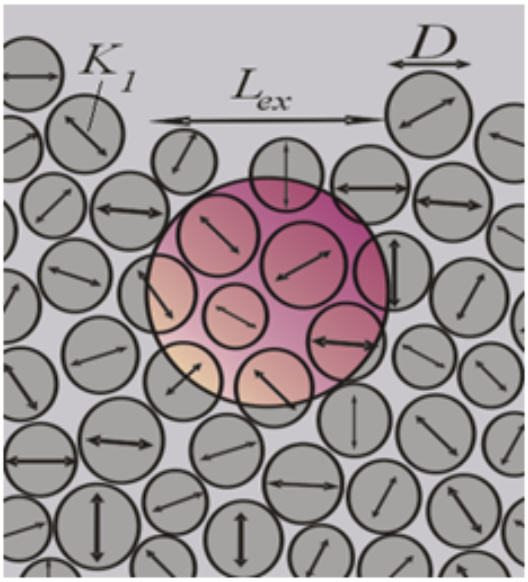

Fig. 4.34. Schematic picture of nanocrystalline structure that consists of randomly oriented crystalline grains embedded into amorphous matrix

1988 [135, 136] and shortly after their discovery they attract attention of many scientists since they combine high saturation magnetization and high structural stability of crystalline materials with low anisotropy of amorphous samples [137, 138, 139] .

4.7.2 Magnetic properties of nanocrystalline materials

Excellent soft magnetic properties of nanocrystalline materials are given by low dimension of nanocrystalline grains that is lower than exchange length, L_{ex} as well as by their random orientation (see Fig. 4.34). The disadvantage of crystalline materials is their strong magnetocrystalline anisotropy that is quantified by the anisotropy constant K_1. The problem is solved by random orientation of crystalline grains in nanocrystalline materials the effect that results in the averaging out of magnetocrystalline anisotropy in a bulk [133]. Hence, the overall effective anisotropy $\langle K \rangle$ of magnetocrystalline materials is given by the 6th power of the grains diameter, D [134, 140]:

$$\langle K^6 \rangle \sim \frac{K_1^4}{A^3} D^6 \tag{4.19}$$

However, such condition is only fullfiled when the diameter of grains, D, is lower than exchange length L_{ex} (see Fig. 4.34). Finally, the magnetization direction will not be given by the crystallographic axis, but by exchange interaction of the ferromagnetic grains [134, 140]. Similarly as in the case of anisotropy, the coercivity H_c and initial susceptibility $\chi_i$will depend on the sixth

power of crystalline grains diameter, D:

$$H_c = p_c \frac{\langle K^6 \rangle}{\mu_0 M_s} \sim p_c \frac{K_1^4 D^6}{\mu_0 M_s A^3} \tag{4.20}$$

$$\chi_i = p_u \frac{\mu_0 M_s^2}{\langle K^6 \rangle} \sim p_c \frac{\mu_0 M_s^2 A^3}{K_1^4 D^6} \tag{4.21}$$

where p_c and p_u are material constants. As given in Eq. (4.20) and (4.21), there is a strong dependence of coercivity and initial susceptibility on the crystalline grains diameter. This simple model describes well the most of the magnetic properties of nanocrystalline materials. However, if one want to study them in details, magnetoelastic interaction must be taken into account that arises from magnetoelastic interaction of magnetic moments and stresses introduced by production of amorphous precursors and by subsequent annealing process. In such case, induced anisotropy, K_u, is higher than effective anisotropy given by Eq. (4.19) and coercive force is given by the third power of the crystalline grains [141, 142]:

$$H_c \sim D^3 \tag{4.22}$$

This is also the case of glass-coated microwires, in which the strong stresses introduced by production and by glass-coating cannot be ommited.

4.7.3 Chemical composition of nanocrystalline materials

In order to obtain nanocrystalline structure, one must carefully select the chemical composition. Usually, the nanocrystaline materials are prepared by controlled thermal treatment of amorphous precursor. This condition defined also the first nanocrystalline material FINEMET, having a chemical composition $Fe_{73.5}Si_{13.5}Cu_1Nb_3B_9$ [135]. Each element plays it's role in the production: boron and silicon is neccesary to obtain amorphous structure of precursor since it hinders the crystallization of Fe crystalls. It is possible to replace boron by phosphor or carbon [143]. In addition, Fe and Si crystallizes into bcc Fe_3Si crystalline phase that is characterized by high saturation magnetization. Copper is introduced to increase the number of nucleations centers for crystalline grain in order to get fine crystalline structure [144, 145]. Niobium hinders the grain growth since it cannot fit into the Fe_3Si phase due to its size [145, 146].

According to the above described model, nanocrystalline materials consists of at least four elements $XYWZ$, where X is ferromagnetic element (Fe, Co, Ni) or their alloys, Y belongs to Noble metals (Cu, Ag, Au), W is $4d$ or $5d$ transition metals from the group IV-VIB (Zirconium, Niobium, Hafnium, Tantalum, Molybdenum,...) and Z is metalloid neccessary for amorphous precursor preparation (B, P, C, N). It is possible to improve slightly the soft magnetic properties of FINEMET-based nanocrystalline materials by partial substitution of Fe for $3d$ of $4f$ elements like Ni [147], Cr [148, 149], Pr [150] , Al [151], etc...

Another advantage of FINEMET-based nanocrystalline materials is their low effective magnetostriction. It is given by averaging out of the positive magnetostriction of amorphous residual phase with negative magnetostriction of Fe_3Si crystalline grains. This (together with low magnetocrystalline anisotropy) leads to th extremly low total anisotropy of FINEMET-based nanocrystals.

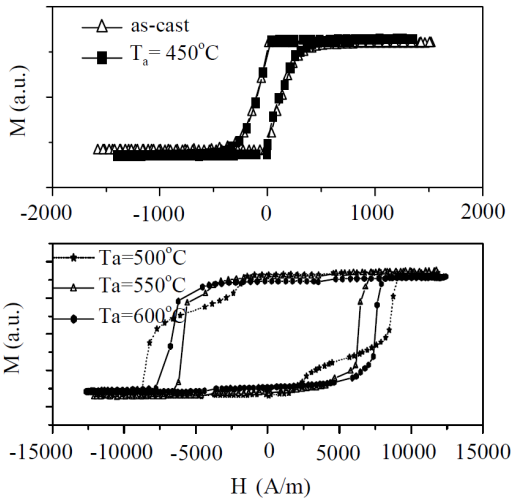

Fig. 4.35. Hysteresis loops of $Fe_{73.5}Si_{13.5}B_9Nb_3Cu_1$ microwire for the different stages of devitrification shows strong magnetic hardening after annealing above crystallization tempetarure (T_x = 540°C) [158].

One of the few disadvantage of FINEMET-based nanocrystalline materials is their relatively low saturation magnetization [145]. This problem has been solved by introducing the new class of nanocrystalline materials based on FeCuNbB. It is called NANOPERM and is characterized by high saturation magnetization ($\sim$ 2 T [152]) as well as by high initial susceptibility. On the other side, NANOPERM-based nanocrystals exhibit low Curie temperature ($\sim$ 80°C [153]). Such low T_c disqualifies NANOPERM-based nanocrystals from applications even just above the room temperature.

Solution has been found by using new nanocrystalline class - HITPERM having composition FeCo(Cu)NbB with the Curie temperature well above 600°C [154]. Moreover, HITPERM-based nanocrystalline materials are characterized by the same high saturation magnetization as NANOPERM. Their lower initial permeability (comparing to FINEMET and NANOPERM) is a result of positive effective magnetostriction due to a positive magnetostriction of crystalline FeCo grains as well as of amorphous matrix.

4.7.4 Finemet

Very early after discovery of nanocrystalline materials, the idea to emply nanocrystalline structure in glass-coated mmicrowires arose [12, 155, 156, 157]. However, it was focused to soft magnetic properties and their stability. Method of production of glass-coated nanocrystalline microwires is a specific because of strong stresses introduced during annealing on metallic nucleus by glass coating due to different thermal expansion coeficient. Due to the mentioned stresses, γ-Fe crystalline phase sometimes appears, which is non-magnetic and plays a role of pinning centers for domain wall propagation [158, 159, 160]. Such a structure deteriorates the good soft magnetic properties of FINEMET-based structure (Fig. (4.35)).

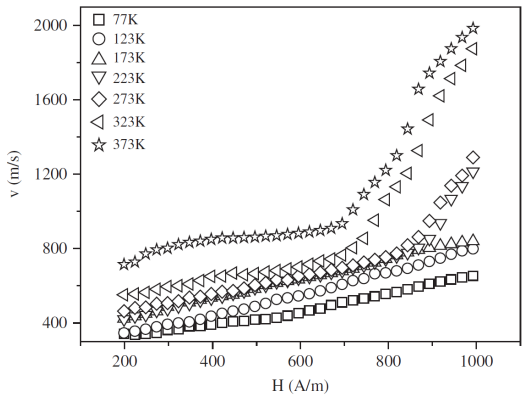

Fig. 4.36. Dependence of domain wall velocity on applied magnetic field for amorphous FeCuNbSiB microwire (temperature as parameter) [161].

On the other hand, small effective magnetostriction of FINEMET-based nanocrystalline glass-coated microwire leads sometimes to the lose of magnetic bistability [155]. These are the problems that must be solved when one decides to employ FINEMET-based microwire to study the domain wall dynamics and therefore the domain wall dynamics study in nanocrystalline glass-coated microwires appears a bit later [73, 161, 162].

Even in amorphous state, FINEMET-based precirsor shows fast domain wall propagation (Fig. 4.36), having linear dependence of the domain wall velocity on the applied magnetic field (see Eq. (3.3)) with a negative critical propagation field H_0 as found in other amorphous glass-coated microwires. Such linear dependence appears at lower temperatures (below 223K). However, other region with higher domain wall mobility appears at high fields when the temperature exceeds 200 K that was ascribed to the change of the domain wall structure from transversal to vortex one. The transversal configuration has lower energy and therefore it appears at low fields. Moreover, it is has lower domain wall mobility ($\sim$ 2 m^2/As, see Fig. 4.37) and it is preffered in thinner magnetic wires [105]. On the other hand, vortex configuration of the domain wall has higher domain wall energy and therefore it appears at higher fields. As it was shown theoretically, it appears at thicker wires and it has higher mobility ($\sim$ 0.25 m^2/As, see Fig. 4.37) that is not so temperature dependent.

Such hypotesis is confirmed by the change of the domain structure in microwires, which was studied by measurement of the temperature dependence of remanent (M_r) and saturation (M_s) magnetization (Fig. 4.38). The difference between the M_r and M_s gives us information about the radial domain structure [163]. It appears as a result of the stresses introduced through the different thermal expansion coefficient of the glass coating and metallic nucleus. It is clear from Fig. 4.38 that the radial domain structure is thicker at low temperatures and decreases with the temperature due to stress relief. Hence, the diamter of axial domain increases with temperature and allows the vortex domain wall to be created.

The annealing of FINEMET-based amorhous precursor below the Curie temperature of the alloy usually leads to a strong induced anisotropy in amorphous microwires. During such an-

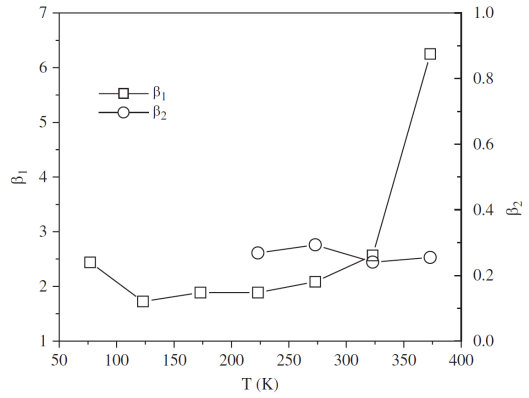

Fig. 4.37. Temperature dependence of the domain wall damping for both transversal (β_1) and vortex (β_2) domain wall in amorphous FeCuNbSiB microwire [161].

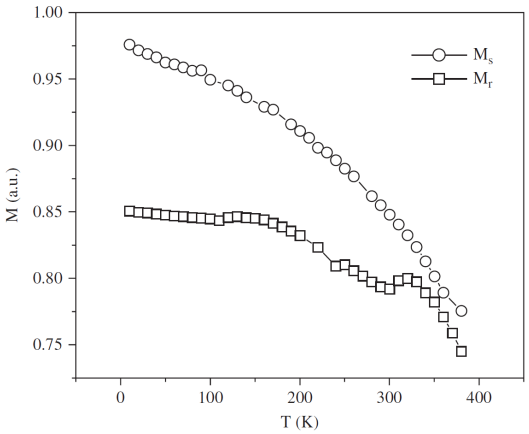

Fig. 4.38. Temperature dependence of the remanent (M_r) and saturation (M_s) magnetization of amorphous FeCuNbSiB microwire [161].

nealing, the existing domain pattern is stabilized. As a consequence, due to the decrease in the domain wall mobility the initial susceptibility diminishes [164] and a higher critical field must be applied to remove the domain wall from their equilibrium position [165]. The largest effect of such stabilization is typically observed at around 473 K. The domain wall dynamics of FINEMET-based microwire heat-treated at 473 K is shown in Fig. 4.39. As in almost all cases in microwires, the domain wall velocity v is found to be exactly proportional to the applied field H according to Eq. (3.3). However, some peculiarities are found in that dynamics. First, the domain wall velocity decreases with measuring temperature, which is quite controversial in comparison with previous results [8, 9]. Typically, the magnetic moments freedom increases with the tem-

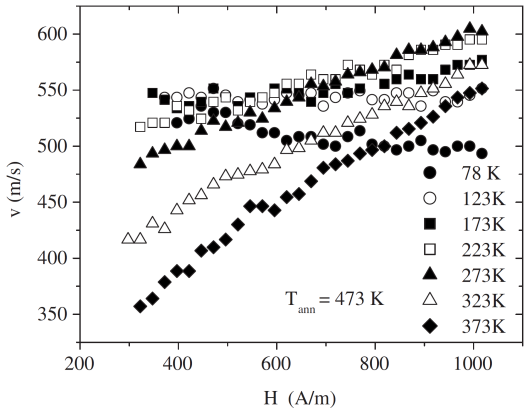

Fig. 4.39. Domain wall dynamics of FeSiBNbCu microwire annealed at 473 K for 1h, with the measuring temperature as a parameter [73].

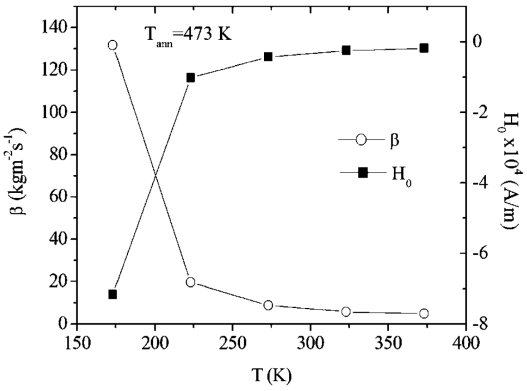

Fig. 4.40. Temperature dependence of domain wall damping and critical propagation field for the FeSiBNbCu microwire annealed at 473 K for 1h [73].

perature due to their thermal activation and so does the domain wall velocity. Furthermore, the domain wall velocity is mainly driven by two parameters: the domain wall mobility S, which is inversely proportional to the domain wall damping β and the critical propagation field, H_0. Although the domain wall mobility S decreases at low temperature, the domain wall velocity remains high due to the large and negative critical propagation field H_0.

Opposite to the domain wall velocity, the wall mobility S increases with the temperature. According to the Eq. 3.4, the wall mobility is mainly driven by the domain wall damping β because the saturation magnetization decreasing with temperature in the measured temperature range. As shown in Fig. 4.40, the domain wall damping strongly increases at low temperature and reaches even negative values at around 78 K. The negative domain mobility has already been

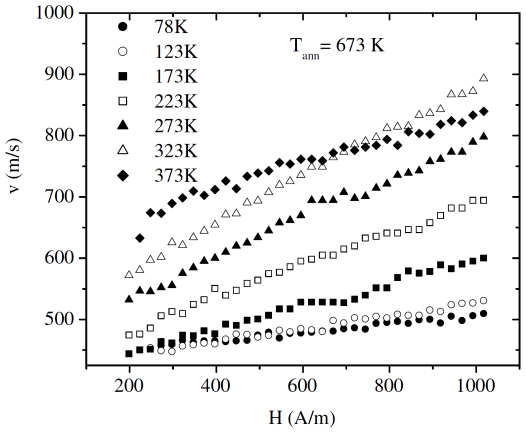

Fig. 4.41. Domain wall dynamics of FeSiBNbCu microwire annealed at 673 K for 1h, with the measuring temperature as a parameter [73].

explained in Section 4.2 in terms of domain structure stabilization. It just must be stressed that such stabilization leads to the variation of domain wall damping that is almost two orders in the temperature interval 75-375 K.

Annealing at 673 K (above T_C, but still below the crystallization temperature $\sim$ 813 K) has a few effects on the structure of FeSiBNbCu microwires. Such a temperature is high enough to release the stresses induced during the fabrication procedure, leading to an anisotropy homogenization of the material and consequently, the coercivity decreases [158]. The domain structure disappears above the Curie temperature, hence the local defects will be randomly distributed making the domain structure destabilized. It is manifested by very small pinning field [165]. However, the FeSiBNbCu microwire still remains in amorphous state, therefore its structural relaxation occurs even at low temperatures [66]. Thus, the domain wall dynamics is similar to the corresponding one in the as-cast microwire. The domain wall velocity increases with the temperature and so does the domain wall mobility (Fig. 4.41). Moreover, the annealing at such high temperature leads to the stress relief and homogenization of the structure. In fact, annealing at 673 K leads to a maximum decrease in the switching field in amorphous Finemet microwire [166] and the domain wall velocity increases comparing to that of the microwire annealed at 473 K.

However, additional stresses are induced on the metallic nucleus by glass coating due to their different thermal expansion coefficient when the microwire is cooled down to room temperature. In this case, the domain wall damping is around one order of magnitude lower than that after annealing at 473 K and decreases with temperature (Fig. 4.42). It could be ascribed to the lower local anisotropy due to the random redistribution of the defects after annealing at temperature above T_C. In addition, the decrease in the domain wall damping due to the diminishing of the mobile defects concentration c_0 given by Eq. (3.9) should be also taken into account as has been already found for FeSiB microwires annealed at 673 K [40].

The most important parameters controlling the domain wall dynamics in amorphous microwires are the distribution and strength of induced stresses on the metallic nucleus by the glass

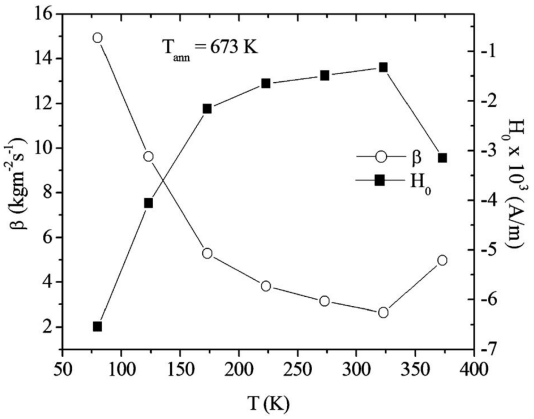

Fig. 4.42. Temperature dependence of domain wall damping and critical propagation field for the FeSiBN-bCu microwire annealed at 673 K for 1h [73].

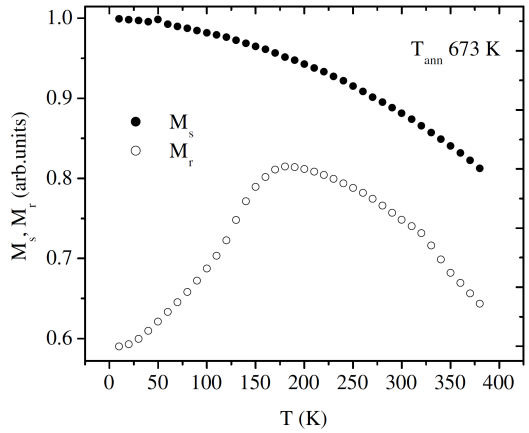

Fig. 4.43. Temperature dependence of remanent (M_r) and saturation (M_s) magnetization for the FeSiBN-bCu microwire annealed at 673 K for 1h [73].

coating. One can see from Fig. 4.43 that the domain structure remains constant in the temperature range between 175 and 375 K. Below this range, the radial domain structure in the shell increases in volume. The annealing temperature at 673 K is high enough (in comparison with the one at 473 K) to relax significantly the stresses induced during the microwire fabrication. Hence, the effect of the stresses induced by glass coating when the temperature cools down to RT is stronger. However, although the variation in the axial core domain volume is higher than for the microwire annealed at 473 K, the temperature dependence of the domain wall damping together with the variation in the critical propagation field are not as high as in the case of the microwire

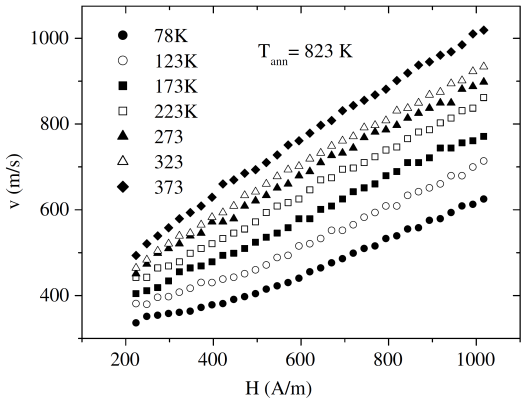

Fig. 4.44. Domain wall dynamics of FeSiBNbCu microwire annealed at 823 K for 1h, with the measuring temperature as a parameter [73].

annealed below T_C. This points out the fact that the locally induced magnetic anisotropy through the structural relaxation is the dominant factor in determining the domain wall velocity at least in amorphous materials, which allows the existence of structural relaxation even at low temperatures [39, 165]. The annealing at 673 K significantly reduces the mobile defect concentration c_0 with respect to annealing process at lower temperature [165]. Therefore, the effect of structural relaxation on the domain wall dynamics is weaker than in the case of annealing at 473 K.

The fastest domain wall value of 1000 m/s has been found for the microwire annealed at 823 K. The annealing treatment at 823 K leads to the development of the nanocrystalline microstructure that consists of α-FeSi grains randomly distributed into an amorphous matrix [12]. The nanocrystalline structure in the material has some advantages. First, the random orientation of the nanocrystalline grains are interexchange-coupled averaging out the magnetocrystalline anisotropy since their diameter is much smaller than the exchange correlation length [133]. Moreover, the crystalline α-FeSi grains have a negative magnetostriction coefficient in contrary to the positive one of the amorphous matrix. Thus, the effective magnetostriction of nanocrystalline FeSiBNbCu microwire is nearly zero and a negligible role in the magnetic properties is played on the nanocrystallized material by the magnetoelastic anisotropy. Therefore, a large magnetic susceptibility and very low-switching field are characteristic properties of nanocrystalline material [157]. As a consequence of the low anisotropy, the domain wall velocity reaches a high value above 1000 m/s for rather low applied magnetic field of 1000 A/m (Fig. 4.44). The highest domain wall velocity measured in thin crystalline ferromagnetic wires was about 1500 m/s in a FeNi microwire, although it was reached for a much larger applied magnetic field of around 4000 A/m [101]. In addition, the low anisotropy results in a small domain wall damping value less than 2.5 kg/m^{2}s that does not change significantly with the temperature because of the stable crystalline structure developed in the material Fig. 4.45. Vanishing magnetocrystalline and magnetoelastic anisotropies are confirmed also by magnetization measurements (Fig. 4.46). The single-domain structure is confirmed only in the temperature range from 250 to 325 K. Outside this range, the single domain structure is destroyed, which is confirmed not only by the sharp

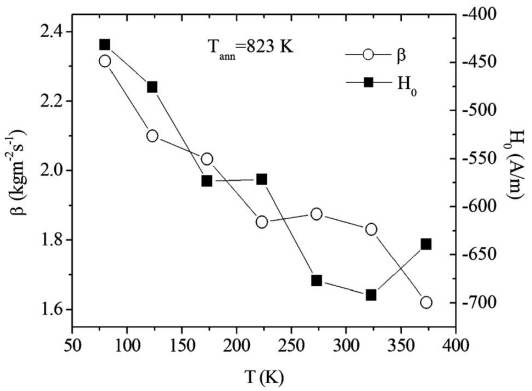

Fig. 4.45. Temperature dependence of domain wall damping and critical propagation field for the FeSiBNbCu microwire annealed at 823 K for 1h [73].

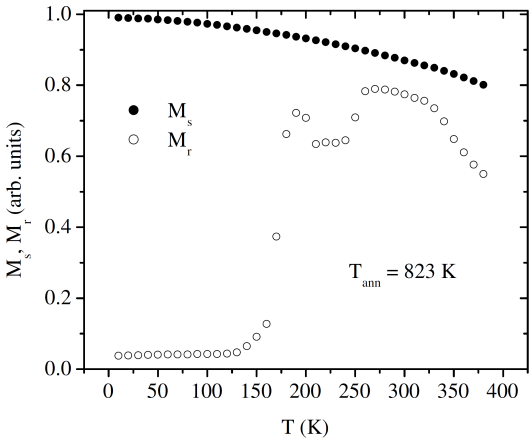

Fig. 4.46. Temperature dependence of remanent (M_r) and saturation (M_s) magnetization for the FeSiBNbCu microwire annealed at 823 K for 1h [73].

decrease in the remanent magnetization but also by hysteresis loops measurement (Fig. 4.47). Besides, the shape anisotropy strongly influences the domain structure of nanocrystalline FeSiBNbCu microwires. It must be pointed out that 1 cm long samples were used for magnetization measurement whereas 10 cm long samples were employed for domain wall damping measurements that clearly show magnetic bistability (i.e., single-domain structure). The critical length, to observe the magnetic bistability is typically on the order of a few mm for highly magnetostrictive microwires [14].

For low-magnetostriction nanocrystalline FINEMET microwires, a length of sample of around 1 cm is not enough for the magnetic bistability appearance. Due to the vanishing values of both

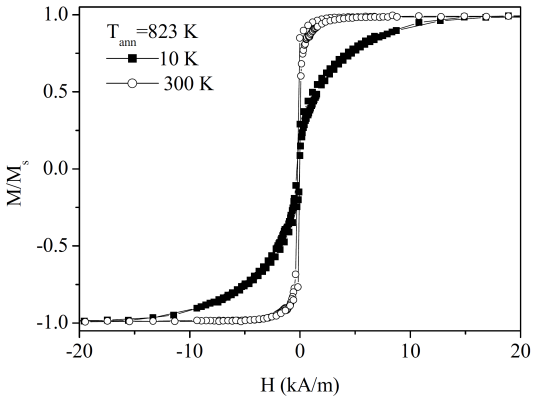

Fig. 4.47. Hysteresis loops measured at 10 and 300 K for FeSiBNbCu microwire annealed at 823 K for 1h [73].

magnetocrystalline and magnetoelastic anisotropies, the most important parameter governing the domain wall damping arises from the eddy current. Nanocrystalline microwires have much lower resistivity comparing to the amorphous ones [129]. Thus, the small decrease of the domain wall damping with the temperature can be ascribed to the temperature dependence of the resistivity in nanocrystalline FeSiBNbCu microwires. Although the domain wall damping slightly changes with temperature, the domain wall velocity increases due to the temperature dependence of the critical propagation field H_0, which also remains negative in the nanocrystalline state. However, its amplitude is one order of magnitude lower than that the value obtained after annealing at 673 K, and two orders of magnitude lower than that the corresponding one after annealing at 473 K.

This feature makes nanocrystalline materials ideal for stable domain wall dynamics in a wide range of temperatures. Hence, we have dealt with another compositions, too.

4.7.5 FeHfSiB

Another studied nanocrystalline glass-coated microwires is NANOPERM-based one having composition $Fe_{79}Hf_7Si_2B_{12}$ [167, 168]. Such composition creates α-Fe crystalline grains directly during the microwire's production. The crystalline grain size is 17 nm and increases up to 34 nm after annealing at 600°C (Fig. 4.48). The grain size is higher than in the case of FIENEMT-based microwires and this will result in magnetic hardening (see Eq. (4.20)). The coercivity is higher (comparing to FINEMET) ~ 1000 A/m and decreases with annealing (Fig. 4.49) The decrease of coercivity can be appointed to the release of the stress induced by production. However, neither high temperature (600°C) annealing decreases the coercivity below 600 A/m.

The biggest disadvantage is their low magnetostriction. Neither high stresses applied on the metallic nucleus by glass-coating induce monodomain structure and such microwire does not exhibit magnetic bistability (Fig. 4.50). Hence they are not suitable for domain wall dynamics study.

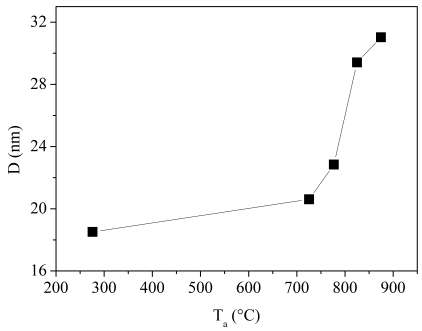

Fig. 4.48. Dependence of grain size on annealing temperature for FeHfSiB nanocrystalline microwire [168].

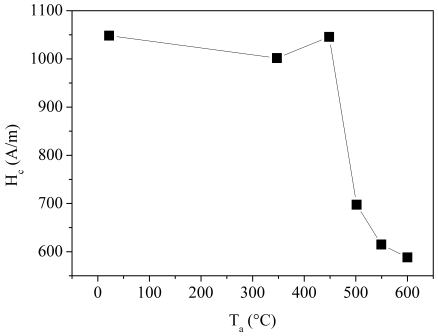

Fig. 4.49. Dependence of coercivity on annealing temperature for FeHfSiB nanocrystalline microwire [167].

4.7.6 FeNiMoB

As it was shown above, the low magnetistriction of FINEMET- and HITPERM-based nanocrystalline microwires results in lose of their magnetic bistability due to low magnetostriction. Low total magnetostriction is a result of counterplay of negative magnetostriction of crystalline phase with positive magnetostriction of amorphous matrix. In contrary, magnetic bistability appears in positive magnetostrictive microwires. In order to get bistable nanocrystalline microwire, positive total magnetostriction is necessary, too.

One possibility is to employ new $Fe_{40}Ni_{38}Mo_4B_{18}$ composition. It has been shown that it is possible to prepare nanocrystalline ribbons of such composition with very good soft magnetic properties [168, 169, 170]. They are prepared by controlled annealing of amorphous precursor and their structure consists of γ-FeNi crystalline grains of diameter $\sim$ 10 nm embedded in amorphous matrix. In contrary to FINEMET and NANOPERM-based microwire, where nega-

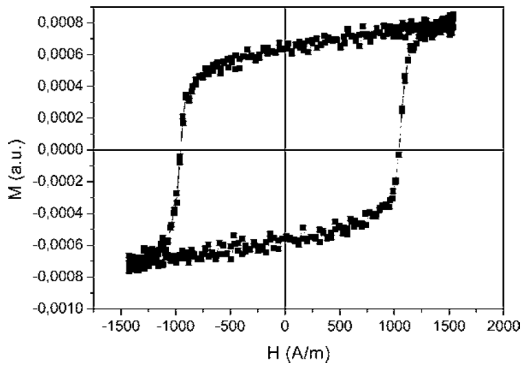

Fig. 4.50. Hysteresis loops for as-cast FeHfSiB nanocrystalline microwire [168].

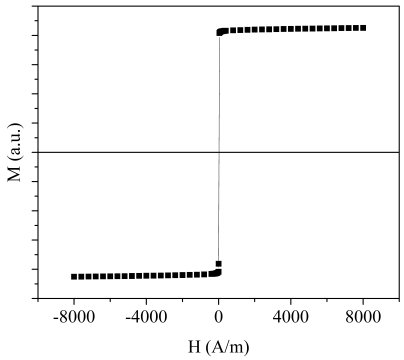

Fig. 4.51. Hysteresis loops for nanocrystalline FeNiMoB microwire [171].

tive magnetostriction α-Fe(Si) phase appears, γ-FeNi phase has positive magnetostriction. This leads to positive total magnetostriction of nanocrystalline microwires and magnetic bistability is kept until the highest annealing temperatures [171] (Fig. 4.51).

In addition, such composition solves two more problems of nanocrystalline glass-coated microwires. Firstly, it has been mentioned in Section 4.7.4 that in some cases γ-Fe phase appears in FINEMET-based microwires. Such a phase has higher density (comparing to α-Fe(Si)) and therefore it is sometimes preffered during annealing under stress. However, it is non-magnetic and hence it deteriorates good soft magnetic properties. In contrary, γ-FeNi phase is soft magnetic and improves the good magnetic behaviour of nanocrystalline microwires. As a result, the switching field of FeNiMoB nanocrystalline microwire is much lower than that of FeHfSiB (Fig. 4.52).

Secondly, replacing Nb or Zr for Mo leads to decrease of crystallization temperature down to

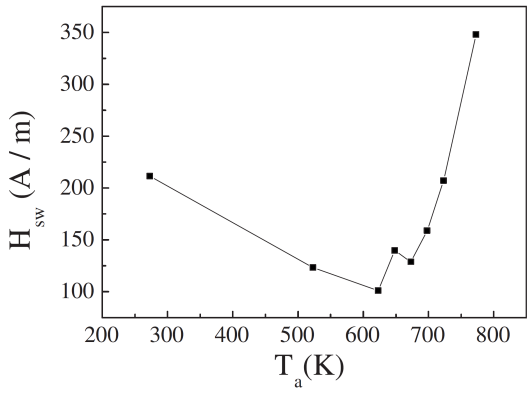

Fig. 4.52. Dependence of coercivity on annealing temperature for FeNiMoB amorphous and nanocrystalline microwire [171].

375°C [168, 169, 170, 171]. This is particularly important in the case of glass-coated microwires, in which strong stresses are introduce by glass during annealing as a result of different thermal expansion coefficient of metallic nucleus and glass-coating. Hence, one can get very good soft magnetic properties when it is annealed properly (see Fig. 4.52).

However, the magnetic properties of FeNiMoB nanocrystalline microwire are still strongly dependent on the stress applied by glass-coating when it is cooled down to room temperature . Therefore, thermal treatment must be provided very carefully otherwise magnetic hardening appears when annealed over optimum annealing temperature ($\sim$ 400°C (see Fig. 4.52) [171, 172]). Therefore we have applied similar composition FeCoMoB to get final product for stable and fast domain wall dynamics.

4.7.7 FeCoMoB

All of the above mentioned problems regarding the applications of nanocrystalline glass-coated microwires are solved in HITPERM-based alloys [173, 174]. They combine the advantages of FeNiMoB nanocrystalline microwires (low crystallization temperature, appearance of magnetic crystalline phase,...) with high magnetization and Curie temperature, together with high structural stability of FeCo-based nanocrystalline materials. In addition, they exhibit magnetic bistability as a consequence of the positive magnetostriction of α - FeCo crystalline grains. Moreover, their excellent soft magnetic properties are maintained in a wide range of temperatures. The combination of FeCo crystalline grains with high magnetization and Curie temperature ($\sim$ 900°C) brought about new materials that can be employed even at a very high temperature [174,175,176].

The optimum annealing conditions to obtain nanocrystalline structure of FeCoMoB microwire was estimated from the measurement of the temperature dependence of resistance, which is known to be a powerful method to determine the structural changes of materials [129]. Figure 4.53 shows temperature dependence of resistance measured up to 600°C. Starting from the amorphous state at 27°C, the resistance slightly increases up to 200°C as a result of the thermal

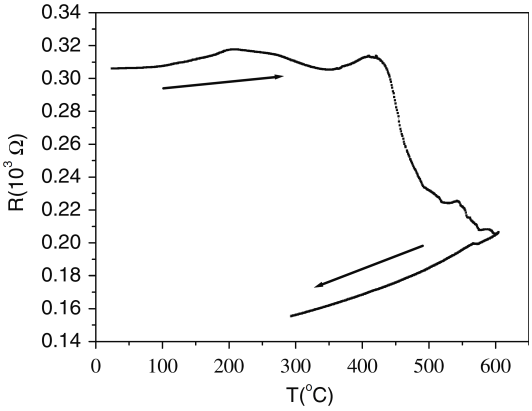

Fig. 4.53. The temperature dependence of resistance for FeCoMoB microwire. Arrows show the temperature running. [129].

activation of the atomic structure. Above 200°C,structural relaxation takes place up to 350°C. Within this range, the stresses and structural defects introduced during the preparation (by rapid quenching and drawing) partly relax and the amorphous structure becomes homogenized, which is characterized by a smooth decrease in the resistance of the studied material. Above 350°C, the structural relaxation has already completed and the resistance linearly increases up to 420°C as expected in metallic conductors. At 420°C, the resistance steeply drops due to the crystallization of α-FeCo nanocrystalline grains that are embedded in the residual amorphous matrix, as was confirmed also by the x-ray measurement. The first crystallization step completes at 540°C. The crystalline grains in HITPERM-based alloys typically consist of bcc α-FeCo B2 (ordered) phase [154] whose grain size was roughly estimated to be around 19 nm according to Scherrers formula. Above this temperature, a kind of secondary crystallization takes place that completes above 600°C. However, no new phases were recognized from the X-ray , and the crystalline grain size remains nearly constant at 19 nm; hence the second crystallization step should be rather ascribed to the increase in volume fraction of the crystalline phase. As it was shown in case of FeNiMoB nanocrystalline microwires [171], strong stresses are generated during annealing in the metallic nucleus by glass coating as a result of different thermal expansion coefficients. These stresses inhibit the crystal growth due to the suppression of atomic mobility. Thus, the crystalline grain size remains nearly constant, which is a requirement for nanocrystalline alloys to show excellent and stable soft magnetic properties [133]. The temperature dependence of resistance for nanocrystallized microwire shows a monotonic decrease with decreasing temperature, confirming the high structural stability of nanocrystalline materials.

An additional advantage of the proposed FeCoMoB composition is its magnetic bistability. In contrast to the classical nanocrystalline compositions (FINEMET, NANOPERM), the α-FeCo nanocrystalline grains exhibit positive magnetostriction. Thus, the overall magnetostriction remains positive, which is a necessary condition for magnetic microwires to obtain monodomain structure and hence, magnetic bistability. Figure 4.54 shows the bistable hysteresis loops of the

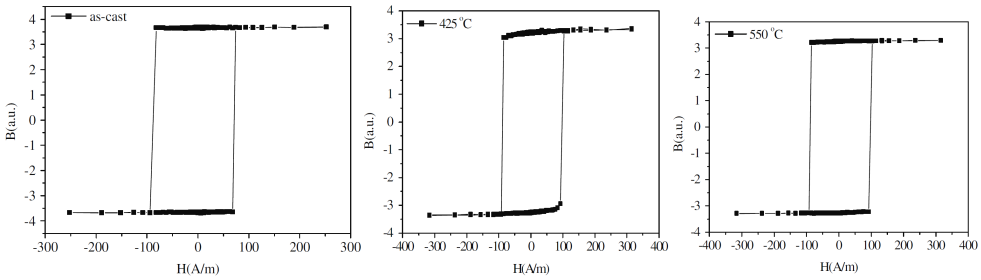

Fig. 4.54. Hysteresis loops of as-cast FeCoMoB microwire and microwires annealed for 1 h at temperatures 425°C and 550°C, respectively, show magnetic bistability. [129].

FeCoMoB microwire in the as-cast state and after annealing at 425 and 550°C. Note that magnetic bistability is confirmed by the lack of experimental points between the two stable magnetic configurations. The loops measured in the as-cast state and annealed below 425°C (not shown) are perfectly bistable, whereas annealing at 425°C leads to a slight reduction in the differential susceptibility within the range 100 to 100 A/m. This could be assigned to the onset of the crystallization process. However, the crystalline precipitates are small and separated by a long distance and they play the role of pinning centres for the domains. Anyway, the main magnetization process is a single Barkhausen jump of a single domain wall at a field of 100 A/m as it is typical for a positive magnetostriction microwire. Annealing at temperatures above 425°C leads to a further crystallization, during which the α-FeCo nanocrystalline grains grow within the amorphous matrix. In this state, the size of the grains is significant and the distance between the grains embedded in the amorphous matrix is smaller than the ferromagnetic exchange length $\sim$ 46 nm [177], which (together with the random distribution of their crystallographic axis) results in the averaging out of an effective magnetocrystalline anisotropy. Thus, the microwires remain magnetically soft, and the loops are perfectly bistable due to the positive magnetostriction of crystalline grains as well as amorphous matrix.

The dynamic switching field and its dependence on the annealing process (Fig. 4.55) reflect the structural changes introduced by annealing. Thermal treatment below 350°C releases the stresses introduced during the microwire production (as shown also in the resistance measurement in Fig. 4.53), which results in the decrease in magnetoelastic anisotropy and therefore to decrease in the switching field. Annealing at temperatures close to 450°C leads to the formation of crystalline grains which being spatially separated play the role of pinning centres for domain wall motion . Therefore, a strong increase in the dynamic switching field is observed after annealing at 425°C. Such an increase is not observed in the case of quasistatic loops (Fig. 4.54) because the dynamic switching field measured by the induction method [178] is strongly dependent on the domain wall propagation, whereas quasistatic loops measure only static magnetization state. In the case of well-separated crystalline pinning centres, the domain wall propagation is hindered and the measured dynamic switching fields are higher than static ones. Such a hardening is frequently observed after annealing of nanocrystalline samples just below the optimum annealing temperature [157]. An important fact is that the switching field remains nearly constant after annealing above 425°C in contrast to nanocrystalline microwires with different alloy com-

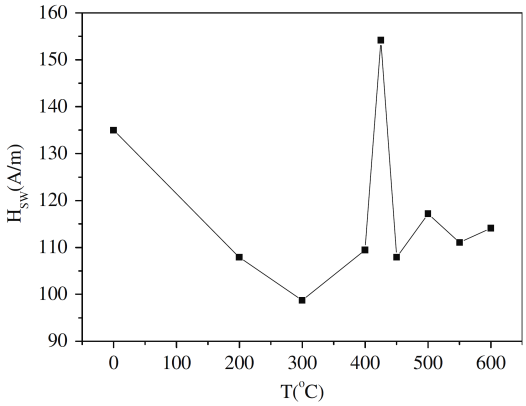

Fig. 4.55. Dependence of coercivity on annealing temperature for FeNiMoB amorphous and nanocrystalline microwire [171].

positions (where annealing at higher temperatures results in a steep increase in the switching field [157,159,171]). The coercivity of soft nanocrystalline materials is mainly driven by a small magnetocrystalline anisotropy, which is a result of randomly oriented crystalline grains. Their diameter ($\sim$ 19 nm) is much smaller than the exchange length; hence they are exchange-coupled through the amorphous matrix. As a result of such interaction, the effective magnetocrystalline anisotropy is almost zero. The crystalline grain diameter does not change within a wide range of annealing temperatures because of the stress resulting from the glass coating on the metallic nucleus. So, the optimum annealing temperature interval to obtain soft magnetic, bistable microwire is enhanced from 450 to almost 600°C, in contrast to the classical nanocrystalline materials, where the optimum annealing temperature ranges typically within a very narrow interval at more elevated temperatures (from 530 to 560°). The crystallization temperature decreases in comparison with the HITPERM alloys by 100°C. This is seemingly a consequence of using Mo in order to inhibit grain growth. As it was shown in [179], Mo decreases the crystallization temperature of the nanocrystalline phase in opposition to Zr or Nb [173, 174, 175]. However, good soft magnetic properties remain and the given composition belongs to the group of softest magnetic nanocrystalline microwires. This is another important fact for production specially in the case of glass-coated microwires, where high temperature annealing results in a strong applied stress due to the different thermal expansion coefficients of metallic nucleus and glass coating [157, 159, 171].

The independence of the switching field on the annealing tepmerature above 450°C can be explained by measurements of anisotropy field as obtained from FMR measurements [99]. The evolution of the anisotropy field H_k with annealing temperature for FeCoMoB microwire is shown in Fig. 4.56. Strong stresses introduced during the microwires production result in large magnetoelastic anisotropy at the as-cast state. Annealing below the crystallization temperature leads to stress relaxation and sample homogenization so, indicating that the strong anisotropy field decreases after annealing below 400°C. Annealing above crystallization temperature (425°C) has a little effect on the anisotropy field. Such behavior reflects well the switching field dependence

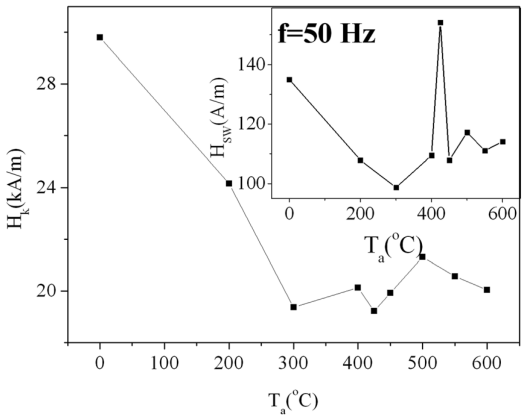

Fig. 4.56. Evolution of anisotropy field with annealing of the glass-coated FeCoMoB microwire. Inset shows the switching field dependence on the annealing temperature [99].

on the annealing temperature obtained by induction measurement method (see Fig. 4.55 or inset of Fig. 4.56). In contrary to the switching field, no maximum appears at 425°C as a result of appearance of precipitates of crystalline phase since FMR at high frequencies is not sensible to the domain wall propagation. Above this temperature, the nanocrystalline structure appears with an exchange interaction between the crystalline grains. Such a structure is very stable and the anisotropy field H_k remains almost constant similarly to the switching field.

Large internal stresses are induced inside of metal core during production process and these stresses significantly determine the magnetic behavior of the microwire. Both quenching stresses as well as those resulting from the difference between thermal expansion coefficients of metal core and glass-cover are present in the microwires. Knowing the anisotropy field H_k (estimated from FMR measurement - Fig. 4.56), it is possible to calculate the internal stresses using the relationship [20]:

$$\sigma = \frac{\mu_0 M_s H_k}{3\lambda_s} \tag{4.23}$$

for samples after different thermal treatment. The dependence of internal stresses on the annealing temperature is shown in Fig. 4.57. Although saturation magnetostriction increases with annealing temperature [180], internal stresses decrease sharply from initial maximum value in the as-cast state. This sample, in its as-cast amorphous state, is characterized by strong internal stresses frozen during the production process. Stress relaxation takes place during annealing process at higher temperatures. Therefore, internal stresses quickly decrease in amorphous samples with increasing annealing temperature from maximal value $\sim$ 800 MPa down to minimal values $\sim$ 250 MPa in the nanocrystalline state. Finally, microwires in a nanocrystalline state have almost constant and low values of internal stresses. This can explain the results of the switching field dependence on annealing temperature, where very weak dependence of the switching field was observed on the annealing temperature above 450°C.

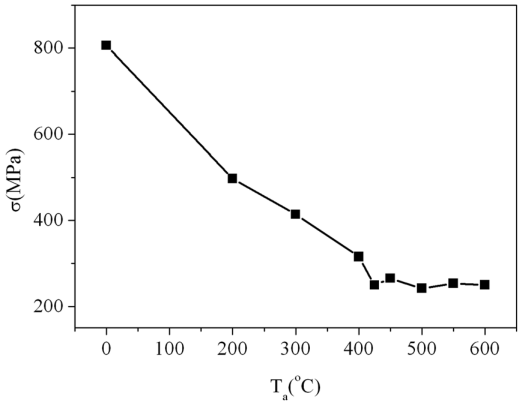

Fig. 4.57. The dependence of the internal stresses on the annealing temperature for FeCoMoB amorphous and nanocrystalline microwire [99].

One of the most important information that can be obtained from FMR measurements are damping parameters. Gilbert damping is the main parameter that influences the domain wall dynamics, and one of the very promising direction of microwires application is their use in modern spintronic devices based on the domain wall propagation in thin magnetic wires. Fast domain wall velocity observed in glass-coated microwires is usually ascribed to very low values of Gilbert damping that can be estimated from FMR spectra. Figure 4.58 shows the evolution of measured values of Gilbert damping that range from 0.0127 up to 0.0746. Gilbert damping increases at low annealing temperatures because of stress relaxation takes place, homogenization of sample and stabilization of domain structure. Gilbert damping shows the highest value of 0.0746 above crystallization temperature, exactly at temperature 425°C. In fact, the structure is changed from amorphous to nanocrystalline at this temperature. The number of crystallites is still low and they are separated by a large distance, that is, the structure is highly nonhomogeneous. At higher annealing temperatures, Gilbert damping decreases very shortly down to the lowest value 0.0127. At higher annealing temperatures, the volume fraction of grains is significant and distance between them is smaller than ferromagnetic exchange length L_{ex} (~ 46 nm). Therefore, exchange interaction between them leads to the averaging out of magnetocrystalline anisotropy, which result in drop of switching field values and as well as Gilbert damping values. The obtained values of Gilbert damping correspond well to the ones obtained in glass-coated CoFeSiB microwires [97, 98] and its temperature dependence reflects also the temperature dependence of the switching field as described above.

Relatively high resistance of nanocrystalline FeCoMoB materials (which is higher than that of pure crystalline phase) together with low dimensions of glass-coated microwires leads to a small eddy current damping of domain wall (see Eq. (3.6)). Low anisotropy and low Gilbert damping (as described above) should results in a low magnetic relaxation damping (see Eq. (3.8)). Moreover, small structural relaxation of nanocrystalline materials [181], leads to small structural relaxation damping of the domain wall (Eq. (3.9)). These features results in a very low overall domain wall damping that allows the domain wall to achieve the very fast propagation velocities

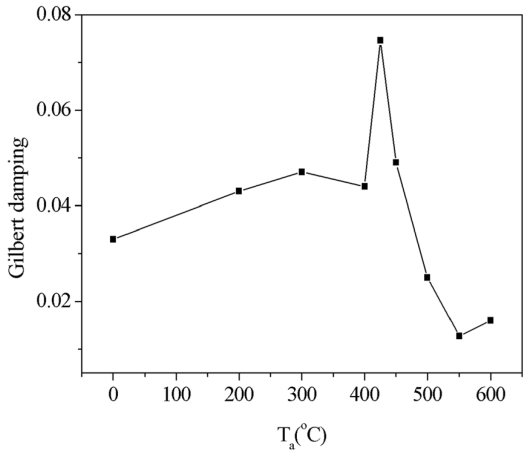

Fig. 4.58. Dependence of Gilbert damping on the annealing temperature for FeCoMoB amorphous and nanocrystalline microwire [99].

of domain wall [182, 183].

Amorphous glass-coated FeCoMoB microwires are characterized by very fast the domain wall velocity even at low applied magnetic fields. Figure 4.59 shows the domain wall velocity v versus applied magnetic field H for amorphous FeCoMoB microwire for a wide temperature range. Starting at 80 K, wide range of linear dependence of v on H (according to Eq. (3.3)) is observed. Above 800 A/m, one can see a steep increase of the domain wall mobility that has already been ascribed to the change of the domain wall structure from transversal to vortex one. At the field $H_w \sim 1100$ A/m, the maximum of the domain wall velocity 2000 m/s is observed that is followed by a region of negative domain wall mobility (the domain wall velocity decreases with the applied field H). This is typical behavior for Walker limit - the limit above which the periodic transformation of the domain wall structure appears that is accompanied by the oscillation of the local domain wall velocity [46]. It results in the decrease of the average domain wall velocity. At higher temperature (180 K), the domain wall dynamics looks similar. However, the field at which the domain wall transformation appear decreases to around 600 A/m and so does the Walker field H_w ($\sim$ 850 A/m). On the other hand, the Walker velocity v_w increases to 2350 m/s. This is a result of decrease of the magnetoelastic anisotropy that is mainly determined by the complex stress distribution in glass-coated microwires induced during their production by quenching. Moreover, strong stresses σ are applied on the microwire as a result of different thermal expansion coefficients of the glass-coating and metallic nucleus. These stresses are proportional to the temperature change ΔT:

$$\sigma(T) \approx E_Y(\alpha_g - \alpha_m)\Delta T \tag{4.24}$$

where E_Y is the Youngs modulus of the metallic core, and α_g and α_m are the corresponding thermal expansion coefficients of the glass and metallic core, respectively. The higher is the temperature, the lower are the stresses and the lower is the anisotropy field. Hence, the Walker field decreases, too. At even higher temperatures (280 K and above), the region of negative

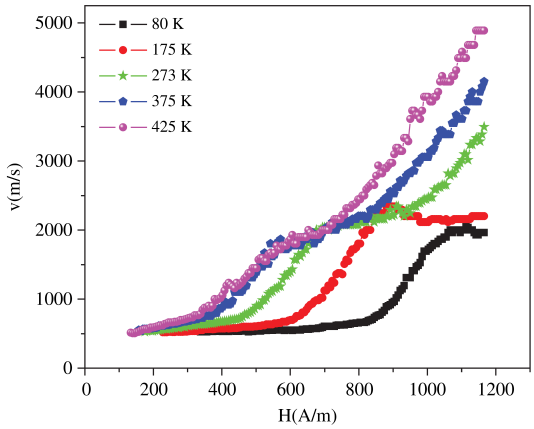

Fig. 4.59. The domain wall dynamics for amorphous as-cast FeCoMoB microwire. [182].

domain wall mobility is suppressed and the domain wall velocity increases up to 5000 m/s. The higher is the temperature, the lower is the magnetoelastic anisotropy and the lower are the field of transition and Walker field. Here we must mention that such fast velocities cannot be explained by only the low anisotropy. It was shown before, that there are more reasons for fast domain wall propagation in magnetic microwires. Among the low anisotropy, it is also the existence of two, perpendicular anisotropies that can averaged out each other.

As many times before, the fast domain wall in amorphous FeCoMoB microwire is paid by low temperature stability. Some improvements can be done by proper thermal treatment. For examle, annealing of the wire at 575 K leads to the homogenization of the microwires structure and to the stress relief [129]. The domain wall dynamics at 80 K is similar to that of as-cast microwire showing the Walker limit at 950 A/m (Fig. 4.60). However, the maximum velocity is higher than that of as-cast alloy (4200 m/s). Above 80 K, the domain wall dynamics becomes more stable with temperature. The domain wall mobility changes weakly with the temperature and the most affected parameter that varies with temperature is the critical propagation field H_0. It decreases with the temperature reflecting the decrease of the anisotropy field due to the decrease of the stresses introduced by the glass-coating on the metallic nucleus. The maximum velocity also increases with temperature and exceeds the value of 5000 m/s even at the temperature 280 K. Further increase of the temperature leads just to a small increase of maximum velocity to 5300 m/s. Also such domain wall dynamics is more stable with temperatrure (comparing to as-cast state), huge variations of domain wall velocity are measured at a given field when temperature varies.

The problem of temperature stability can be definitely solved by inducing the nanocrystalline structure. It was induced by thermal annealing at 775 k for 1 hour. Nanocrystalline materials are characterized by high structural stability that is comparable to their crystalline counterparts. Moreover, HITPERM-based materials show also high Curie temperature. The combination of these two conditions leads to extremely stable domain wall dynamics (in the range of velocities below 1500 m/s) that depends very weakly on temperature (see Fig. 4.61). The dependence of the domain wall velocity v on applied magnetic field H shows two regimes: linear one that was

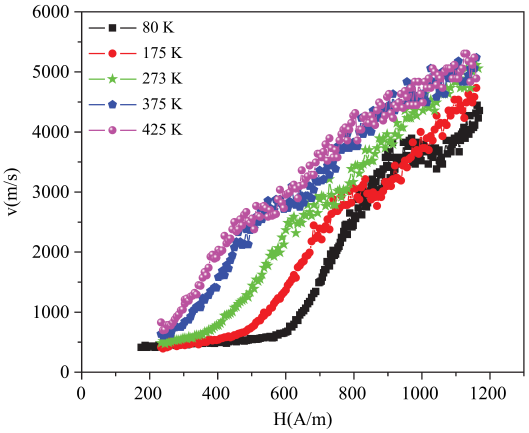

Fig. 4.60. The domain wall dynamics for amorphous FeCoMoB microwire annealed at 575 K for 1 h. [182].

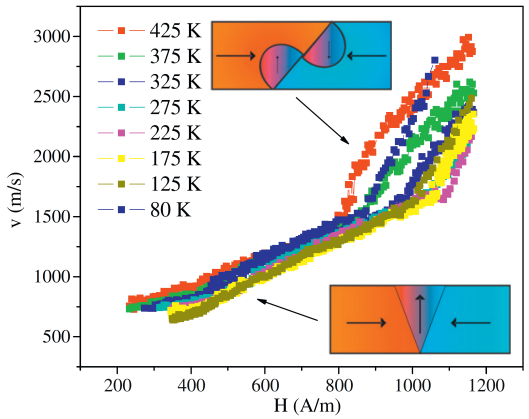

Fig. 4.61. Domain wall dynamics in nanocrystalline FeCoMoB microwires measured in a wide range of temperature. [183].

ascribed to transversal doman wall structure at low fields having lower domain wall mobility and vortex one (which is non-linear) showing higher domain wall mobility and appears at higher magnetic field. The domain wall mobility for transversal domain wall (Fig. 4.62) are comparable to that for amorphous microwires [5, 9], but its temperature stability is much higher [9]. Although, the domain wall velocity at given field slightly varies with temperature, the domain wall mobility in both regimes (transversal and vortex one) is almost constant.

Small variation of domain wall mobility reflects the temperature dependence of the saturation magnetization as given in Eq. (3.4) ($S \sim M_s$) see Fig. 4.62. This confirms the fact that domain wall damping β in nanocrystalline HITPERM-based microwires remains nearly constant within a wide temperature range (80-425 K). Since the temperature dependence of saturation magnetization shows no scattering [129], the small scattering of domain wall mobility is the most probably the result of small temperature variation of magnetoelastic anisotropy that is a result of complex

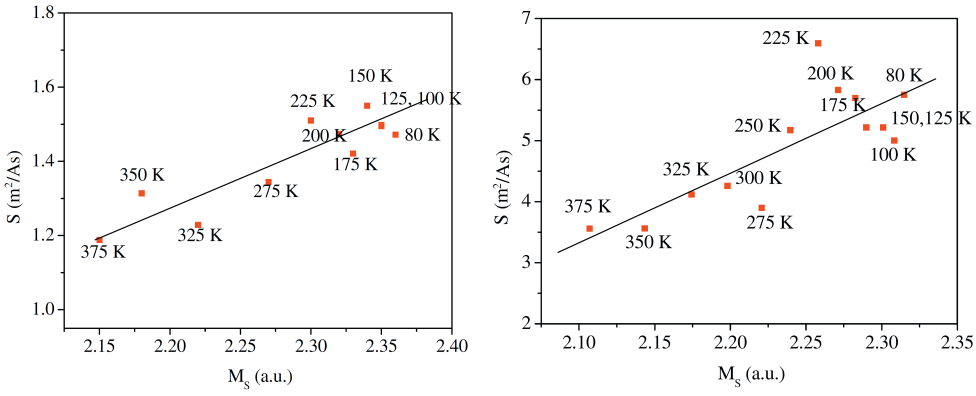

Fig. 4.62. The dependence of domain wall mobility for transversal (left) and vortex (right) wall on saturation magnetization (temperature of measurement as a parameter). Full line corresponds to the linear fit according to Eq. (3.4) [183].

stress distribution introduced by the glass-coating due to different thermal expansion coefficient of glass and metallic nucleus.

The only parameters that are clearly affected by the measuring temperature are the critical fields. There are three critical fields observed in the domain wall dynamics in nanocrystalline FeCoMoB microwire: two critical propagation fields (given by Eq. (3.3)) for transversal, H_0^t, and vortex domain wall H_0^v, and the transition field when the domain wall mobility increases. Both critical propagation fields exhibit the same temperature dependence (see Fig. 4.63). They firstly slightly increase (up to 225 K) and above 225 K both decrease almost linearly. However, the critical field for transversal domain wall is negative in contrary to the positive critical propagation field for vortex domain wall. Negative critical propagation field points to the negative restoring pressure applied on the domain wall in the center of the microwire, which is a result of the specific shape transversal domain wall potential in the center of the wire [68]. The negative restoring force is one of the parameter that can be used to increase the domain wall velocity at low fields even in the case of low domain wall mobility. Similarly to the domain wall mobility, the critical propagation fields can be fitted to the inverse saturation magnetization $1/M_s$ (see Eq. (3.5)). Figure 4.63 shows that such dependence is almost linear at least at temperatures above 200 K. That points to the high temperature stability of the restoring force for FeCoMoB nanocrystalline microwire in this temperature range. The variations at low temperatures (below 200 K) can be described in terms of variable axial domain diameter. It has been shown [184] that nanocrystalline FeCoMoB microwire has very stable domain structure (comparing to that of amorphous one). However, a decrease of temperature results in additional stresses introduced by the glass-coating on the metallic nucleus which results in the decrease of the inner domain diameter. As a result, the critical propagation field decreases, too. Similarly, the slight increase of the critical propagation fields at higher temperatures can be explained by a slight increase of the inner domain diameter above 320 K [183].

These are very promising results on the fast domain wall dynamics in thin magnetic wires.

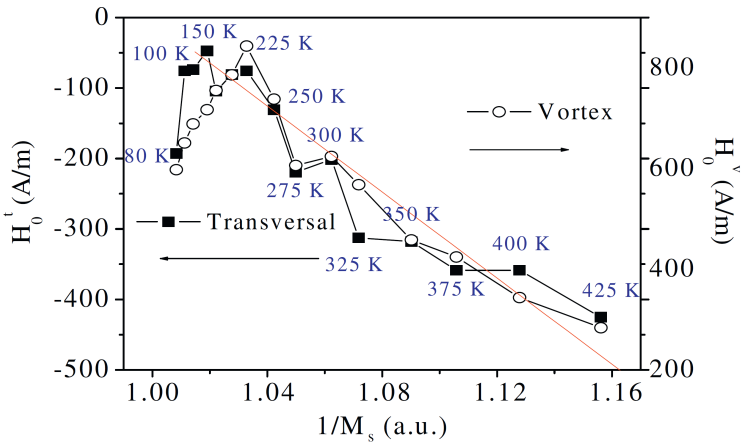

Fig. 4.63. The dependence of the critical propagation fields for transversal and vortex domain wall in nanocrystalline FeCoMoB microwire on the saturation magnetization. Full line corresponds to the linear fit according to Eq. (3.5) [183].

They show that it is possible to produce a material that is characterized by very high domain wall velocity in a reasonable range of magnetic fields. Further thermal treatment (annealing in perpendicular magnetic field, current annealing, etc.) can also be used to combine even faster domain wall velocity with a high temperature stability of nanocrystalline FeCoMoB microwire. It's high Curie temperature as well as the presence of two different ferromagnetic elements (Fe and Co) should help to induce various kind of anisotropy by pair ordering.

5 Switching field of domain wall

The strong dependence of the domain wall dynamics on external parameters can be succesfully employed in construction of miniaturized sensors that sense magnetic field, electrical current, temperature, mechanical stress, etc... [185]. The biggest advantages of glass-coated microwires are their small dimansions that allow embeding of microwires into the studied materials without destroying its mechanical proparties, glass-coating that serves as electrical and chemical (it avoids oxidation at higher temperatures) insulator, fast response that is given by the domain wall velocity, wide temperature range that is given mainly by the Curie temperature (there are no restriction to the low-temperature limit), etc... The easiest way to employ bistable microwires for sensing is to use strong dependence of the switching field on external parameters. As given in Section 2, amorphous microwires with positive magnetostriction are characterized by the magnetic bistability (only two values of magnetization are allowed: $\pm M_s$). The switching between the two values appears at the switching field H_{sw} - the field high enough to depin the domain wal from it's potential well at the end of the wire.

The magnetization process of magnetically bistable amorphous microwires runs by a single giant Barkhausen jump between two stable remanent states (see Fig. 4.8). Therefore, the depinning of a domain wall from the closure structure at one end is responsible for the coercivity mechanism. The switching field of single domain wall in microwire is given by the shape of the domain wall potential. Without the action of the external magnetic field, the position x of the pinned 180° domain wall is given by its potential $W(x)$ minimum which in amorphous materials is mainly determined by magnetoelastic interaction of magnetic moments with local stress induced by production. Under the action of the applied magnetic field H the total free energy $F(x)$ of the domain wall (see Fig. 5.1) is given by [29]:

$$F(x) = W(x) - 2\mu_0 M_s H S_{dw} x, \tag{5.1}$$

where S_{dw} is the area of domain wall (which will be assumed to be constant in this case). If the

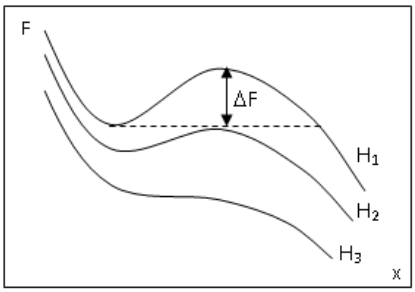

Fig. 5.1. Dependence of the free energy F of the closure domain wall on its position x at different external magnetic field $H_1 < H_2 < H_3$. [65, 187].

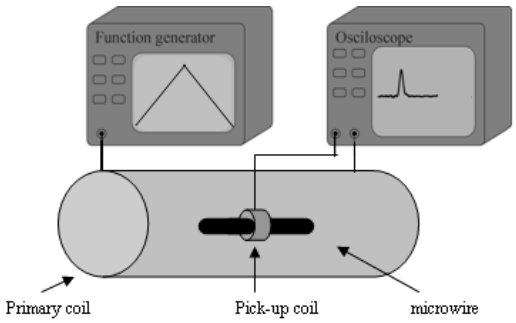

Fig. 5.2. Schematic picture of apparatus for measuring the switching field by induction method [186].

external field H is lower than the switching field H_{sw}, the equilibrium position of the domain wall is given by the local minimum of its total free energy F (see Fig. 5.1). The energy barrier ΔF exists, which does not allow the domain wall to jump into a more favorable position. When the external field H reaches the value of the switching fields H_{sw}, the domain wall depins from its original position and starts to propagate along the wire.

In equilibrium, the domain wall will occupy the position that is given by a minimum of free energy F:

$$\frac{\partial F}{\partial x}|_H = 0. \tag{5.2}$$

Hence, the switching field will be given by a maximum of the first derivation of domain wall potential $W(x)$:

$$H_{sw} = \frac{1}{2\mu_0 M_s S_{dw}} \frac{\partial W(x)}{\partial x}|_{max} \tag{5.3}$$

Therefore it is important to know the shape and origin of domain wall potential in glass-coated microwires.

5.1 Experimental method

The advantage of magnetization process in bistable microwire (single Barkhausen jump) is that one can use a simple induction method to measure the switching field (Fig. 5.2) [64, 186]. Primary coil is fed by triangular shape signal in order to produce linearly increasing magnetic field. When the external field exceeds the switching field, domain wall propagates along the wire (placed coaxially in the primary and pick-up coil) and *emf* maximum is induced in the pick-up coil. Switching field can be easily estimated from the position of maximum. Whole system can be placed into the cryostat and the switching field can be measured in a wide temperature range 80-450 K. Moreover, mechanical stress (up to 150 MPa) can be applied in the whole temperature range. The system can even be improved to recognize the influence of external magnetic field. The problem arises when the microwire is influenced by external parasitic magnetic field

(e.g. Earth's magnetic field). In such case, the measured switching field is a sum of external parasitic and intrinsic switching field. Both components can be distinguished when the switching field is measured in both directions of applied excitation field. Hence, two values of tyhe switching field will be measured, H_{sw}^{+} when excitation field increases and H_{sw}^{-} when excitation field decreases. Finally, the intrinsic switching field, H_{sw} is proportional to the difference of both components [185]:

$$H_{sw} = \frac{H_{sw}^{+} - H_{sw}^{-}}{2}, \tag{5.4}$$

while external parasitic field, H_{ext}, is given by a sum of both components:

$$H_{ext} = \frac{H_{sw}^{+} + H_{sw}^{-}}{2}. \tag{5.5}$$

Such a method is particularly interesting for applications, since two values can be obtained from a single measurements: i) amplitude of axial (with respect to the wire's axis) magnetic field (that in some cases defines also the position of object) and ii) intrinsic switching field that is influenced by temperature, mechanical stress, etc...

5.2 Model for single domain wall potential

One of the simple and very usefull method to study the single domain wall potential is the measurements of the switching field distribution. Energy barrier ΔF (described above) can be overcomed even in the field lower than switching field either by thermal fluctuations (at high enough temperatures) or by tunnelling (at low temperatures) [188].

As it was shown in [64, 65, 187, 189, 190, 191], it is possible to estimate the dependence of the amplitude of energy barrier ΔF on applied magnetic field H.

In order to obtain the dependence of the energy barrier ΔF on the external magnetic field H, let us call x_0 the equilibrium position of the domain wall in the zero external magnetic field. The potential of the domain wall can be expanded as a function of the position x close to x_0 ($\Delta x = x - x_0$) as [189]:

$$W(x) = W_0 + W_0'.\Delta x + \frac{1}{2}W_0''.(\Delta x)^2 + \frac{1}{6}W_0'''.(\Delta x)^3, \tag{5.6}$$

where due to Δx smallness, 4th and higher power terms will be neglected. At the zero applied magnetic field, $H = 0$, the domain wall stays at position $x = x_0$ where the potential wall is minimum

$$W_0' = 0. \tag{5.7}$$

The giant Barkhausen jump occurs when the switching field, H_{sw}, is reached at

$$\frac{\partial F}{\partial x}|_{H=H_{sw}} = 0 \tag{5.8}$$

and

$$\frac{\partial^2 F}{\partial x^2}|_{H=H_{sw}} = 0. \tag{5.9}$$

It follows from Eqs. (5.7)−(5.9) that:

$$W_0'' = \frac{k^2}{\chi_0} \tag{5.10}$$

and

$$W_0''' = -\frac{k^2}{2\chi_0^2 H_{sw}}, \tag{5.11}$$

where χ_0 is the initial susceptibility of the domain wall at the zero external field and $k = 2\mu_0 M_s S_{dw}$.

The dependence of the energy barrier on the external magnetic field can be calculated by inserting Eqs. (5.6), (5.7), (5.10), and (5.11) into Eq. (5.1). In the local extreme of the free energy:

$$\frac{\partial^2 F}{\partial x^2}|_{H<H_{sw}} = 0. \tag{5.12}$$

The energy barrier $\Delta F(H)$ given by the difference between the local maximum and minimum of the free energy is:

$$\Delta F(H) = F_{max}(H) - F_{min}(H), \tag{5.13}$$

and taking into account Eqs. (5.1), (5.12), and (5.13), it can finally be expressed as:

$$\Delta F(H) = \frac{8}{3}\chi_0 \sqrt{H_{sw}}(\Delta H)^{3/2}, \tag{5.14}$$

where $\Delta H = H_{sw} - H$. The 3/2-power law has been also found when calculating the energy barrier dependence on the external magnetic field in [190, 192].

Due to thermal fluctuations of the switching field, its probability, dp, lies within the range between ΔH and $\Delta H + d(\Delta H)$ and is given by [191]:

$$dp = B \exp(-\Delta F/kT) d(\Delta H), \tag{5.15}$$

where B is a constant, and kT is a thermal energy. Inserting the field dependence of the energy barrier Eq. (5.14) into Eq. (5.15) and introducing the reduced fluctuation $\Delta h = \Delta H/H_{sw}$, a linear dependence of the logarithm of the probability density $\ln(dp/d(\Delta h))$ on the $(\Delta h)^{3/2}$ is found:

$$\ln(dp/d(\Delta h)) = \beta_h - \alpha_h (\Delta h)^{3/2} \tag{5.16}$$

where

$$\alpha_h = \frac{8}{3}\frac{\chi_0 H_{sw}^2}{kT} \tag{5.17}$$

$$\beta_h = \frac{2}{3}\ln(\alpha_h)\ln(2)\ln[y(\alpha_h)^{1/3}], \tag{5.18}$$

and

$$y(\alpha_h)^{1/3} = \int_0^{\alpha_h^{1/3}} z \exp(\alpha_h^{1/3}) dz, \tag{5.19}$$

The linear dependence in Eq. (5.16) will be very useful for the evaluation of the switching field distribution. Parameter α_h gives us information about the shape of the domain wall potential. If the switching field value H_{sw} is measured simultaneously with the distribution, the initial susceptibility χ_0 can be obtained which gives us information about the shape of the domain wall potential bottom.

5.3 Domain wall potential in glass-coated microwires

The probability of switching can be easily measured. In contrary to other methods [188,190,192] we have used continuously increasing applied magnetic field during measurement instead of a constant one. The problem during the data analysis arises from the fact that the measured distribution of the switching field does not represent the distribution of the probability of overcoming the barrier since the switching events are not independent. In our case, the probability $p(H^*)$ that the domain wall will overcome the energy barrier at the measured magnetic field H^* is given:

$$p(H^*) = \frac{p'(H^*)}{[1 - \sum p'(H \geq H^*)]}, \tag{5.20}$$

where $p'(H^*)$ is the probability that the switching occurs at the field H^* and quantity $[1 - \sum p'(H \geq H^*)]$ is the probability that the switching was not observed at lower field. Assuming also the frequency dependence of the model according to [191, 193], we finally obtain the probability density that the domain wall will overcome the barrier at the reduced magnetic field Δh:

$$\frac{dp}{d(\Delta h)} = \left[\sum_{k=1}^{k_m} \frac{N_k}{\sum_{i=k}^{k_m} N_i} \right]^{-1} \frac{N_k}{\delta h \frac{dH}{dt} \sum_{i=k}^{k_m} N_i}, \tag{5.21}$$

where N_k is a number of switching events from the interval $(H_k; H_{k+1})$, $\delta h = (H_{max} - H_{min})/k_m$, k_m is a number of divisions of the interval $(H_{min}; H_{max})$, and dH/dt is the sweep rate of the applied field. Equation (5.21) takes into account the fact that conditions for the appearance of large and small fluctuations are nonequivalent due to the experimental method.

The temperature dependence of the switching field distribution is shown in Fig. 5.3. The largest switching field and broadest distribution function are found at the lowest measuring temperature. With increasing temperature, the average switching field of the distribution shifts towards lower values and the distribution width notably decreases. These results are in contradiction to the model presented in [189, 192, 193].

Moreover, in contrary to a simple linear dependence evaluated in Eq. (5.16), a more complex form of the switching field distribution has been found in bistable microwires, that consists of two linear dependencies (see Fig. 5.4). Such discrepancy can be explained by a complex form of the domain wall potential. The unexpected form of the switching field distribution is supposed

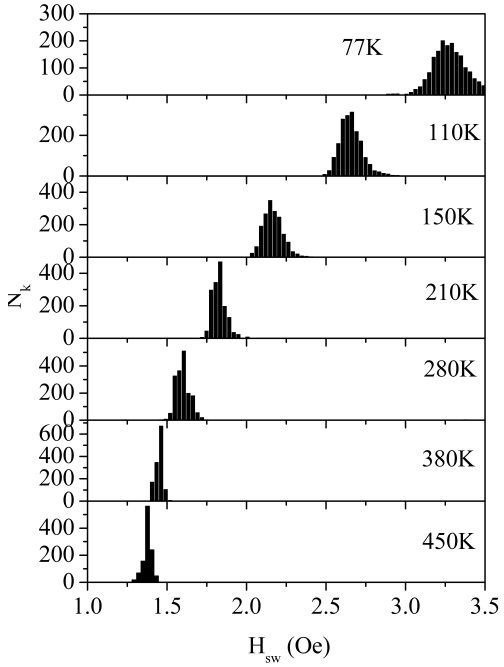

Fig. 5.3. Temperature dependence of the switching-field distribution function of the as-cast sample. N_k denotes number of the events at the given field [64].

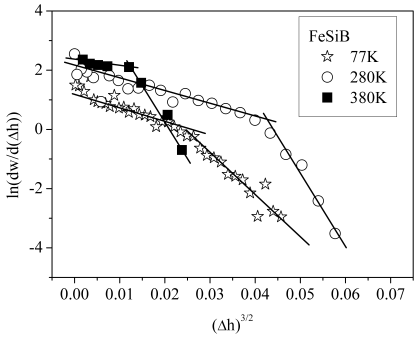

Fig. 5.4. Logarithm of the probability density of the switching-field fluctuations measured at different temperatures [64].

to be a result of the combination of long-range magnetoelastic pinning and short-range pinning coming from the structural relaxation of the atomic-scale defects [65].

The type of the domain structure in the magnetic materials is decided by long-range interactions which would be mainly represented by magnetoelastic ones in the case of glass-coated microwires. However, the exact position of the domain wall is given by the short-range interaction of the domain wall with local defects. The magnetoelastic contribution to the domain wall potential arises from the interaction of the closure domain walls with the residual stress existing within the microwires and stress centers that are present due to the amorphous structure of the wire. Its energy density is proportional to the magnetostriction through:

$$E_\sigma = \frac{3}{2}\lambda_s \sigma, \tag{5.22}$$

In our case, the total stress σ is given by the sum of residual intrinsic stresses introduced by the quenching and drawing during the microwires production and additional applied stresses arising from the different thermal expansion coefficient of the glass-coating and metallic nucleus. The short-range contribution to the domain wall potential arises from the interaction of the domain wall with the defects on the atomic level. Due to the interaction energy with the local spontaneous magnetization these mobile defects try to orient their anisotropy into the most favorable orientation. Amorphous alloys, in general, have a lower packaging density because of the steric misfit between atoms of different atomic radii. Therefore, even at low temperatures, small rearrangements of atoms are possible by jumps of atoms into the neighboring free volumes [39]. This leads to the stabilization of the domain wall position. The total interaction energy of the domain wall with the mobile defects, also called stabilization energy, can be expressed by Eq. (4.1).

Surely, there is another contribution to the long range potential coming from the magnetostatic energy which arises due to the decrease of the stray field energy by the formation of the closure domain structure as well as the shape anisotropy energy. But, as it was deduced from the temperature dependence of the switching field, their contributions can be neglected in comparison to the two above mentioned contributions.

As a result, the total free energy F of the single domain wall without the action of an applied field has a complex shape as schematically shown in Fig. 5.5. In the low magnetic field H_1 regime, the free-energy minimum is given by the shape of the stabilization potential coming from the short range pinning. At an intermediate field H_2, two local minima coexist in the free energy of the domain wall. This happens because of the specific shapes of two potentials. For a field close to the switching field, H_3, the second minimum disappears, but a small local minimum still exists coming from the pinning on the atomic-scale defect.

Based on this assumption, the specific shape of the probability density dependence on the reduced magnetic field can be explained. It has no linear dependence, but it consists of the addition of two linear dependencies as schematically depicted in Fig. 5.6. The slope of the linear curve is given at each temperature (according to Eq. (5.16)) by the susceptibility and coercivity (through the coefficient α_h) of the corresponding potentials.

Considering the thermally activated model [192, 193], the switching field distribution width, ΔH, should be a function of $T^{2/3}$. Nevertheless, the width of the distribution experimentally decreases with the temperature, which can be explained considering a temperature dependence of the switching field. Its value can be determined from the relationship [189]:

$$\Delta H = (1/\alpha_h)^{2/3} C.H_{sw}, \tag{5.23}$$

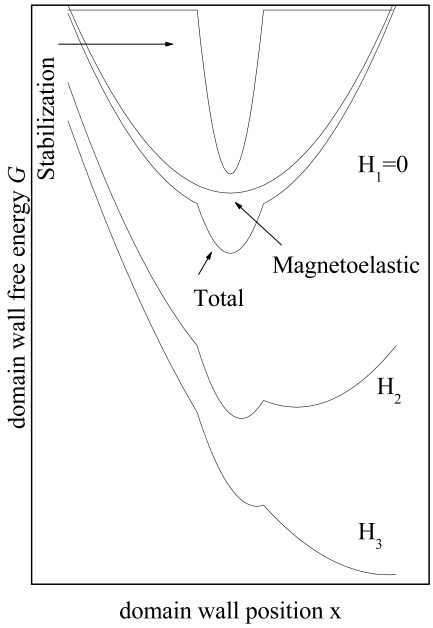

Fig. 5.5. Dependence of the free energy of the closure domain wall on its position (under the action of the external applied magnetic fields $H_1 < H_2 < H_3$). The arrows point to the local minima that appear [187].

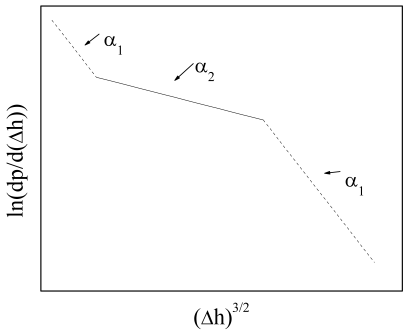

Fig. 5.6. Theoretical dependence of the probability density on the reduced magnetic field [65].

where C is a constant parameter. In the first approximation, the distribution width is proportional to the coercivity (see Fig. 5.7), where the temperature dependence of α_h has been neglected.

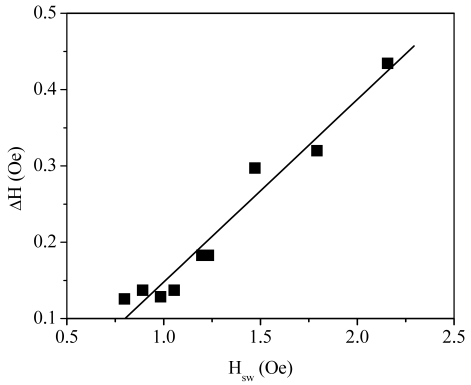

Fig. 5.7. The dependence of the switching field distribution width ΔH on the switching field H_{sw} measured at different temperatures [65].

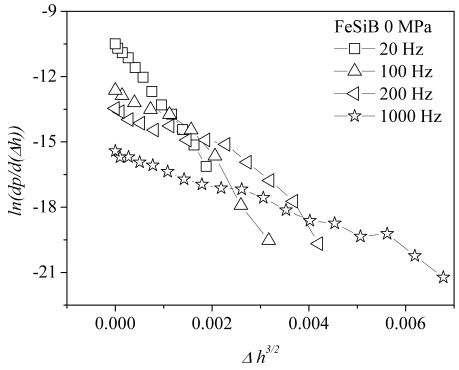

Fig. 5.8. Probability density as a function of the reduced field $\Delta h^{3/2}$ measured at different frequencies without applied load [187].

The exact role of each particular contribution to the domain wall potential in glass-coated microwires has been identified by the series of experiments under applied stress (to enhance the magnetoelastic contribution) as well as at various frequencies (to enhance the evolution of the time-dependent relaxation contribution) [187].

The probability density as a function of the reduced magnetic field measured at different frequencies is given in Fig. 5.8. At low frequency, when the time of the measurement is long enough to the evolution of the structural relaxation contribution to the domain wall potential, a linear dependence is found as seen in Eq. (5.16). In such cases, the relative strength of the

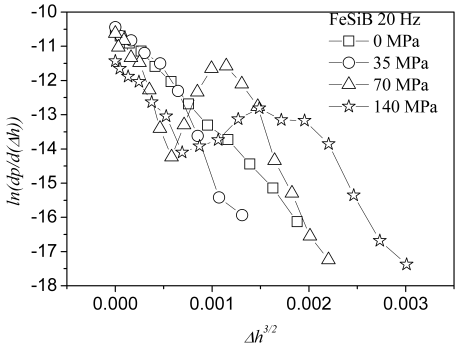

Fig. 5.9. Probability density as a function of the reduced field $\Delta h^{3/2}$ measured at frequency 20 Hz with applied load [187].

stabilization potential is high enough, so the second local minimum (shown in Fig. 5.5) does not appear. When the time for relaxation decreases (higher frequency 100 and 200 Hz), a nonlinear behavior was found. This is a result of the appearance of the second local minimum in the position dependence of the domain wall free energy (Fig. 5.5) when the external magnetic field is applied. The shape of the probability density as a function of $\Delta h^{3/2}$ depends on the relative strength of a particular contribution. At lower fields, the domain wall free-energy minimum is given by the sum of two contributions: magnetoelastic and relaxation ones. At medium fields, the second minimum appears, which is given only by the magnetoelastic contribution. Here, the probability to overcome the complex barrier p is given as a product of both probabilities p_1, p_2 that the particular barriers will be overcome ($p = p_1.p_2$). Therefore, the slope of the probability density decreases. Finally, at the fields close to the switching fields, the free-energy minimum is given again by the sum of two contributions. At a high frequency (1000 Hz), the time of the measurement is too short for the defects to stabilize the domain wall and the domain wall potential is given almost by a simple magnetoelastic interaction. A small portion of stabilization is visible at high fields ($\Delta h^{3/2} \rightarrow 0$), close to the switching fields. The slope α_h measured at high frequency is the same as the intermediate slope measured at 100 or 200 Hz.

By applying stress, the magnetoelastic contribution becomes more important (Fig. 5.9). The second local minimum that appears in the position dependence of the domain wall free energy is deep which results even in the decrease of the probability density with the increasing field (note that field increases when Δh decreases). By increasing the applied stress, the relative strength of the magnetoelastic contribution is more important and the effect is more visible.

The evolution of the relaxation contribution under applied stress (Fig. 5.10) will help us to understand the shape of the probability density. At low frequency, when the relaxation is developed, the slope of the probability density is the same at low fields, as well as at the fields close to the switching fields. The decrease of the probability density occurs only at intermediate fields, when the second maximum in the domain wall free energy appears. By increasing the frequency of the measurements, the shoulder appears at intermediate fields, that has a slope

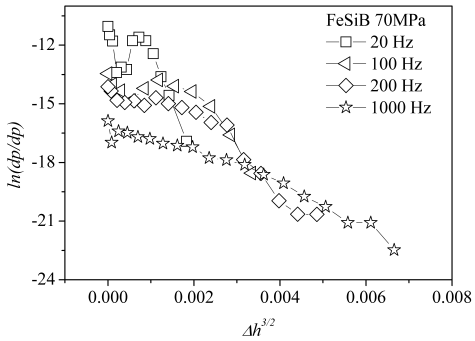

Fig. 5.10. Probability density as a function of the reduced field $\Delta h^{3/2}$ measured at different frequencies with applied load 70 MPa [187].

similar to the slope of the probability density at 1 kHz. Moreover, the strength of the minimum in the probability density decreases and almost disappears at 1 kHz when the relaxation has no time for development.

6 Dependence of the switching field on external parameters

The two contributions to the domain wall potential in glass-coated microwires results in two contributions to the switching field. Let us first consider that during fabrication, glass-coated microwires undergo large internal stresses. They are generated during quenching due to thermal gradient, drawing stresses and additionally from the Pyrex cover as a consequence of the different thermal expansion coefficient of insulating coating and metallic nucleus. Since the Fe-based microwires have large magnetostriction, it is reasonable to assume, that the switching field will be driven mostly by the magnetoelastic interaction between internal stresses σ and the domain walls at the closure structure at the ends. The magnetoelastic contribution to the switching field, H_{sw}^{σ} can be expressed as [194]:

$$H_{sw}^{\sigma} \approx \frac{\sqrt{3A\lambda_s\sigma}}{M_s}. \tag{6.1}$$

On the other hand, as a result of the fabrication technique, the structure of amorphous wires is in metastable state and for this reason quite large relaxation effects can be expected. Due to this relaxation phenomena, an additional magnetic field is required in order to push the domain wall out of its position. This additional pinning field is known to contribute significantly to the total coercive field [197]. For relaxation effects due to local structural rearrangements, the pinning field contribution H_{sw}^{p} is obtained from Eq. (4.1):

$$H_{sw}^{p} \approx \frac{1}{M_s}\frac{\left\langle (\epsilon_{eff}^2) \right\rangle c_0}{kT} G(t,T). \tag{6.2}$$

These are the two strongest contributions to the switching field. They define magnetic properties of amorphous glass-coated microwires. As will be shown below, they are sufficient to describe most of variations of the switching field with external parameter.

6.1 Frequency dependence of the switching field

The simple frequency dependence of the coercivity was previously found in magnetic wires or ribbons [198,199]. It was shown that the magnetoelastic contribution to coercivity in amorphous wires at low frequency f can be expressed as:

$$H_{sw}^{\sigma} = H_{c_0} + const(f.H_A)^{1/n}, \tag{6.3}$$

where H_{c_0} is the static coercivity, H_A is the amplitude of the applied field, and n is a coefficient ranging from 1 to 3 depending on the geometry and hysteresis mechanism of the materials. It was theoretically estimated [198] to be:

- 1 in case of small domain wall mass, m_{dw}, and small measuring frequencies
- 3/2 in case of small stiffnes coeficient, α (see Eq. (3.1)) and large measuring frequencies
- 2 in case of of small stiffnes coeficient, α and small measuring frequencies
- 3 in case of small domain wall mass, m_{dw}, and large measuring frequencies

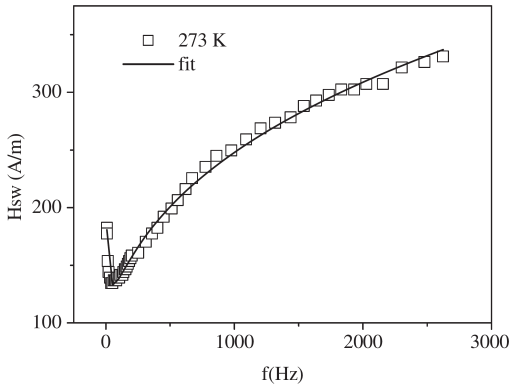

Fig. 6.1. Frequency dependence of the switching field in amorphous glass-coated FeNiMoB microwire [200].

However, our measurement in the FeNiMoB microwire showed a more complex frequency dependence of the switching field (Fig. 6.1 [200]). A similar dependence was also found in [201, 202]. It consists of two parts: at low frequencies the switching field decreases with increasing frequency; in the frequency range above 50 Hz the switching field depends on $f^{1/3}$, fitting well the calculations for small domain wall mass [198]:

$$H_{sw}^{\sigma} = (1/3)H_{c_0} + [4x_{cr}(\beta + 2M_s D)/M_s](4fH_A)^{1/3}, \tag{6.4}$$

where x_{cr} is the critical displacement of the domain wall to be depinned. The field from the micro-eddy current is proportional to $D(dx/dt)$ (D is proportionality constant).

On the other hand, the decrease in the coercivity at low frequency can be explained satisfactorily in terms of structural relaxation [197, 203]. As a result of their preparation, the structure of amorphous wires is associated with the metastable state of the amorphous structure, and for this reason quite large relaxation effects can be expected. As the measuring frequency decreases, the measuring time increases and a stabilization of the domain structure through structural relaxation takes place. Such an effect has already been observed for domain wall potential study in amorphous glass-coated microwires (see Section 5.3).

To confirm the origin of both contributions, the temperature and stress effect on the switching field were measured [200]. The slope of the high-frequency part increases with the temperature (Fig. 6.2), reflecting the changes in saturation magnetization M_s (which decreases with temperature) as well as the critical displacement of the domain wall x_{cr} (see Eq. (6.4)). This is a result of changes accompanied by the application of tensile stress arising from the different thermal expansion coefficients of the metallic nucleus and the glass-coating. Such a change reflects the stress dependence of the frequency-independent magnetoelastic part, H_{c_0}, of H_{sw}. The lower is the temperature, the higher are the stresses σ and the higher is the H_{c_0} ($H_{c_0} \sim (\lambda_s \sigma)^{1/2}$). On the other hand, the relaxation contribution changes as a result of the change in relaxation time. The relaxation time decreases with temperature according to the Arrhenius law given by Eq. (3.11). Therefore, the minimum in the frequency dependence of the switching field shifts to

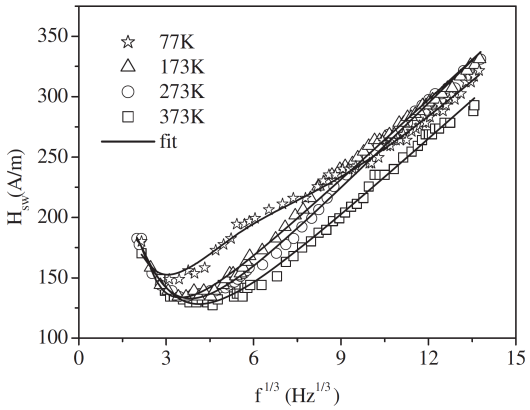

Fig. 6.2. Frequency dependence of the switching field in amorphous glass-coated FeNiMoB microwire. Temperature as a parameter [200].

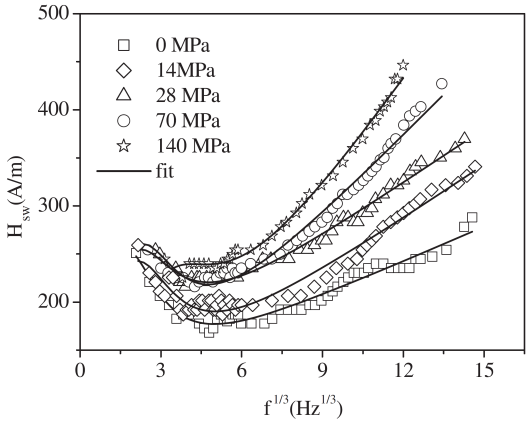

Fig. 6.3. Frequency dependence of the switching field in amorphous glass-coated FeNiMoB microwire. Applied tensile stress as a parameter [200].

higher frequencies at higher temperatures. Using the pre-exponential factor $\tau_0 = 5 \times 10^{16} s$ found for relaxation measurements in the ribbon of the same composition, we obtain the activation energies 0.26, 0.59, 0.93 and 1.27 eV for the temperatures 77, 173, 273 and 373 K, respectively. These activation energies belong to the range of activation energies found for the ribbon of the same composition (0 - 1.7 eV) [169].

On the other side, applying stress has almost no influence on the relaxation contribution (Fig. 6.3). The relaxation time and the amplitude of the structural relaxation, obtained by fitting, are almost the same for all measurements. This is because the relaxation time is not influenced strongly by the applied stress. However, the magnetoelastic contribution, which is defined by the stress applied on the sample, increases. Firstly, an increase in the frequency-independent part of the switching field H_{c_0} (see Eq. (6.4)) is observed at low applied tensile stress (below

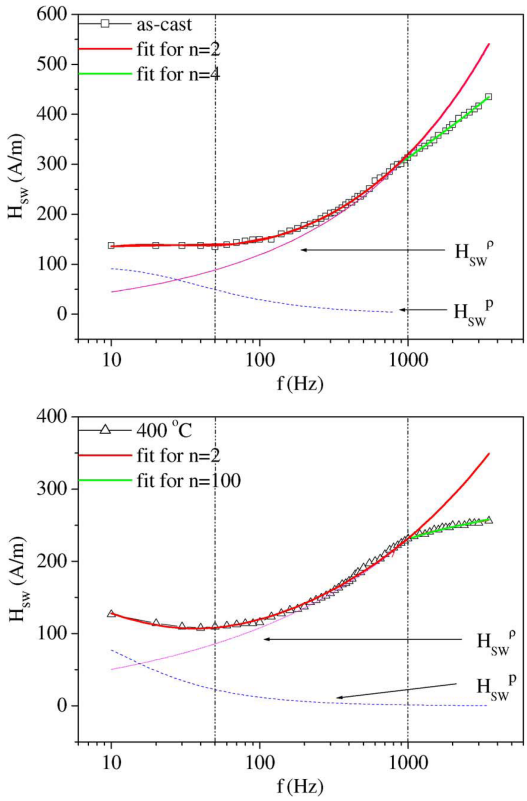

Fig. 6.4. Frequency dependence of switching field in amorphous and annealed at 400°C FeCoMoB microwire consists of three different regions [202].

30 MPa), whereas the slope of the frequency dependence changes slightly. At higher applied stresses, the slope of the frequency dependence increases, most probably because of the increase in the damping coefficient β [108, 204]. However, the simple model cannot describe all cases. Figure 6.4 shows the frequency dependence of the switching field measured in amorphous and nanocrystalline FeCoMoB microwire. In contrary to previous results described above, three frequency ranges are recognized. The relaxation contribution prevails at low frequency and could be neglected above 1000 Hz. In contrary, magnetoelastic contribution increases with the frequency and is dominant above 30 Hz. The fitting for medium frequency range (50-1000 Hz) gives parameter n to be equal to 2, which fits condition of small stiffnes constant α and low excitation frequencies f [198]. Anisotropy of amorphous and nanocrystalline microwires is quite low (therefore, α is low) in comparison to that of crystalline materials. Thus, we can express magnetoelastic contribution in the case small anizotropy and low frequency of applied field [198]:

$$H_{sw}^{\sigma} = H_{c_0} + 4D[H_A(x_{cr}M_s/\beta + 2M_sD)]^{1/2}(f)^{1/2}. \tag{6.5}$$

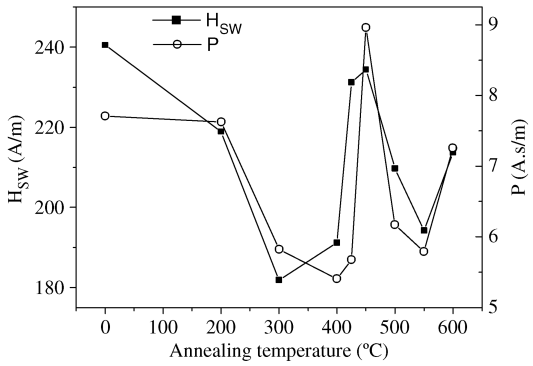

Fig. 6.5. Dependence of the switching field in amorphous and nanocrystalline FeCoMoB microwires (measured at 500 Hz) and the proportionality constant P on the annealing temperature [202].

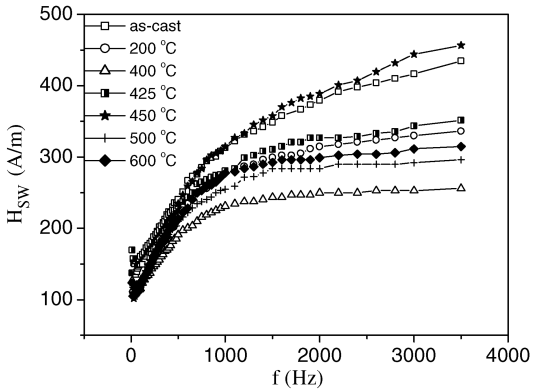

Fig. 6.6. The frequency dependence of switching field in amorphous and nanocrystalline FeCoMoB microwires. Temperature of annealing as a parameter [202].

The situation is different at the frequencies above 1 kHz (see Figs. 6.4 (up) and (down)). The relaxation contribution has no influence in this range and fitting the data with Eq. (6.3) gives parameter n=4, which has no physical meaning according to the theory given in [198]. However, it reflects somehow the structure of studied microwires as will be shown below.

Annealing of the microwire within the temperature range from 200 to 400° leads to the partial relaxation of stresses induced during fabrication and as well as partial homogenization of sample. As a result, the switching field is reduced (Fig. 6.5). The frequency dependence still consists of three regions (Fig. 6.6), however, the magnetoelastic contribution decreases. This is confirmed also by the decrease of the proportionality constant P obtained from Eq. (6.5):

$$P = 4D[H_A(x_{cr}M_s/\beta + 2M_sD)]^{1/2}. \tag{6.6}$$

Annealing at 425°C leads to a precipitation of crystalline phase (see also Section 4.7.7). However, the precipitates are small and the distance between them is large. Hence, they play a role of the pinning centers for the domain wall displacement and the switching field increases. The proportionality constant P increases, too.

After annealing at 450°C , nanocrystalline state is already formed, where FeCo crystalline grains appears. However, the filling of the space by nanocrystalls is low and they still can play a role of the pinning centers for the domain.

Annealing of the microwire at the temperatures above 450°C results in homogenization of the microwire. Its structure consists of crystalline grains embedded in the amorphous residual matrix. Random distribution of their easy axis together with their exchange interaction leads to the vanishing crystalline anisotropy. In addition, the switching field decreases as a result of homogenization and so does the proportionality constant P, too (Fig. 6.5).

A similar behaviour of proportionality constant P and switching field H_{sw} with the annealing temperature could tell us something about the most important parameters that controls P. Taking into account that switching field H_{sw} is proportional to critical displacement x_{cr} (Eq. (5.3)):

$$H_{sw} = \alpha x_{cr}, \tag{6.7}$$

one can assume, that the change of P with annealing is driven mainly by the change of the critical displacement of the domain wall x_{cr}. A small deviations could be ascribed also to the change of the damping coefficient β (as it was found in [182]) or small change of saturation magnetization M_s [184].

In the high frequency range (above 1 kHz), it is not possible to fit the switching field with Eq. (6.3) with reasonable parameter ($n \geq 4$). However, such fitting reveals some information about the homogeneity of the structure of microwire. We have obtained $n = 4$ for as-cast sample (that contains high stresses introduced during production) and for that annealed at 450°C (where homogeneity is destroyed by the large distance between the crystalline grains). On the other hand, the fitting for the homogeneous samples (where also the decrease of the switching field reveals homogenization) gives $n = 100$, which results to a quite weak frequency dependence of in this frequency range (Fig. 6.6). One possible explanation could be a change of the domain wall structure. Two different domain wall structures has been assumed in amorphous microwires: transversal one at low fields and vortex one at higher magnetic fields [182, 183]. Let us assume that the different domain wall has a different frequency dependence of the switching field. The pinning field of the transversal domain wall is lower then the nucleation field of the vortex one, but it has steeper frequency dependence. When the switching field of the transversal domain wall exceeds the nucleation field of the vortex one, the domain wall changes (as in the case of the domain wall dynamics [182]) and different frequency dependence could be observed. However, this is only a hypothesis and more measurements are in progress in order to get full understanding of frequency dependence of the switching field in whole range.

Anyway, the existence of different frequency ranges, where different contributions play major role, gives us possibility to tailor the temperature and stress dependence of the switching field that could be succesfuly employed in the multifunctional sensoric applications.

6.2 Temperature dependence of the switching field

The two contributions to the domain wall potential in glass-coated microwires have different temperature dependence.

Firstly, the temperature dependence of magnetoelastic contribution is given by the mechanical stresses σ applied on metallic nucleus and temperature dependence of saturation magnetostriction λ_s and saturation magnetization M_s. In case of amorphous glass-coated microwires the temperature dependence of stresses σ is given:

$$\sigma = \sigma_a(T) + \sigma_r, \tag{6.8}$$

where σ_r are residual intrinsic stresses coming from quenching and drawing, and $\sigma_a(T)$ are the stresses which presently depend on the temperature and arise from the different thermal expansion coefficients of the glass and of the metallic nucleus (see Eq. (4.24)).

As early found in previous works [195], the temperature dependence of the magnetostriction of amorphous alloys can be described by the so-called scaling laws:

$$\lambda_s = cM_s^k. \tag{6.9}$$

Here, c is a constant and the power exponent k depends on the mechanism of magnetostriction and is expected to take value of 3 for Fe-based amorphous alloys, when the magnetostriction originates from a single-ion anisotropy of uniaxial character and 2 for Co-based amorphous alloys, when where the magnetostriction originates from an anisotropic two-ion exchange contribution of uniaxial symmetry [196]. Thus, Eq. (6.1) can be simplified into the form:

$$H_{sw}^{\sigma} \approx lM_s^{k/2}(T)(1 + r(\Delta T))^{1/2}. \tag{6.10}$$

Here l is a constant proportional to residual stress σ_r and r is proportional to the difference between the thermal expansion coefficient of metallic nucleus and glass-coating ($r \sim E_Y(\alpha_g - \alpha_m)/\sigma_r$).

On the other hand, temperature dependence of structural relaxation contribution to the switching field is given mainly by its proportionality to the reciprocal value of thermal energy ($H_{sw}^p \sim 1/kT$), temperature dependence of the saturation magnetization M_s and temperature dependence of the relaxation time given by Arrhenious law (Eq. (3.11)). Finally, the temperature dependence of the structural relaxation contribution is given:

$$H_{sw}^p \approx o\frac{F(t,T)}{M_s T}, \tag{6.11}$$

where $o \sim \left\langle (\epsilon_{eff}^2) \right\rangle c_0/k$.

As both contributions to the switching field have very different temperature dependence, this gives us possibility to tailor the temperature dependence of total switching field in glass-coated microwires according to desired conditions. In next paragraphs, few ways how to do it are introduced.

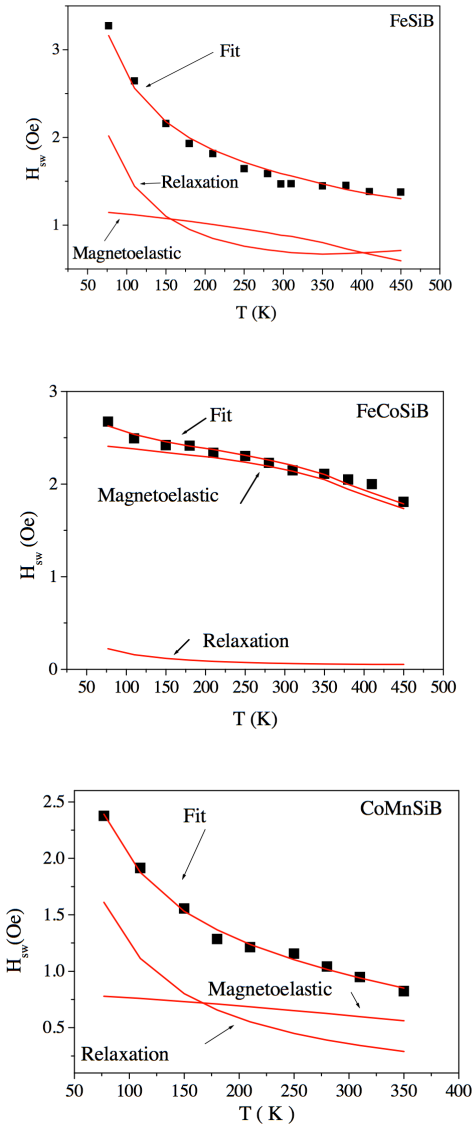

Fig. 6.7. Temperature dependence of switching field for 3 different (FeSiB, CoFeSiB, CoMnSiB) amorphous glass-coated microwire [205].

6.2.1 Effect of chemical composition

One possibility to tailor the temperature dependence is to select appropriate chemical composition. Figure 6.7 shows the results for 3 different chemical compositions that differs by the relative

amplitude of both contributions to the switching field [205].

The switching field distribution of the amorphous FeSiB microwire has strong increase of the coercivity at low temperature, which can be ascribed to the increase of the relaxation time of the mobile atomic defects. They loosing their mobility and increases the local anisotropy. With increasing the temperature, the mobility of the defects increases and the coercivity decreases. Above 170 K, the magnetoelastic pinning dominates in the coercivity mechanism because of high saturation magnetization of FeSiB composition. In this case, the switching field decreases to its half amlitude in the temperature range 80-450 K.

The different situation is in the amorphous FeCoSiB microwire, where magnetoelastic pinning dominates over all temperature range. The contribution from structural relaxation is ten times smaller then magnetoelastic one and can be registered only at lowest temperatures as a small increase of coercivity. It was found on the ribbons of the similar composition [206] that low temperature relaxation has very small effect on the coercivity in amorphous FeCoSiB alloys with the same compound of Fe and Co. The high temperature annealing is necessary to see the effect of magnetic relaxation in this ribbon [207]. In the case of FeCoSiB microwire, the switching field decreases almost linearly by one quarter of its value in the temperature range 80-450 K

In the case of the amorphous CoMnSiB microwires, which has the smallest magnetostriction from the observed microwires, the structural relaxation contribution also dominates at low temperatures. At higher temperatures the magnetoelastic pinning is prevailing, but the pinning on atomic scale defects is still comparable. Here, the switching field is most sensible to the temperature and it decreases by 60% in the whole temperature range.

Since the most important anisotropy that determines the magnetic properties of glass-coated microwires is magnetoelastic, stress distrbution will be one of the most important parameters (among the saturation magnetostriction, λ_s) to control the temperature dependence of the switching field.

The influence of the stress distribution on the magnetic domain structure can be successfully studied by the magnetization measurement [163]. Assuming the domain structure given in Fig. 2.4, the saturation magnetization corresponds to the magnetization of the whole microwire, whereas remanent magnetization corresponds to the magnetization of the axial domain. Hence, one can estimate the radius of axial core domain as well as thickness of the radial domain structure that defines the relative strength of axial and radial stresses introduced on metallic nucleus.

The temperature dependence of both magnetizations and for FeNiSiB microwire is given in Fig. 6.8. The saturation magnetization decreases with the temperature (as typically) due to thermal activation of magnetic moments. The temperature dependence of remanent magnetization, M_r, varies in a non-monotonous way with temperature, reflecting the change of the stress distribution in the microwire. In order to explain the variation of with temperature, the stresses (either axial or radial), introduced by the different thermal expansion coefficient of metallic nucleus and the glass coating, should be taken into account (see Eq. (4.24)).

At high temperatures, the stresses are minimal. When the temperature decreases, the stresses introduced by glass coating increase. In the temperature range from 400 down to 200 K, the axial stresses prevail resulting in the increase of the axial domain volume and increase of . Further decrease of temperature down to 10 K favours the radial stresses, which are connected to the increase of the radial domain structure at the temperature below 200 K and the decrease of M_r. The temperature effect of the induced stresses is the strongest for 35 at.% of Ni, whereas for

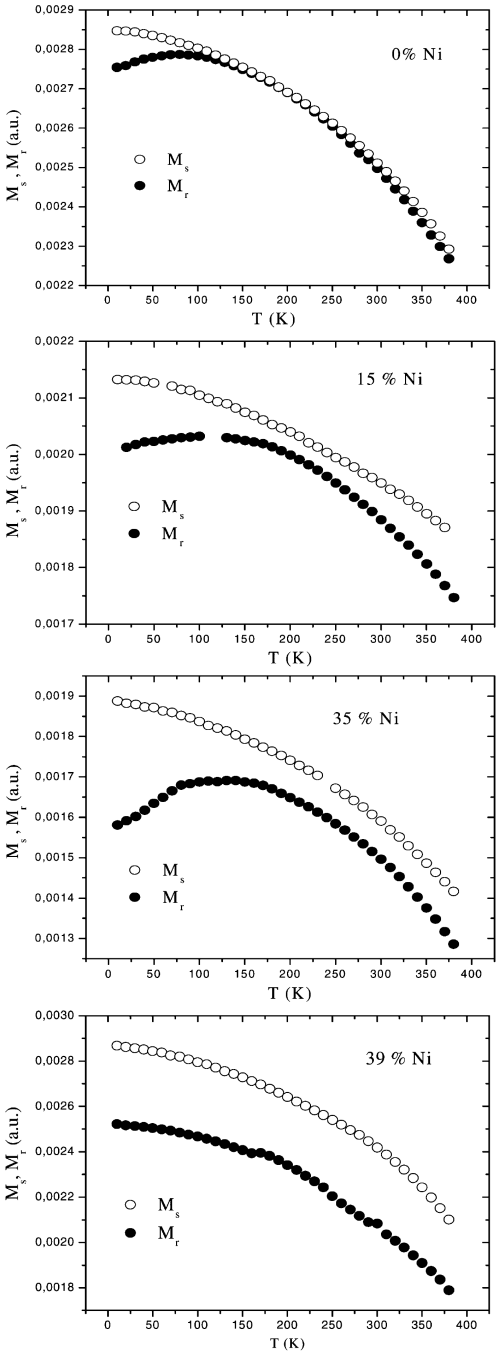

Fig. 6.8. Temperature dependence of saturation M_s and remanent M_r magnetization for $Fe_{77.5-x}Ni_xSi_{7.5}B_{15}$ microwires. The difference between them corresponds to the magnetic moments from the radial domain structure [163].

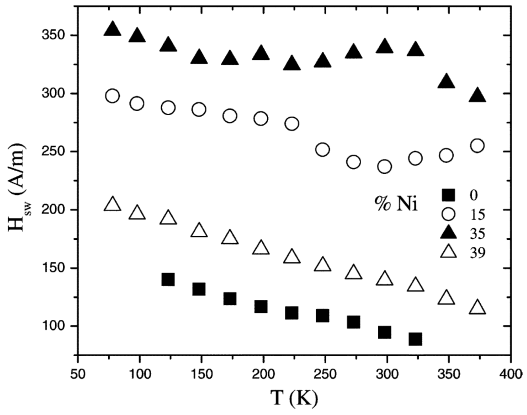

Fig. 6.9. Temperature dependence of the switching field for $Fe_{77.5-x}Ni_xSi_{7.5}B_{15}$ microwires [163].

39 at.% of Ni the radial domain structure almost does not change. Here, the compositional dependence of thermal expansion coefficient with change of Ni content should be taken into account. In pure (without Si and B) crystalline Fe-Ni alloys, the minimum thermal expansion coefficient appears for 35 at.% of Ni and it increases when the Ni content decreases [74].

The stress distribution in amorphous glass-coated microwires strongly affects their magnetic properties. The temperature dependence of the switching field for selected microwires is given in Fig. 6.9. Generally, the switching field decreases with temperature for all microwires, reflecting the relief of the stresses induced by the glass-coating. Small deviations from the monotonous decrease of the switching field for microwires with 15 and 35 at.% of Ni could be ascribed to the structural relaxation.

Another possibility how to improve the temperature dependence of the switching field is to employ the alloys with high stability and low Curie temperature. Typical example is Fe-CrSiB microwire [208]. Studied composition has some specific properties. Firstly, addition of Cr decreases magnetostriction and also the Curie temperature. The Curie temperature has been reported to be 398 K, close to room temperature, in amorphous ribbons with the same chemical composition as the studied microwires [209]. However, the Curie point of the amorphous microwire will be higher due to strong internal stresses introduced during production process [210]. Small Curie temperature increases the sensitivity of the switching field to the external parameters (like temperature, stress) at room temperature. Secondly, addition of chromium stabilizes amorphous structure (due to the higher Cr affinity to B atoms) [211] that is highly desirable for practical applications. As a result, the stress distribution will also show high structural stability in a wide range of temperatures as confirmed from magnetization measurements (Fig. 6.10) [208]. Saturation magnetization M_s decreases slowly with temperature reflecting the thermal activation of magnetic moments. The same is valid for remanent magnetization M_r. However, the difference between M_s and M_r is not constant within the whole temperature range (10-380 K) and slightly decreases with increasing temperature. The diameter of the axial monodomain decreases with increasing the measuring temperature. This is understood to be a consequence of

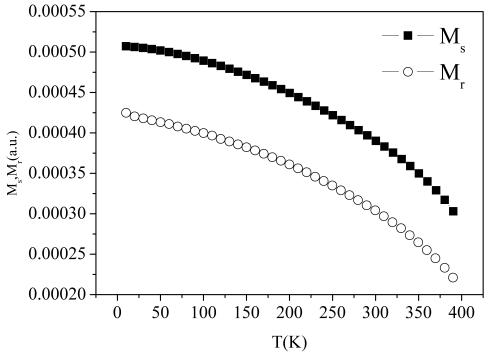

Fig. 6.10. Temperature dependence of saturation M_s and remanent M_r magnetization for FeCrSiB microwire shows high stability of stress distribution and weak decrease of radial domain structure thickness [208].

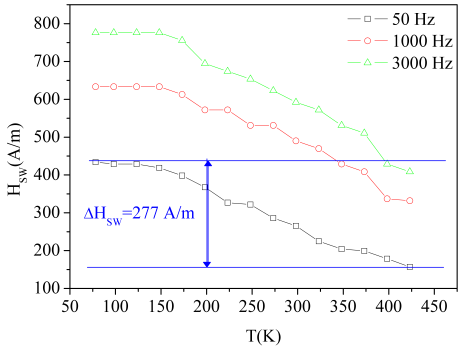

Fig. 6.11. Temperature dependence of the switching field of amorphous FeCrSiB microwire measured at selected frequencies (50Hz, 1000 Hz and 3000 Hz) [208].

the changing axial stresses applied on the metallic nucleus by glass coating at low temperatures (Eq. (4.24)).

These features results in a strong and almost linear temperature dependence of the switching field in a wide temperature range from 125-425K (Fig. 6.11) [208]. Generally, the switching field decreases with temperature, reflecting the relief of the stresses induced by the glass-coating due to different thermal expansion coefficient comparing to metallic nucleus. Here, the temperature dependence of the switching field is enhanced by the low value of the Curie temperature. Close to the Curie temperature, the anisotropy decreases steeply and this results in an enhancement of the switching field reduction. Finally, the switching field decreases from 428 A/m at 125 K

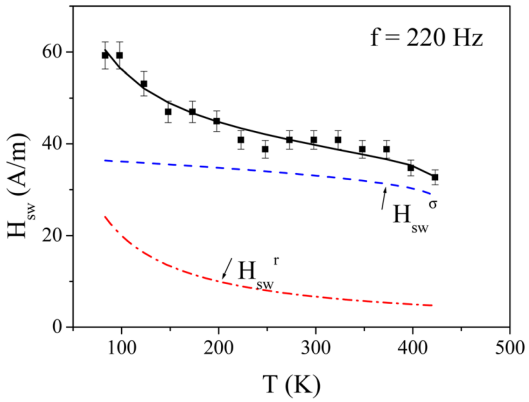

Fig. 6.12. Temperature dependence of the switching field measured at 220 Hz. Full lines correspond to the fit according to Eq. (6). [212].

down to 157 A/m at 425 K. So, it shows a variation of almost 200% compared with the high temperature value. As previously shown, the temperature dependence of the switching field in amorphous microwires can be tuned by the frequency of the applied field [212], as a result of the different frequency dependence of both contributions to the switching field. In the case of FeSiBCr microwire, the temperature dependence of the switching field is not influenced by the frequency since the structural relaxation contribution is very small.

6.2.2 Effect of frequency

As given above, the switching field is usually sensible to the frequency of applied magnetic field as a result of two contributions to the domain wall potential. Since both contributions have also different temperature dependence, such an effect can be employed to control the temperature dependence of the total switching field. However, one must properly choose the chemical composition. Amorphous FeNbSiB microwires shows high structural relaxation even at low temperature and sufficiently large saturation magnetostriction to see an effect. Therefore, the two contributions to the switching field are comparable and can be used to tune the temperature dependence of the switching field. [212].

Figure 6.12 shows the temperature dependence of the switching field measured at medium frequency of 220 Hz. Two contributions (magnetoelastic and structural relaxation) are well recognized having different temperature dependencies. The magnetoelastic contribution (H^{σ}_{sw}) decreases with the temperature concavely whereas the relaxation contribution (H^{r}_{sw}) shows convex increase at low temperature. Consequently, by tuning the frequency of applied magnetic field one can tune the temperature dependence of the total switching field. At low frequencies (50 Hz), the switching field is low and decreases firstly at low temperatures but is temperature independent in the range from 270 to 370 K (Fig. 6.13). It is because at low frequencies the structural relaxation contribution is not negligible (see Section 6.1) and defines the temperature dependence of the switching field (see the temperature dependence of the H^{r}_{sw} in Fig. 6.12).

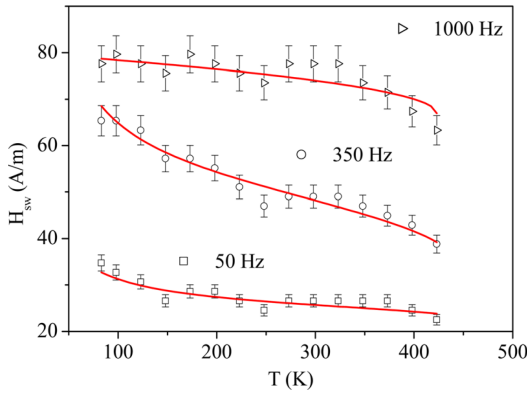

Fig. 6.13. Temperature dependence of the switching field measured at various frequencies of applied magnetic field. Lines represents the fits according to Eqs. (6.1) and (6.2) [212].

On the other hand, high frequency (1000 Hz) temperature dependence shows almost temperature independent range up to 325 K that is followed by the decrease of the switching field. At higher frequencies, the structural relaxation vanishes (see Section 6.1) and the overall temperature dependence of the switching field is given by the temperature dependence of its magnetoelastic contribution. The discrepancy between the fit and experimental data at highest temperature can be ascribed to the temperature dependence of saturation magnetization and magnetostriction that has not been taken into account here. The saturation magnetostriction should decrease with the temperature following the temperature dependence of magnetization through the power law.

At intermediate frequencies, both contributions contribute to the temperature dependence of the switching field in amorphous microwires. In such a way, almost linear dependence of the switching field on the temperature can be obtained by measuring at 350 Hz (Fig. 6.13).

Such behaviour can be employed in multifunctional contact-less sensor, in which the function of the sensor can be selected by frequency of measuring field. At low frequency (50 Hz), the magnetic field can be sense (see Section 5.1) and thermal stability is increased in the range 270 to 370 K by temperature insensitivity of the switching field , whereas at medium frequency (350 Hz) the switching field is sensible to the temperature and can be employed to sense the temperature.

6.2.3 Effect of thermal treatment

The switching field sensitivity on temperature can also be tailored by thermal treatment.

Fig. 6.14 shows the temperature dependence of the switching field for as-cast and thermally treated FeCoMoB microwire [213]. Due to the production process (rapid quenching, drawing), there is a complex stress distribution of the stresses induced in as-cast microwires. Therefore, the temperature dependence of switching field is also complex. Firstly, it decreases at low temperature, then it rises, close to the 300 K, showing discontinuos behaviour at high temperatures. Such temperature dependence can be understood taking into account the complex stress distribution

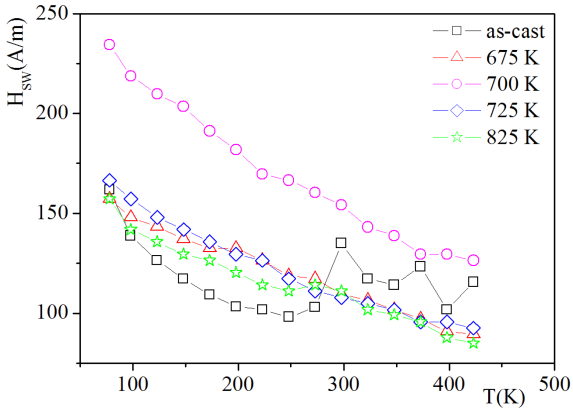

Fig. 6.14. Temperature dependence of switching field for heat-treated FeCoMoB microwire. Annealing temperature as a parameter [213].

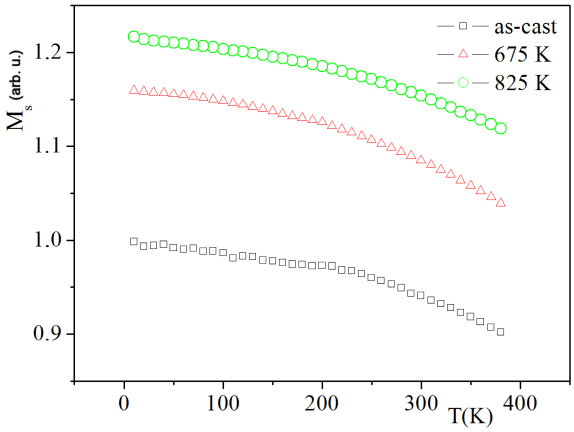

Fig. 6.15. Temperature dependence of saturation magnetization for heat-treated FeCoMoB microwire. Annealing temperature as a parameter [213].

and the additional stresses applied on microwire due to a different thermal expansion coefficient of metallic nucleus, α_m, and glass-coating, α_g. Varying the temperature of microwires, the complex stress distribution in as-cast microwires varies, too.

Similar behaviour can be found from the measurement of saturation magnetization M_s (see Fig. 6.15) [213]. Small discontinuities in the saturation magnetization are visible at low temperatures. The temperature dependence of magnetization is not smooth reflecting the changes in the complex stress distribution due to stress arising from glass coating. However, the applied field of 1 T is strong enough to saturate the sample and such laborious behaviour is observed

only below 200 K. At higher temperature, the temperature dependence of M_s is smooth. Annealing of microwires at 675 K leads to the stress relaxation and homogenization of the stress distribution in microwires. However, this temperature is still low enough for microwires to be amorphous [129]. The main anisotropy that determines magnetic properties of amorphous microwires is magnetoelastic one. Hence the homogenization of the stress distribution leads to the smooth temperature dependence of the switching field. It decreases with a temperature following the decrease of the stress σ applied on microwire by glass-coating due to the change of temperature (see Eq. (4.24)). Moreover, the above-mentioned annealing (together with homogenization of the stress distribution) leads to the increase of M_s, which has also very smooth temperature dependence.

Annealing at 700 K leads to an increase of the switching field. It was found that crystallization process starts close to this temperature [129]. However, crystalline precipitates are small, having a long distance between them. Hence, they act the role of the pinning centers for the domain wall and it results in the increase of H_{sw} (Fig. 6.15). Annealing at the temperatures higher than 700 K leads to the appearance of nanocrystalline structure that is characterized by the small crystalline grains (smaller than exchange length) embedded in amorphous matrix. Exchange interaction of crystalline grains leads to the averaging out of magnetocrystalline anisotropy that results in a magnetic softness (switching field decreases). FeCoMoB composition was selected due to its positive magnetostriction in order to obtain bistable hysteresis loop. Therefore, the temperature dependence of H_{sw} is driven mainly by magnetoelastic interaction of magnetic moments with the stress applied due to the glass-coating. The nanocrystalline FeCoMoB microwire is as soft as the amorphous one after the stress relaxation (by annealing at 675 K). The advantage of FeCoMoB composition is that magnetic softness obtained by annealing is almost independent on the temperature of annealing within wide range of temperatures 725 - 875 K [129]. The temperature dependence of H_{sw} is also similar for different temperature of annealing within this range. However, its structural stability of nanocrystalline microwires is much higher even at high temperatures. Moreover, the saturation magnetization of nanocrystalline microwires is higher than that of amorphousone (Fig. 6.15).

Such treatment brings material that is easy to prepare (the annealing temperature do not need to be controlled very precisely) and variation of the switching field is reasonable (over 70% with respect to high temperature value). Moreover, annealing at high temperatures solve the proeblem of aging that is always connected to amorphous composition.

6.3 Stress dependence of the switching field

Since the magnetoelastic anisotropy dominates in glass-coated microwires, they are ideal material for sensing in stress applications. However, strong and complicated stress distribution is introduced during their production [18,19,20]. Understanding the complexicity of the effect, one can get interesting results that can be employed in the multisensoric applications.

6.3.1 Effect of frequency

Amorphous FeNbSiB microwire has been selected to show the complex dependence of the switching field on the applied mechanical stress [214]. It is characterized by high structural relaxation in as-cast state and reasonably high magnetostriction to obtain magnetic bistability.

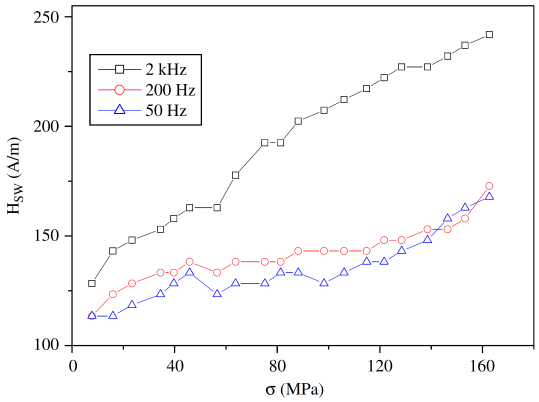

Fig. 6.16. Stress dependences of the switching field for FeNbSiB microwire measured at various frequencies of the applied magnetic field [214].

The stress dependence of the switching field for three different frequencies of external magnetic field is given in Fig. 6.16. At low frequency (50 Hz), the switching field increases weakly with the applied stress up to 100 MPa. Above this stress, the slope of the stress dependence increases. At medium frequencies (200 Hz), the behavioris similar, but the change of the switching field is more sensitive up to 140 MPa and a change in the slope appears at higher stress ($\sim$ 150 MPa). At high frequency (2 kHz), the switching field gradually increases in the whole studied interval.

Similarly to the temperature dependence of the switching field given in Section 6.2.2, the differences in the stress dependence of the switching field can be explained in terms of two contributions to the switching mechanism in glass-coated microwires. Figure 6.17 shows the frequency dependence of the switching field of FeNbSiB microwire. It is clear, that at low frequencies, the relaxation contribution H_{sw}^{r} is responsible for frequency dependence of the switching field, whereas it decreases with the frequency. On the other hand, the magnetoelastic contribution H_{sw}^{σ} is the only one responsible for the increase of the switching field at frequencies above 2 kHz. Similarly, the stress dependence of the switching field can be treated in terms of the same two contributions to the domain wall potential. Firstly, magnetoelastic contribution to the switching field is given by Eq. (6.1). Here, mechanical stress σ is given by the sum of the stresses induced during the microwires production together with the stresses applied on the microwire by glass-coating due to different thermal expansion coefficients of metallic nucleus and glass-coating (σ_i) and the stress applied on the microwire during measurement(σ_a):

$$\sigma = \sigma_i + \sigma_a \tag{6.12}$$

On the other hand, the stress dependence of the relaxation contribution is represented by the stress dependence of the interaction energy of the mobile defects with spontaneous magnetization ϵ_{eff} (as given in Eq. (6.2)). The interaction energy ϵ_{eff} is given by a sum of three terms: magnetoelastic(ϵ_σ), exchange(ϵ_{ex}), and dipole-dipole contribution(ϵ_d) [66]:

$$\epsilon_{eff} = \epsilon_\sigma + \epsilon_{ex} + \epsilon_d \tag{6.13}$$

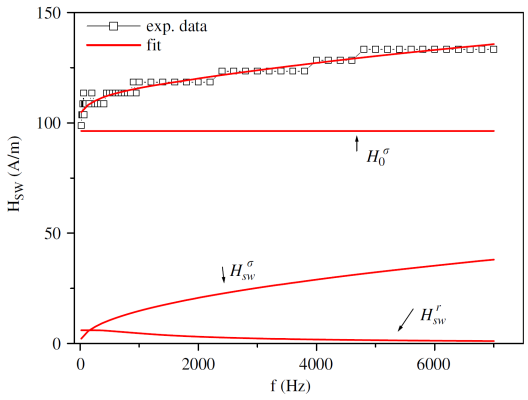

Fig. 6.17. Frequency dependence of switching field for FeNbSiB microwire. Full lines represent the fits by the two contributions to the switching [214].

The most important in our case is the magnetoelastic contribution, ϵ_σ, that is given by a local magnetoelastic energy:

$$\epsilon_\sigma = \lambda_s \sigma_l \tag{6.14}$$

where σ_l denotes the local stress that surrounds the relaxing defects.

Finally, the stress dependence of the switching field is given by a sum of two contributions given by Eqs. (6.1) and (6.2). Figure 6.18 shows the fitting of experimental data according to such a sum. It is clear that magnetoelastic contribution is responsible for stress dependence at low stress. However, at higher stress (above 40 MPa), relaxation contribution must be taken into account. Increasing the measuring frequency to 200 Hz, the relaxation contribution amplitude decreases (see Fig. 6.17) and at 2 kHz the relaxation contribution is negligible and the magnetoelastic contribution is the only one that can explain the stress dependence of the switching field according to Eq. (6.1) and (6.12).

This is an important point for application in multipurpose miniature sensors. Combination of results presented in Fig. 6.16, 6.13 and measuring technique presented in Section 5.1 leads to the contact-less sensor that can simultaneously measure magnetic field (position, electrical current, etc..) and temperature or mechanical stress. The switching between the function is made by a simple variation of the measuring frequency. At low frequency, the switching field is weakly sensible to temperature ad mechanical stress. At medium frequency, the switching field is sensible to temperature, but still weakly sensible to the mechanical stress. At higher frequency, the switching field is sensible to mechanical stress, but weakly sensible to temperature.

6.3.2 Effect of thermal treatment

Due to the complex stress distribution introduced into the metallic nucleus during the production of microwire, annealing process is sometimes necessary to improve the stress sensitivity of the switching field. A typical example is amorphous $Fe_{49.5}Ni_{28}Si_{7.5}B_{15}$ microwire [215].

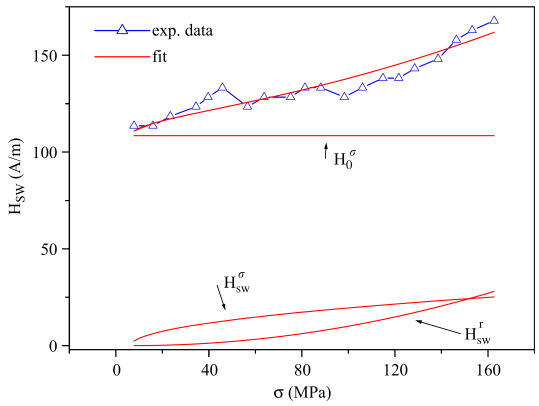

Fig. 6.18. Stress dependence of the switching field for FeNbSiB microwire measured at 50 Hz. Full lines represent the fits according to Eqs. (3.2) and (3.5) [214].

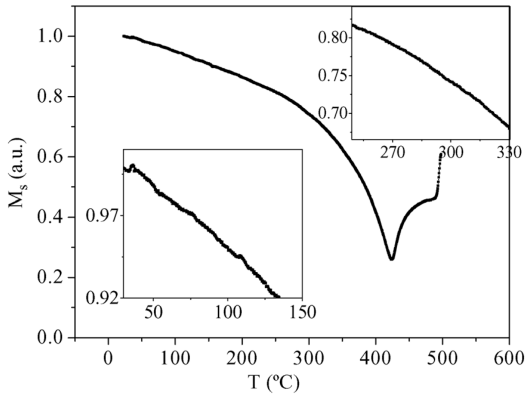

Fig. 6.19. Temperature dependence of magnetization for amorphous $Fe_{49.5}Ni_{28}Si_{7.5}B_{15}$ microwire [215].

In order to estimate the optimum temperature of thermal treatment, temperature dependence of magnetization was measured firstly. It shows monotonous decrease from room temperature up to the 425 °C (Fig. 6.19). At this temperature, the magnetization starts to increase as a result of the crystallization of new Fe-Ni phase. The Curie temperature of amorphous phase is above the crystallization temperature. Detailed analysis shows the roughness of the curve below the 200 °C, which points to the structural relaxation of the complex stress distribution introduced into the wire during the production process (see inset of Fig. 6.19). Above 200 °C, the temperature dependence is smooth pointing to the homogenization of the structure and stress relief (see inset of Fig. 6.19). According to the temperature dependence of magnetization, three temperatures were selected for the further thermal treatment of the microwire: 200, 300, and 400 °C above the temperature where structural relaxation takes place, but well below the crystallization

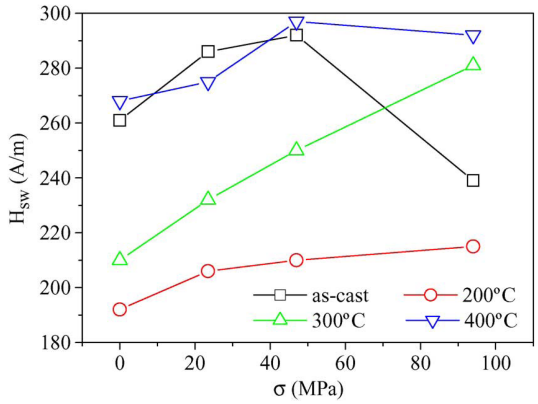

Fig. 6.20. Stress dependence of the switching field for amorphous $Fe_{49.5}Ni_{28}Si_{7.5}B_{15}$ microwires annealed at different temperatures [215].

temperature to avoid the crystallization and lose of magnetic bistability.

Figure 6.20 shows the stress dependence of the switching field for amorphous FeNiSiB microwires annealed at different temperatures. In the as-cast state, the stress dependence of the switching field is complex it increases at low stress (below 50 MPa) then it decreases to 240 A/m. This can be a result of complex stress distribution where axial and radial stresses compete in between changing the domain structure of microwire. Annealing at 200 °C leads to the stress relief (σ_i decreases) and homogenization of the structure. Apart from decrease of the switching field, the stress dependence of the switching field becomes monotonous. Assuming the nucleation-propagation model, the switching field should be proportional to the square root of the applied stress (see Eq. (6.1)) [194]. Such a stress dependence of the switching field roughly fits to the measured data. Annealing at higher temperature 300 °C further decreases the stress and homogenizes the structure of metallic nucleus. As a result, the switching field is more sensible to the applied stress and increases monotonously from 210 A/m to 280 A/m at 94 MPa. The higher is the temperature of annealing, the higher is the relaxation of the stresses introduced during the wires production. However, additional stress arising from the glass coating should be taken into account in the case of glass-coated microwire. Hence, annealing at 400 °C introduces strong stresses from the glass coating when the wire is cooled down after treatment. Moreover, the annealing at 400 °C is close to the Curie temperature of the wire, hence the mono-domain structure described in the introduction is not present during thermal treatment. Finally, the stress dependence of the switching field becomes complex and weak after such treatment and is similar to the one measured for as-cast sample.

Hence, the optimum temperature was estimated to be 300 °C, at which the switching field increase monotonously by 30% with applied stress up to 90 MPa. Moreover, the stability of the switching field increase, too, as it was shown by measurement of the switching field distribution [215].

Another possibility how to tailor the stress dependence of the switching field is the use of nanocrystalline composition. The disadvantage of nanocrystalline FeNiMoB microwire was its

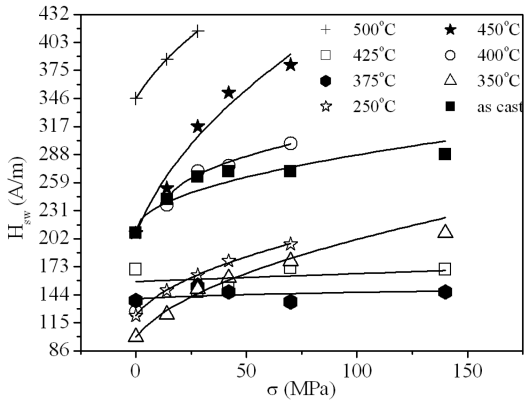

Fig. 6.21. Stress dependence of the switching field in amorphous glass-coated $Fe_{40}Ni_{38}Mo_4B_{18}$ microwire after different thermal treatments. Full lines correspond to fit according to Eq. (2). [172].

high sensitivity to thermal treatment (see Section 4.7.6). On the other hand, this disadvantage can be use to sense the mechanical stress.

Figure 6.21 shows the stress dependence of the switching field of amorphous glass-coated FeNiMoB microwires treated at different temperatures from 250 up to 500 °C. As-cast sample shows strong dependence of the switching field on the applied stress where the switching field monotonously increases with the applied stress σ. Annealing of the microwires at low temperatures causes the release of the internal stresses introduced during microwires production. This results in the decrease of the switching field as well as in the decrease of its stress dependence. Moreover, the magnetostriction of amorphous FeNiMoB alloys decreases by annealing, too [169]. The minimum value of the switching field H_{sw} was observed for the annealing temperature T_a = 350 °C. After annealing of the microwire at temperature 375 °C, the sample shows no stress dependence of the switching field, because the stresses are almost completely removed by the annealing. After annealing at 400 °C, the crystalline γ-FeNi phase appears [171]. However, the crystallites are very small and the distance between them is more than the exchange length. They act as the pinning centers for the closure domain wall and the switching field increases a little bit. As a result of the stresses introduced by the pinning centers, the switching field shows the strong stress dependence.

The annealing at 425 °C has been shown to be the optimum annealing temperature to obtain the nanocrystalline FeNiMoB alloy with the best soft magnetic properties (the lowest magnetostriction, the lowest coercive field, and the highest initial susceptibility) [169]. In the case of nanocrystalline FeNiMoB microwire, the switching field shows no stress dependence, probably as a result of very low magnetostriction. On the other hand, the switching field does not reach the minimum value. In the case of glass-coated microwire, one should take into account the stresses introduced by the glass coating (as a result of the different thermal expansion coeffcient of the glass and metallic nucleus) during cooling after annealing. The annealing at the temperature above the optimum annealing temperature (at 450 °C) leads to the strong stress dependence of the switching field in the nanocrystalline FeNiMoB microwire. The diameter of the grains in-

creases and therefore the switching field increases, following the D^6-law (see Eq. (4.20) [133]). Moreover, after the treatment at 500 °C, the samples become brittle and the maximum applied stress can be no higher than 30 MPa.

Finally, such thermal treatment allows one to tailor stress dependence of the switching field without a need to vary chemical composition. At low temperatures, the strong switching field dependence on the stress can be obtained, which is useful for stress sensing elements. Close to the optimal annealing temperature (425 °C), no stress dependence of the switching field was detected. Such behaviour is useful for the different sensing elements (temperature, current), which must not be stress sensitive.

7 Summary and perspectives

The given manuscript gives a review on magnetization processes in glass-coated microwires with positive magnetostriction. They are characterized by a single domain structure and magnetization process that runs through a single domain wall propagation along entire wire, which makes them ideal material for single domain wall propagation studies.

The domain wall dynamics in glass-coated microwires is characterized by various peculiar characteristics. Firstly, it is structural relaxation damping that arises from the amorphous nature of metallic nucleus. Secondly, it is a negative critical propagation fields that arises from a peculiar shape of a single domain wall potential in glass-coated microwires. Both effects allows one to effectively tailor the domain wall dynamics and to obtain fast domain wall even in the case of low domain wall mobility. Under the special condition, the domain wall dynamics is characterized by the constant velocity that does not depends on the amplitude of applied magnetic field. In addition, it is possible to manipulate the domain wall dynamics in order to obtain negative domain wall mobility. Such mobility can be controlled by frequency of applied field or by temperature of measurement.

In the low-field range, the domain wall propagation is no more viscous. In turn, it is affected by the local distribution of the defects and the domain wall propagation consists of intermittent jump at various domain wall velocity. The local domain wall velocity is given by a local pinning field. As a result, the average domain wall velocity on long scale is given by a power law. At high temperatures, the pinning of the domain wall on local defect is weak and the domain wall propagates in a rigid form. Local pinning increases at low temperatures changing the shape of propagating domain wall into the flexible one. This leads to the variation of the power exponent.

The main parameter that influence the domain wall velocity is its mobility. It is given by the reciprocal value of domain wall damping. In case of glass-coated microwires, the eddy-current damping is negligible. Magnetic relaxation damping is also low due to a low anisotropy and Gilbert damping of amorphous wires. Hence, the domain wall mobility in glass-coated microwires is high and the domain wall is very fast.

In high-field region, the domain wall mobility increases by one order as a result of change of the domain wall structure from transversal to vortex one. The energy of vortex domain wall is higher than that of transversal one. Therefore, it appears at higher fields. Moreover, the vortex domain wall does not create surface magnetic poles that hinders the domain wall propagation. Hence it shows higher mobility. Finally, such domain wall are extremly fast (up to 18 km/s).

Three reasons responsible for fast domain walls in glass-coated microwires were recognized: 1) low anisotropy and Gilbert damping; 2) existence of the two perpendicular anisotropies; and 3) existence of radial domain structure below the surface of metallic nucleus that hinders the domain wall pinning on surface defects.

Interaction of the domain wall with phonons generated due to magentostriction is sometimes observed at high velocities that are comparable to the sound speed. Different interaction has been observed that correspond to different elastic waves - longitudinal, transversal and Lambe's waves.

The main parameter that defines the domain wall velocity is anisotropy. The magnetoelastic anisotropy is the most important in case of glass-coated amorphous microwires. Properly selected thermal treatment leads to a decrease of magnetoelastic anisotropy that leads to the sharp increase of domain wall damping and velocity.

However, fast domain walls can be observed even in the case of highly anisotropic microwires. Application of transversal magnetic field (with respect to the wire's axis) leads to a compensation of axial anisotropy. This results in the incerase of the domain wall velocity even though the domain wall mobility decreases. Finally, fast domain wall (9 km/s) is observed that is almost independent on applied axial magnetic field.

Transversal anisotropy (that is neccessary to obtain fast domain wall) can even be induced by thermal treatment in transversal magnetic field. Similar effect is obtained by current annealing that introduces circular anisotropy.

Fast domain wall due to high domain wall mobility in amorphous microwires is paid by its poor time and temperature stability. Solution can be found in application of nanocrystalline structure for metallic core. Nanocrystalline materials are composite materials. They consist of crystalline grains (of nanometer size) embedded in amorphous matrix. They combine high structural stability of crystalline materials with low anisotropy of amorphous structure. As a result, the domain wall velocity in nanocrystalline is relatively high (1 km/s), but its domain wall mobility is almost temperature independent.

Glass-coated nanocrystalline FeCoMoB microwires are even better materials for fast and stable domain wall dynamics. They are characterized by high magnetic moment, high Curie temperature, low anisotropy and positive magnetostriction. This leads to even faster domain wall (3 km/s). In addition, the domain wall dynamics at low field is temperature independent in a wide range of temperatures from 80 to 450 K.

The strong dependence of the domain wall dynamics on external parameters can be employed in the applications for construction of miniaturized sensors of magnetic field, position, temperature, mechanical stress, etc...

The most appropriate parameter to sense external parameters is the switching field. It can easily be measured contactlessly by induction method. Moreover, two external parameters can be simultaneously obtained from a single measurements: magnetic field and temperature (or mechanical stress).

The switching field is given by the shape of the single domain wall potential that consists of two contribution: 1) magnetoelastic one that arises from the interaction of magnetic moments with the local stress distribution induced during the production; and 2) structural relaxation that arises from the metastable structure of amorphous metallic nucleus of glass-coated microwires.

Two contributions to the domain wall potential lead to the two contributions to the switching field of the domain wall. Both contributions have different frequency dependence. At low frequencies, the structural relaxation prevails, while magnetoelastic one is dominant at higher frequencies (above 100 Hz).

In addition, both contributions to the switching field have different temperature and stress dependence. Combination of their frequency, temperature and stress dependence leads to a multipurpose miniature sensing element. Its function is defined by the applied frequency of exitation field. At low frequency, the microwire is very weakly temperature and stress dependent. At medium frequency (200 - 300 Hz), the switching field is temperature dependent, but weak stress dependence is observed. At higher frequencies ($\sim$ 1 kHz), the switching field is almost temperature independent, but increases with applied stress linearly.

The stress and temperature dependence of the switching field can even be tailored by properly selected thermal treatment. Annealing at high enough temperatures reduces the internal stresses induced by microwire's production. This leads to increase of switching field sensitivity to applied

mechanical stress as well as to the stress introduced by glass as a result of different thermal expansion coefficient of metallic nucleus and glass-coating.

The presented features of bistable glass-coated microwires can be employed in technical applications to sense temperature, stress, magnetic field, electrical current, position, etc... The dimensions of glass-coated microwires allow their embedding into many technical structures without destroying their mechanical properties. However, the sensitivity of the switching field in the technical region of temperatures (-50 to 150°C) or mechanical stresses (up to 10 MPa) must be enhanced. Enhancement of the switching field dependence on temperature in the range from 20 to 50°C could lead to the possible applications of glass-coated microwires in biomedicine. Glass-coating of amorphous microwires increases their biocompatibility. Moreover, easy, cheap and efficient production process leads to very high added value of glass-coated microwires.

Amorphous nucleus of glass-coated microwires can be replaced by many other metallic structures like for example modern Heusler compositions [216, 217]. Complex stress distribution introduced by glass brings new effects also in these alloys. One of examples is the increase of efficiency of magnetocaloric effect at low magnetic field in Heusler NiMnInCo glass-coated microwire due to the presence of Hopkinson effect [218].

Acknowledgement: This work has been done in colaboration with my colleagues from ICMM CSIC Madrid, UPV San Sebastian and Universidad de Oviedo in Spain, Technical University in Kosice, Slovakia and Slovak Academy of Sciences in Kosice. Hence, author would like to acknowledge the help of his teachers and colleague: Prof. Manuel Vazquez, Prof. Arcady Zhukov, Prof. Blanca Hernando, Prof. Pavol Vojtanik, Assoc. Prof. Eva Komova, Prof. Josef Blazek, Assoc. Prof. Dusan Praslicka, Assoc. Prof. Jozef Hudak, Assoc. Prof. Jan Ziman, Dr. Jozef Kovac. Moreover, author would like to thanks to his students that took part on this work: Mgr. Kornel Richter, Mgr. Yuriy Kostyk, Dr. Peter Klein, Mgr. Jana Gamcova, Mgr. Tomas Ryba, Ing. Rudolf Sabol as well as to the foreign students that stayed in his laboratory and also took part on the study of magnetization processes in magnetic microwires: Dr. Jesus Olivera, Dr. German Infante, Dr. Jesus Santos, Dr. Jacob Torrejon. This work was supported by the project NanoCEXmat Nr. ITMS 26220120019 and ITMS 26220120035, Slovak VEGA grant. No. 1/3036/06, 1/0076/09, 1/0060/13, APVT-20-007804, APVV-0027-11, APVV0266-10 and 6.EUFP - MANUNET - DEWMAGMIWIRTEC and 7.EUFP - MANUNET - SOMAMICSENS.

References

[1] S. S. P. Parkin, M. Hayashi, L. Thomas: *Science* **320** (2008) 190

[2] D. A. Allwood, G. Xiong, C. C. Faulkner, D. Atkinson, D. Petit,R. P. Cowburn: *Science* **309** (2005) 1688

[3] C. Y. You: *Appl. Phys. Lett.* **92** (2008) 152507

[4] D. A. Allwood, G. Xiong, R. P. Cowburn: *Appl. Phys. Lett.* **85** (2004) 2848

[5] R. Varga, A. Zhukov, J. M. Blanco, M. Ipatov, V. Zhukova, J. Gonzalez, P. Vojtanik: *Phys. Rev.* **B 76** (2007) 132406

[6] R. Varga, K. Richter, A. Zhukov: *IEEE Trans. Magn.* **44** (2008) 3925

[7] K. Richter, R. Varga, G. A. Badini-Confalonieri, M. Vazquez: *Appl. Phys. Lett.* **96** (2010) 182507

[8] R. Varga., K. L. Garcia, M. Vzquez, P. Vojtanik: *Phys. Rev. Lett.* **94** (2005) 1017201

[9] R. Varga, A. Zhukov, J. M. Blanco, M. Ipatov, V. Zhukova, J. Gonzalez, P. Vojtanik: *Phys. Rev.* **B 74** (2007) 212405

[10] G. Infante, R. Varga, G. A. Badini-Confalonieri, M. Vazquez: *Appl. Phys. Lett.* **95** (2009) 012503

[11] H. Chiriac, T. A. Ovari: *Progress Mater. Science* **40** (1996) 333

[12] A. Zhukov, J. Gonzalez, M. Vazquez, V. Larin, A. Torcunov *Nanocrystalline and amorphous magnetic microwires in: Encyclopedia of Nanoscience and Nanotechnology* (American Scientific Publishers,2004)

[13] M. Vazquez *Advanced magnetic microwires in Handbook of Magnetism and Advanced Magnetic Materials* (John Wiley & Sons, 2007)

[14] M. Vazquez: *Physica* **B 299** (2001) 302

[15] G. F. Taylor: *Phys. Rev.* **23** (1924) 655

[16] A. V. Ulitovski *Method of continuous fabrication of microwires coated by glass* (authors certifications (USSR patent), No 128427, 1950)

[17] L. Kraus, R. Gemprle, J. Schneider: *proc. of SMM3* (1973) 580

[18] H. Chiriac, T. A. Ovari, G. Pop: *Phys. Rev.* **B 52** (1995) 10104

[19] H. Chiriac, T. A. Ovari, S. Corodeanu, G. Ababei: *Phys. Rev.* **B 76** (2007) 214433

[20] A. S. Antonov, V. T. Borisov, O. V. Borisov, A. F. Prokoshin, N. A. Usov: *J. Phys. D: Appl. Phys.* **33** (2000) 1161

[21] S. A. Gudishnikov, B. Y. Ljubimov, P. S. Pavlanov, Y. V. Prokhorova, V. S. Skomartovski, N. A. Usov, A. V. Torcunov: *Phy. Stat. Solidi* **A 206** (2009) 625

[22] A. Chizhik, A. Zhukov, J. M. Blanco, J. Gonzalez: *J. Magn. Magn. Mater.* **249** (2002) 27

[23] J. Ziman, J. Onufer, M. Kladivova: *Physica* **B 406** (2011) 3576

[24] L. V. Panina, K. Mohri: *Appl. Phys.Lett.* **65** (1994) 1189

[25] N. N. Orlova, A. S. Aronin, S. I. Bozhko, Yu. P. Kabanov, V. S. Gornakov: *J. Appl. Phys.* **111** (2012) 073906

[26] K. H. Liu, Z. C. Lu, T. C. Liu, D. R. Li: *Chin. Phys.Lett.* **30** (2013) 017501

[27] J. Ye, R. P. de Real, G. Infante, M. Vazquez: *J. Appl. Phys.* **113** (2013) 043904

[28] C. W. Chen *Magnetism and metallurgy of soft magnetic materials* (Dover Publications Inc., New York, 1986)

[29] B. D. Cullity *Introduction to magnetic materials* (Addison-Wesley,1972)

[30] T. H. O'Dell *Ferromagnetodynamics* (The MacMillan Press Ltd., 1981)

[31] A. Hubert, R. Schafer *Magnetic Domains* (Springer-Verlag, Berlin, 1998)

[32] S. Chikazumi *Physics of Ferromagnetism* (Claredon Press, Oxford, 1997)

[33] D. X. Chen, N. M. Dempsey, M. Vazquez: *IEEE Trans. Magn* **31** (1995) 781

[34] H. J. Williams, W. Shockley, C. Kittel: *Phys. Rev.* **80** (1950) 1090

[35] A. Thiaville, J. M. Garcia, J. Miltat: *J. Magn. Magn. Mater.* **242-245** (2002) 1061

[36] H. Forster, T. Schrefl, W. Scholz, D. Suess, V. Tsiantos, J. Fidler: *J. Magn. Magn. Mater.* **249** (2002) 181

[37] L. Landau, E. Lifshitz: *Phys. Z. Sowjetunion* **8** (1935) 153

[38] C. Kittel, J. K. Galt: *Solid State Phys.* **3** (1956) 437

[39] H. Kronmuller, M. Fahnle *Micromagnetism and the microstructure of the ferromagnetic solids* (Cambridge Univ. Press., Cambridge, 2003)

[40] R. L. Novak, J. P. Sinnecker, H. Chiriac: *J. Phys. D: Appl. Phys.* **41** (2008) 095005

[41] R. Varga, A. Zhukov, N. Usov, J. M. Blanco, J. Gonzalez, V. Zhukova, P. Vojtanik: *J. Magn. Magn. Mater.* **316** (2007) 337

[42] R. Varga, J. Torrejon, Y. Kostyk, K. L. Garcia, G. Infantes, G. Badini and M. Vazquez: *J. Phys.: Cond. Matter.* **20** (2008) 445215

[43] H. Kronmuller: *Phys. Stat. Sol.* **b 127** (1985) 531

[44] L. M. Garcia, J. Bartolome, F. J. Lazaro, C. de Francisco, J. M. Munoz: *Phys. Rev.* **B 54** (1996) 15238

[45] R. Varga, G. Infante, G. A. Badini-Confalonieri, M. Vzquez,: *J. Phys.:Conf.Series* **200** (2010) 042026

[46] N. L. Schryer, L. R. Walker: *J. Appl. Phys.* **45** (1974) 5406

[47] Y. Nakatani, A. Thiaville, J. Miltat: *Nature Mater.* **2** (2003) 521

[48] F. H. de Leeuw: *IEEE Trans. Magn.* **9** (1973) 614

[49] C. H. Tsang, R. L. White, R. M. White: *J. Appl. Phys.* **49** (1978) 6052

[50] M. V. Chetkin, Yu. N. Kurbatova, T. B. Shapaeva, O. A. Borschegovsky: *Physics Letters A* **337** (2005) 235

[51] M. V. Chetkin, Yu. N. Kurbatova, T. B. Shapaeva, O. A. Borschegovsky: *J. Exp. Theor. Phys.* **103** (2006) 159

[52] A. K. Zvezdin: *J. Exp. Theor. Phys. Lett.* **29** (1979) 553

[53] V. G. Baryakhtar, B. A. Ivanov, A. L. Sukstanskioe: *J. Exp. Theor. Phys.* **51** (1980) 757

[54] K. J. Sixtus, L. Tonks: *Phys. Rev.* **42** (1932) 419

[55] L. Tonks, K. J. Sixtus: *Phys. Rev.* **39** (1932) 357

[56] P. Landeros, S. Allende, J. Escrig, E. Salcedo, D. Altbir, E. E. Vogel: *Appl. Phys. Lett.* **90** (2007) 102501

[57] J. Hudak, J. Blazek, A. Cverha, P. Gonda, R. Varga: *Sensors and Actuators* **A 156** (2009) 292

[58] A. Chizhik, R. Varga, A. Zhukov, J. Gonzalez, J. M. Blanco: *J. Appl. Phys.* **103** (2008) 07E707

[59] M. Tibu, M. Lostun, T. A. Ovari, H. Chiriac: *Rev. Sci. Instr.* **83** (2012) 064708

[60] A. Zhukov: *Appl. Phys. Lett.* **78** (2001) 3106

[61] S. Puerta, D. Cortina, H. Garcia-Miquel, D. X. Chen, M. Vazquez: *J. Non-Cryst. Solids* **287** (2001) 370

[62] M. Neagu, H. Chiriac, E. Hristoforou, I. Darie, F. Vinai: *J. Magn. Magn. Mater.* **226-230** (2001) 1516

[63] H. Chiriac, E. Hristoforou, M. Neagu, and I. Darie: *Mater. Sci. Eng.* **304-306** (2001) 1011

[64] R. Varga, K. L. Garcia, A. Zhukov, M. Vazquez, P. Vojtanik: *Appl. Phys. Lett.* **83** (2003) 2620

[65] R. Varga, K. L. Garcia, M. Vazquez, A. Zhukov, P. Vojtanik: *Phys. Rev.* **B 70** (2004) 024402

[66] H. Kronmuller: *Philos. Mag.* **B 48** (1983) 127

[67] M. Borrous, H. Kronmuller: *Phys. Stat. Sol.* **A 113** (1989) 169

[68] R. Varga, G. Infante, K. Richter, M. Vazquez: *Phys. Stat. Sol.* **A 208** (2011) 509

[69] C. H. Tsang, R. L. White, R. M. White: *AIP Conf. Proc.* **29** (1975) 552

[70] R. Varga, K. Richter,A. Zhukov: *Acta Phys. Pol.* **A 118** (2010) 747

[71] N. L. Schryer, L. R. Walker: *J. Appl. Phys.* **45** (1974) 5406

[72] R. Varga, G. Infante, G. A. Badini-Confalonieri, M. Vazquez: *J. Phys. Conf. Ser.* **200** (2010) 042026

[73] J. Olivera, R. Varga, V. M. Prida, M. L. Sanchez, B. Hernando, A. Zhukov: *Phys. Rev.* **B 82** (2010) 094414

[74] R. M. Bozorth *Ferromagnetism* (A John Wiley & Sons, Inc., 2003)

[75] R. Varga, Y. Kostyk, A. Zhukov, M. Vazquez: *J. Non-Cryst. Sol.* **354** (2008) 5101

[76] Y. Kostyk, R. Varga, M. Vazquez, P. Vojtanik: *Physica* **B 403** (2008) 386

[77] J. Ziman, J. Onufer, M. Kladivova: *J. Magn. Magn. Mater.* **323** (2011) 3098

[78] J. P. Sethna, K. A. Dahmen, O. Perkovic *The Science of Hysteresis, ed. G. Bertotti and I. Mayergoyz* (New York: Academic, 2006)

[79] G. Durin, S. Zapperi *The Science of Hysteresis, ed. G. Bertotti and I. Mayergoyz* (New York: Academic, 2006)

[80] O. Narayan, D. S. Fisher: *Phys. Rev.* **B 48** (1993) 7030

[81] T. Nattermann, S. Stepanov, L. H. Tang, H. Leschhorn: *J. Physique II* **2** (1992) 1483

[82] R. C. OHandley: *J. Appl. Phys.* **46** (1975) 4996

[83] D. Atkinson, D. A. Allwood, C. C. Faulkner G. Xiong, M. D. Cooke, R. P. Cowburn: *IEEE Trans. Magn.* **39** (2003) 2663

[84] P. J. Metaxas, J. P. Jamet, A. Mougin, M. Cormier, J. Ferre, V. Baltz, B. Rodmacq, B. Dieny, R. L. Stamps: *Phys. Rev. Lett.* **99** (2007) 217208

[85] Y. Nakatani, N. Hayashi, T. Ono, H. Miyajima: *IEEE Trans. Magn.* **37** (2001) 2129

[86] S. Yang, J. L. Erskine: *Phys. Rev.* **B 72** (2005) 064433

[87] B. Alessandro, C. Beatrice, G. Bertotti, A. Montorsi: *J. Appl. Phys.* **68** (1990) 2901

[88] J. P. Sethna, K. A. Dahmen, C. R. Myers: *Nature* **410** (2001) 242

[89] D. Spasojevic, S. Bukvic, S. Milosevic, H. E. Stanley: *Phys. Rev.* **E 54** (1996) 2531

[90] S. Zapperi, C. Castellano, F. Colairoi, G. Durin: *Nature Phys.* **1** (2005) 46

[91] D. S. Stone: *Acta Metall. Mater.* **39** (1991) 599

[92] R. Madec, B. Devincre, L. P. Kubin: *Phys. Rev. Lett.* **89** (2002) 255508

[93] D. M. Dimiduk, C. Woodward, R. LeSar, M. Uchic: *Science* **312** (2006) 1188

[94] J. Ziman, V. Suhajova, M. Kladivova: *Physica* **B 407** (2012) 3566

[95] F. Beck, R. C. Gomes, K. D. Sossmeier, F. Bohn, M. Carara: *J. Magn. Magn. Mater.* **323** (2010) 268

[96] M. Ipatov, V. Zhukova, A. Zvezdin, J. Gonzalez, J. M. Blanco, A. Zhukov: *J. Supercond. Nov. Magn.* **24** (2011) 851

[97] K. D. Sossmeier, F. Beck, H. Chiriac, L. F. Schelp, M. Carara: *Phys. Stat. Sol.* **A 206** (2009) 635

[98] M. Ipatov, V. Zhukova, A. Zhukov, J. Gonzalez, A. Zvezdin: *Phys. Rev.* **B 81** (2010) 134421

[99] P. Klein, R. Varga, G. Infante, M. Vazquez: *J. Appl. Phys.* **111** (2012) 053920

[100] A. Himeno, T. Ono, S. Nasu, T. Okuno, K. Mibu, T. Shinjo: *J. Magn. Magn. Mater.* **272-276** (2004) 1577

[101] D. Atkinson, D. A. Allwood, G. Xiong, M. D. Cooke, C. C. Faulkner, R. P. Cowburn: *Nat. Mater.* **2** (2003) 85

[102] E. R. Lewis, D. Petit, L. OBrien, A. Fernandez-Pacheco, J. Sampaio, A. V. Jausovec, H. T. Zeng, D. E. Read, R. P. Cowburn: *Nat. Mater.* **9** (2010) 980

[103] H. Chiriac, E. Hristoforou, M. Neagu, I. Darie, A. E. Moga: *J. Non-Cryst. Solids* **287** (2001) 413

[104] H. Forster, T. Schrefl, W. Scholz, D. Seuss, V. Tsiantos, J. Fidler: *J. Magn. Magn. Mater.* **249** (2002) 181

[105] R. D. McMichael, M. J. Donahue: *IEEE Trans. Magn.* **33** (1997) 4167

[106] A. Kunz: *IEEE Trans. Magn.* **42** (2006) 3219

[107] N. A. Usov, A. Zhukov, J. Gonzalez: *J. Magn. Magn. Mater.* **316** (2007) 255

[108] D. X. Chen, N. M. Dempsey, M. Vazquez, A. Hernando: *IEEE Trans. Magn.* **31** (1995) 781

[109] A. Zhukov, V. Zhukova, J. M. Blanco, A. F. Cobeno, M. Vazquez, J. Gonzalez: *J. Magn. Magn. Mater.* **258-259** (2003) 151

[110] R. Varga, K. Richter, A. Zhukov: *IEEE Trans. Magn.* **44** (2008) 3925

[111] H. Chiriac, E. Hristoforou, M. Neagu, I. Darie, C. Hison: *Sensors Actuators* **81** (2000) 150

[112] S. O. Demokritov, A. Kirilyuk, N. M. Kreines, V. Kudinov, V. B. Smirnov, M. V. Chetkin: *J. Magnetism Magn. Mater.* **102** (1991) 339

[113] M. V. Chetkin, Y. N. Kurbatova, T. B. Shapaeva, O. A. Borshchegovsky: *J. Exp. Theor. Phys.* **103** (2006) 159

[114] M. V. Chetkin, Y. N. Kurbatova, T. B. Shapaeva, O. A. Borshchegovsky: *Phys. Lett.* **A 337** (2005) 235

[115] *Handbook of Chemistry and Physics, 65^{th} edition* (Chemical Rubber Company)

[116] S. Allende, D. Altbir, E. Salcedo, M. Bahiana, J. P. Sinnecker: *J. Appl. Phys.* **104** (2008) 013907

[117] V. L. Sobolev, H. L. Huang, S. C. Chen: *J. Appl. Phys.* **75** (1994) 5797

[118] V. Zhukova, J. M. Blanco, M. Ipatov, A. Zhukov: *J. Appl. Phys.* **106** (2009) 113914

[119] A. Kunz, S. C. Reiff: *Appl. Phys. Lett.* **93** (2008) 082503

[120] M. T. Bryan, T. Schreffl, D. Atkinson, D. A. Allwood: *J. Appl. Phys.* **103** (2008) 073906

[121] K. Richter *Diploma thesis* (UPJS, 2009)

[122] A. Kunz, S. C. Reiff, J. D. Priem, E. W. Rentsch: *Proceedings - 12th International Conference on Electromagnetics in Advanced Applications, ICEAA'10* (2010) 248

[123] A Kunz, J. D. Priem, S. C. Reiff: *Proceedings of SPIE - The International Society for Optical Engineering* **7760** (2010) 776005

[124] K. Richter, R. Varga, A. Zhukov: *Acta Phys. Polonica* **A 118** (2010) 738

[125] K. Richter, R. Varga, J. Kovac, A. Zhukov: *IEEE Trans. Magn.* **48** (2012) 1266

[126] Y. Takemura, H. Tokuda, K. Komatsu, S. Masuda, T. Yamada, K. Kakuno, K. Saito: *IEEE Trans. Magn.* **32** (1996) 4947

[127] H. Kronmuller: *Phys. Status Solidi* **B 118** (1983) 661

[128] R. Varga, P. Klein, K. Richter, A. Zhukov, M. Vazquez: *J. Magn. Magn. Mater.* **324** (2012) 3566

[129] P. Klein, R. Varga, P. Vojtanik, J. Kovac, J. Ziman, G. A. Badini-Confalonieri, M. Vazquez: *J. Phys. D: Appl. Phys.* **43** (2010) 045002

[130] S. Michalik, J. Gamcova, J. Bednarcik, R. Varga: *J. Alloys Comp.* **509** (2011) 3409

[131] F. C. Rossol: *J. Appl. Phys.* **40** (1969) 1082

[132] F. C. Rossol: *Phys. Rev. Lett.* **24** (1970) 1021

[133] G. Herzer: *IEEE Trans. Magn.* **26** (1990) 1397

[134] G. Herzer: *IEEE Trans. Magn.* **25** (1989) 3327

[135] Y. Yoshizawa, S. Oguma, K. Yamauchi: *J. Appl. Phys.* **64** (1988) 6044

[136] Y. Yoshizawa, K. Yamauchi, T. Yamane, H. Sugihara: *J. Appl. Phys.* **64** (1988) 6047

[137] M. E. McHenry, M. A. Willard, D. E. Laughlin: *Progress in Materials Science* **44** (1999) 291

[138] A. Hernando, I. Navarro *Nanophase Materials* (Kluwer Academic Publisher, 1994)

[139] M. Millan, C. F. Conde, A. Conde: *J. Mat. Sci.* **30** (1995) 3591

[140] A. Hernando, M. Vazquez, T. Kulik, C. Prados: *Phys. Rev.* **B 51** (1995) 3581

[141] G. Herzer: *J. Magn. Magn. Mater.* **294** (2005) 99

[142] K. Suzuki, G. Herzer, J. M. Cadogan: *J. Magn. Magn. Mater.* **177** (1998) 949

[143] J. Tan, Y. F. Gao, G. D. Liu, C. L. Zhang, T. Liu, R. Z. Ma: *J. Magn. Magn. Mater.* **164** (1996) 211

[144] G. Henninger, A. Teresiak, F. Prssler, N. Mattern, M. Mller: *J. Magn. Magn. Mater.* **196-197** (1999) 110

[145] P. Marin, M. Vazquez, A. O. Olofinjana, H. A. Davies: *Nanocryst. Mater.* **10** (1998) 299

[146] M. Mller, H. Grahl, N. Mattern, B. Schnell: *Mat. Sci. Eng.* **A 304-306** (2001) 353

[147] P. Vojtanik, E. Komova, P. Petrovi, R. Varga, H. Sassik, R. Grossinger: *Acta Phys. Slovaca* **48** (1998) 719

[148] R. Varga, P. Vojtanik, M. Kon: *J. Magn.Magn. Mater.* **215** (2000) 340

[149] J. Kovac, O. Dusa, M. Konc, T. Svec, P. Sovak: *J. Magn.Magn. Mater.* **157-158** (196) 197

[150] R. Varga, R. Matejko, P. Vojtanik, P. Agudo, R. Grossinger, H. Sassik: *J. Magn.Magn. Mater.* **197** (1999) 227

[151] G. Pavlik, P. Matta, P. Sovak, A. Zorkovska, M. Konc: *Acta Phys. Pol.* **A 97** (2000) 1

[152] K. Suzuki, A. Makino, N. Kataoka, A. Inoue, T. Masumoto: *Mater. Trans. JIM* **32** (1991) 93

[153] E. Komova, R. Grossinger, P. Vojtanik, R. Varga: *Mat. Sci. Eng.* **A 226** (1997) 693

[154] M. A. Willard, D. E. Laughlin, M. E. McHenry, D. Thoma, K. Sickafus, J. O. Cross, V. G. Haris: *J. Appl. Phys.* **84** (1998) 6773

[155] P. Marin, M. Vazquez, J. Arcas, A. Hernando: *J. Magn. Magn. Mater.* **203** (1999) 6

[156] V. Zhukova, S. Kaloshkin, A. Zhukov: J. Gonzalez: *J. Magn. Magn. Mater.* **249** (2002) 108

[157] J. Arcas, C. Gomez-Polo, A. Zhukov, M. Vazquez, V. Larin, A. Hernando: *Nanostr. Mater.* **7** (1996) 823

[158] P. Vojtanik, R. Varga, R. Andrejco, P. Agudo: *J. Magn. Magn. Mater.* **249** (2002) 136

[159] J. Gonzales, A. Zhukov, V. Zhukova, A. F. Cobeno, J. M. Blanco, A. R. de Arellano-Lopez, S. Lopez-Pombero, J. Martinez-Fernandez, V. Larin, A. Torcunov: *IEEE Trans. Magn.* **36** (2000) 3015

[160] R. Varga, C. Luna, A. Zhukov, M. Vazquez, P. Vojtanik: *Czech. J. Phys.* **Suppl.D 54** (2004) 177

[161] J. Olivera, R. Varga, P. Vojtanik, V. M. Prida, M. L. Sanchez, B. Hernando, A. Zhukov: *J. Magn. Magn. Mater.* **320** (2008) 2534

[162] H. Chiriac, M. Tibu, T. A. Ovari: *IEEE Trans. Magn.* **45** (2009) 4286

[163] J. Olivera, M. L. Sanchez, V. M. Prida, R. Varga, V. Zhukova, A. P. Zhukov, B. Hernando: *IEEE Trans. Magn.* **44** (2008) 3946

[164] P. Vojtank, E. Komova, R. Varga, R. Matejko, R. Grossinger, H. Sassik, P. Agudo, M. Vazquez, A. Hernando: *J. Phys. IV* **8** (1998) Pr2-11

[165] R. Grossinger, D. Holzer, C. Kussbach, H. Sassik, R. Sato Turtelli, J. P. Sinnecker, E. Wittig,: *IEEE Trans. Magn.* **31** (1995) 3883

[166] V. Zhukova, A. F. Cobeno, A. Zhukov, J. M. Blanco, V. Larin, J. Gonzalez: *Nanostruct. Mater.* **11** (1999) 1319

[167] C. Garcia, A. Zhukov, J. Gonzalez, V. Zhukova, R. Varga, J. J. del Val, V. Larin, J. M. Blanco: *J. All. Comp.* **423** (2006) 116

[168] J. Li, Z. Su, T. M. Wang, S. H. Ge, H. Hahn, Y. Shirai: *J. Mat. Sci.* **34** (1999) 111

[169] P. Vojtanik, R. Matejko, R. Varga, V. Ocelik: *Mat. Sci. Forum* **373** (2001) 237

[170] R. Andrejco, R. Varga, P. Marko, P. Vojtanik: *Czech. J. Phys.* **Suppl. A 52** (2002) A113

[171] E. Komova, M. Varga, R. Varga, P. Vojtanik, J. Bednarcik, J. Kovac, M. Provencio, M. Vazquez: *Appl. Phys. Lett.* **93** (2008) 062502

[172] E. Komova, M. Varga, R. Varga, P. Vojtanik, J. Torrejon, M. Provencio, M. Vazquez: *Acta Phys. Pol.* **A113** (2008) 135

[173] H. F. Li, D. E. Laughlin, R. V. Ramanujan: *Phil. Mag.* **86** (2006) 1355

[174] Zs. Gercsi, F. Mazaleyrat, L. K. Varga: *J. Magn. Magn. Mater.* **302** (2006) 454

[175] I. Skorvanek, P. Svec, J. Marcin, J. Kovac, T. Krenicky, M. Deanko: *Phys. Stat. Sol.* **A 196** (2003) 217

[176] O. Mohanta, M. Ghosh, A. Mitra, A. K. Panda: *J. Phys. D: Appl. Phys.* **42** (2009) 065007

[177] H. Iwanabe, B. Lu, M. E. McHenry, D. E. Laughlin: *J. Appl. Phys.* **85** (1999) 4424

[178] J. Ziman, J. Zagyi: *J. Magn. Magn. Mater.* **169** (1997) 98

[179] C. F. Conde, A. Conde: *Rev. Adv. Mater. Sci.* **18** (2008) 565

[180] G. Vlasak, M. Pavuk, P. Mrafko, D. Janickovic, P. Svec, B. Butvinova: *J. Magn. Magn. Mater.* **320** (2008) e837

[181] R. Varga, P. Vojtanik, M. Konc: *J. Magn. Magn. Mater.* **215** (2000) 340

[182] P. Klein, R. Varga, G. A. Badini Confalonieri, M. Vazquez: *J. Nanosci. Nanotechnology* **12** (2012) 7464

[183] P. Klein, R. Varga, M. Vazquez: *J. All. Comp.* **550** (2013) 31

[184] P. Klein, R. Varga, G. A. Badini Confalonieri, M. Vazquez: *J. Magn. Magn. Mater.* **323** (2011) 3265

[185] D. Praslicka, J. Blazek, M. Smelko, J. Hudak, A. Cverha, I. Mikita, R. Varga, A. Zhukov: *IEEE Trans Magn.* **49** (2013) 128

[186] P. Klein, R. Varga, G. A. Badini Confalonieri, M. Vazquez: *IEEE Trans Magn.* **46** (2010) 357

[187] R. Varga, A. Zhukov, M. Ipatov, J. M. Blanco, J. Gonzalez,V. Zhukova, P. Vojtanik: *Phys. Rev.* **B 73** (2006) 054408

[188] A. Garg: *Phys. Rev.* **B 51** (1995) 15592

[189] B. K. Ponomarev, A. P. Zhukov: *Sov. Phys. Solid State* **26** (1984) 1795

[190] R. H. Victora: *Phys. Rev. Lett.* **63** (1989) 457

[191] B. K. Ponomarev, A. P. Zhukov: *Sov. Phys. Solid State* **27** (1985) 273

[192] W. Wernsdorfer, E. Bonet Orozco, K. Hasselbach, A. Benoit, B. Barbara, N. Demoncy, A. Loiseau, H. Pascard, D. Mailly: *Phys. Rev. Lett.* **78** (1997) 1791

[193] L. Gunther, B. Barbara: *Phys. Rev.* **B 49** (1994) 3926

[194] P. Aragoneses, J. M. Blanco, L. Dominguez, J. Gonzalez, A. Zhukov, M. Vazquez: *J. Phys. D: Appl. Phys.* **31** (1998) 3040

[195] R. C. OHandley: *Phys. Rev.* **B 18** (1978) 930

[196] A. Hernando, V. Madurga, C. Nunez de Villavicenco, M. Vazquez: *Appl. Phys. Lett.* **45** (1984) 802

[197] H. Kronmuller: *J. Magn. Magn. Mater.* **24** (1981) 159

[198] A. Zhukov, M. Vazquez, J. Velazquez, C. Garcia, R. Valenzuela, B. Ponomarev: *Mater. Sci. Eng.* **A 226-228** (1997) 753

[199] S. U. Jen, C. J. Weng: *J. Appl. Phys.* **64** (1988) 4627

[200] E. Komova, M. Varga, R. Varga, P. Vojtanik, J. Torrejon, M. Provencio, M. Vazquez: *J. Phys.: Cond. Matter* **19** (2007) 236229

[201] P. Aragoneses, J. M. Blanco, L. Dominguez, A. Zhukov, J. Gonzalez, K. Kulakowski: *J. Phys. D: Appl. Phys.* **31** (1998) 494

[202] P. Klein, R. Varga, G. A. Badini-Confalonieri, M. Vazquez: *IEEE Trans. Magn.* **46** (2010) 357

[203] P. Allia, F. Vinai: *Phys. Rev.* **B 26** (1982) 6141

[204] K. Richter, R. Varga, A. Zhukov: *J. Phys.: Condens. Matter.* **24** (2012) 296003

[205] R. Varga, K. L. Garcia, C. Luna, A. Zhukov, P. Vojtanik, M. Vazquez, *RECENT RESEARCH DEVELOPMENT IN NON-CRYSTALLINE SOLIDS 3* (Transworld Research Network, 2003)

[206] P. Vojtanik, J. Degro, O. V. Nielsen: *Acta Phys. Slov.* **42** (1992) 364

[207] J. Degro, P. Vojtanik, O. V. Nielsen: *Phys. Stat. Sol.* **A 132** (1992) 183

[208] P. Klein, K. Richter, R. Varga, M. Vazquez: *J. All. Comp.* **569** (2013) 9

[209] R. Varga, P. Vojtanik, J. Kovac, P. Agudo, M. Vazquez, A. Lovas: *Acta Phys. Slov.* **49** (1999) 901

[210] N. Lupu, H. Chiriac, S. Corodeanu, G. Ababei: *IEEE Trans. Magn.* **47** (2011) 3791

[211] R. Varga, P. Vojtanik: *J. Magn. Magn. Mater.* **196-197** (1999) 230

[212] R. Sabol, R. Varga, J. Hudak, J. Blazek, D. Praslicka, P. Vojtanik, G. Badini, M. Vazquez: *J. Appl. Phys.* **111** (2012) 053919

[213] P. Klein, R. Varga, M. Vazquez: *Acta Phys. Polonica* **A 118** (2010) 809

[214] R. Sabol, R. Varga, J. Hudak, J. Blazek, D. Praslicka, P. Vojtanik, G. Badini, M. Vazquez: *J. Magn. Magn. Mater.* **325** (2013) 141

[215] R. Varga, J. Gamcova, P. Klein, J. Kovac, A. Zhukov: *IEEE Trans. Magn.* **49** (2013) 30

[216] R. Varga, T. Ryba, Z. Vargova, K. Saksl, V. Zhukova, A. Zhukov: *Scripta Materialia* **65** (2011) 703

[217] V. Vega, L. Gonzalez, J. Garca, W. O. Rosa, D. Serantes, V. M. Prida, G. Badini, R. Varga, J. J. Sunol, B. Hernando: *J. Appl. Phys.* **112** (2012) 033905

[218] T. Ryba, Z. Vargova, R. Varga, V. Zhukova, A. Zhukov: *IEEE Trans. Magn.* **49** (2013) 54